A detailed investigation of clear cell renal cell carcinoma cell and organoid cultures to find putative therapeutic targets and novel therapy approaches

Dissertation

zur

Erlangung des Doktorgrades (Dr. rer. nat.)

der

Mathematisch-Naturwissenschaftlichen Fakultät

der

Rheinischen Friedrich-Wilhelms-Universität Bonn

vorgelegt von

Laura Kristin Eßer

aus

Siegen

Bonn, 2022

Angefertigt mit Genehmigung der Mathematisch-Naturwissenschaftlichen Fakultät der Rheinischen Friedrich-Wilhelms-Universität Bonn.

1. Gutachterin: Prof. Dr. Marieta Toma

2. Gutachter: Prof. Dr. Hubert Schorle

Tag der Promotion: 30.03.2022

Erscheinungsjahr: 2022

Teile dieser Arbeit wurden bereits als folgende Originalpublikationen akzeptiert oder veröffentlicht:

Esser, L. K., Branchi, V., Shakeri, F., Simon, A. G, Kristiansen, G., Buness, A., Schorle, H., Toma, M. I. "Overexpression of Parkin in clear cell renal cell carcinoma decreases tumor aggressiveness by regulating CKS2 levels." (in press). *Int. J. Oncol.*

Esser, L. K., Branchi, V., Leonardelli, S., Pelusi, N., Simon, A. G., Klümper, N., Ellinger, J., Hauser, S., Gonzalez-Carmona, M. A., Ritter, M., Kristiansen, G., Schorle, H., Hölzel, M., Toma, M. I. 2020. "Cultivation of Clear Cell Renal Cell Carcinoma Patient-Derived Organoids in an Air-Liquid Interface System as a Tool for Studying Individualized Therapy." *Front. Oncol.* 10:1775. doi: 10.3389/fonc.2020.01775.

List of abbreviations

786-O^{C431S}: 786-O transduced with pLVX-EF1α-PARK2(C431S)-IRES-mCherry

786-O^{EV}: 786-O transduced with pLVX-EF1α-IRES-mCherry

786-O^{PARK2}: 786-O transduced with pLVX-EF1α-PARK2-IRES-mCherry

A260/280: ratio of absorbance at 260 nm and 280 nm

A260/230: ratio of absorbance at 260 nm and 230 nm

ADMEM/F12: Advanced DMEM/F12

ALI: air-liquid interface

ALI PDO: air-liquid interface patient-derived organoid

ATCC: American Type Culture Collection

BAP1: BRCA1 associated protein-1

BCA: bicinchonic acid

CA9: carbonic anhydrase 9

CC1: cell conditioning 1

ccRCC: clear cell renal cell carcinoma

chRCC: chromophobe renal cell carcinoma

CI: confidence intervall

CID: collision induced dissociation

CKS1: cyclin-dependent subunit 1

CKS2: CDC28 protein kinase regulatory subunit 2

CLS: Cell Lines Service

CT: computed tomography

Da: Dalton

DAB: diaminobenzidin

df: degree of freedom

DPBS: Dulbecco's balanced salt solution

DSF: disease-free survival

DSB: double-strand breaks

DUB: deubiquitinase

dUTPase: deoxyuridine 5'-triphosphate nucleotidohydrolase

E. coli: Escherichia coli

EGF: epidermal growth factor

EMT: epithelial-mesenchymal transition

EV: empty vector

FA: formic acid

FAT10: HLA-F adjacent transcript 10

FBS: fetal bovine serum

FDR: false discovery rate

GSEA: Gene Set Enrichment Analysis

g: gram

H2AC21: Histone H2A type 2-B

H2AW: histone H2A type 3

H2AX: histone H2AX

H3K36: lysine 36 at histone 3

h: hours

HE: hematoxylin-eosin

HECT: homologous to E6-associated protein C-Terminus

HIF-1: hypoxia-inducible factor 1

HIST2H2AC: histone H2A type-c

HPF: high power field

HRE: hypoxia-response elements

HRG: histidine rich glycoprotein

IBR: in-between RING

ICI: immune checkpoint inhibitor

IHC: immunohistochemistry

IT: immunotherapy

K11: 11 lysine site

K48: 48 lysine site

K63: 63 lysine site

K477: 477 lysine site

KRT16: keratin 16

l: liter

LB: lysogeny broth

LCA: leucocyte common antigen

LDHA: lactate dehydrogenase A

LC-MS: liquid chromatography-mass spectrometry

MCA: multiplex human cell line authentication test

MFN2: mitofusin 2

mg: milligram

min: minutes

ms: millisecond

mTORC1: mechanistic target of rapamycin complex 1

m/z: mass-to-charge ratio

NaCl: sodium chloride

$NaHCO_3$: sodium bicarbonate

NaOH: sodium hydroxide solution

NCBI: National Center for Biotechnology Information

NES: normalized enrichment score

NGS: Next Generation Sequencing

nm: nanometer

OS: overall survival

OSBPL10: oxysterol binding protein like 10

PAX8: paired box 8

PBRM1: polybromo 1

PCA: Principle Component Analysis

PD-1: programmed death protein 1

PD-L1: programmed death ligand 1

PDO: patient-derived organoid

PDX: patient-derived xenograft

PEI: polyethyenimine

PES: polyethersulfone

PGD: phosphogycerate

PI3K: phosphoinositide 3-kinase

PKM2: pyruvate kinase M2

pmol: picomoles

pRCC: papillary renal cell carcinoma

PSM: peptide-spectrum match

pT: pathologically examined tumor

qPCR: quantitative PCR

RBR: RING-in-between-RING

RCC: renal cell carcinoma

RCC-MH^{C431S}: 786-O transduced with pLVX-EF1α-PARK2(C431S)-IRES-mCherry

RCC-MH^{EV}: 786-O transduced with pLVX-EF1α-IRES-mCherry

RCC-MH^{PARK2}: 786-O transduced with pLVX-EF1α-PARK2-IRES-mCherry

RING0: ring finger protein 0

RING1: ring finger protein 1

RING2: ring finger protein 2

RING: really interesting new gene

ROS: reactive oxygen species

RT: room temperature

SDC: sodium deoxycholate

SETD2: SET domain containing 2

siRNA: small interfering RNA

SRA: Sequence Read Archive

SRM: serum-reduced medium

SSBP1: single stranded DNA binding protein 1

SWI/SNF: switch/sucrose non-fermentable

TBS-T: Tris-buffered saline with 0.1% Tween)

TEAB: triethylammonium bicarbonate

TKI: tyrosine kinase inhibitor

TMA: tissue microarray

TMT: tandem mass tag

TNM: tumor-node-metastasis

t-stat: t-statistic

TT: targeted therapy

U: units

UBA6: ubiquitin-like modifier-activating enzyme 6

UBE1: ubiquitin activating enzyme 1

UBE2Z: ubiquitin-conjugating enzyme E 2Z

UBL: ubiquitin-like

USE1: UBA6-specific E2 enzyme 1

VEGF: vascular endothelial growth factor

V: volt

VHL: von Hippel Lindau

WT: wild type

µg: microgram

µl: microliter

°C: degrees celsius

Table of Contents

Table of figures

Index of tables

Summary

Therapy options for metastasized renal cell carcinoma are limited. While immune checkpoint inhibitors and therapies targeting the tumor microenvironment have drastically changed treatment options, response rates are hardly predictable. Despite the development of novel therapies, clear cell renal cell carcinomas account for the most deaths of renal cancer, namely 180,000 in 2020. The scarcity of effective therapies highlights the importance of novel therapeutic targets and alternative therapy approaches for this cancer entity.

Therefore, in the first part of this thesis I investigated PARK2, which codes for the protein Parkin. It was first described in autosomal recessive juvenile Parkinson's disease, however, evidence is growing that it can also function as a tumor suppressor gene. Thus, I aimed to thoroughly investigate Parkin's function in clear cell renal cell carcinoma cell lines.

I found that overexpression of PARK2 in clear cell renal cell carcinoma cells leads to reduced aggressiveness *in vitro* indicated by decreased migration and invasion. Moreover, lack of Parkin caused accumulation of CKS2, which was shown by mass spectrometry. CKS2 has been described to be highly expressed in many cancers, therefore, it was intriguing to examine the link between Parkin and the expression levels of CKS2. When mutating the catalytic site of PARK2, which results in E3 ligase deficiency, the migratory capacities of clear cell renal cell carcinoma cells were abolished leading to a similar migratory phenotype as wild-type cells, which lack Parkin. Next, I found that aggressiveness can be reduced by silencing of CKS2 resulting in decreased migration, which was comparable to cells expressing Parkin. Furthermore, analysis of a patient cohort showed that high CKS2 levels are associated with high tumor grading and poor survival.

In conclusion, this first part of the thesis suggests a link between Parkin and CKS2, which affects tumor aggressiveness. Parkin may influence CKS2 levels via its E3 ubiquitin ligase which causes reduced migration and invasion. Altogether, this provides valuable information that CKS2 may be a potential biomarker in clear cell renal cell carcinoma and may serve as a novel therapeutic target in the future.

Since therapy responses in patients are hardly predictable, I was interested in researching a novel tool, which assists present platforms, for its suitability in clear cell renal cell

carcinoma therapy testing and its potential for developing more personalized therapy approaches.

For that, I used fresh tissue from 42 patients, which underwent complete or partial nephrectomy, to generate patient-derived organoids based on an air-liquid interface culture system. The generated air-liquid interface patient-derived organoids were thoroughly characterized to validate them as a novel tool for therapy testing. For that, the obtained tissue was partly minced and cultured, and partly used for isolating RNA to conduct RNA sequencing. Further, immunohistochemistry was performed to verify the similarity of the cultured air-liquid interface patient-derived organoids and the tumor of origin. Common pathological markers and cells of the tumor microenvironment could be identified. Lastly, to test it as a tool for therapy testing, ten air-liquid interface patient-derived organoids were treated with the targeted therapy agent cabozantinib or the immune checkpoint inhibitor nivolumab and responses were obtained. In agreement with observations in the clinics, the response rates varied drastically. This indicates that this model system may give valuable information about the response rates in patients and possible therapy options.

In conclusion, these findings show that the established patient-derived organoids are a promising tool for therapy testing under a controlled setting. Moreover, they resemble the tumor of origin and therapy responses can be quickly obtained.

1. Introduction

In 2020, kidney cancer accounted for 4.6% of all diagnosed cancers and was the 10th most common cancer for men and the 14th most common for women worldwide. In that year, an estimated number of 430,000 new incidences and 180,000 deaths occurred globally. 270,000 cases were diagnosed in men and 160,000 in women depicting an incidence risk rate of 1.7 for men compared to women (Ferlay et al. 2020). Hence, men are more prone to being diagnosed with renal cell carcinoma (RCC), the most common form of kidney cancer, yet the exact causes have not been identified. Possible reasons for that may be a lifestyle with higher risk factors per se. Risk factors include obesity, smoking, workplace exposures, and alcohol consumption as well as hypertension, overuse of certain medications, advanced kidney disease, genetic and hereditary risk factors and family history of kidney neoplasms (American Society of Clinical Oncology 2021).

Up to 2008, incidence rates were rising steadily by 3.4% each year in the United States. The reasons for that are unknown, but may be explained by better screening methods, such as computed tomography (CT) scans. However since 2008, kidney cancer cases have been almost stable (+0.7% per year) and death rates have been falling slightly from 2000 to 2015 (-0.9%) and decreased even more from 2015 to 2018 (-2.6% per year) (SEER*Explorer 2021).

Predominantly, kidney cancer is detected incidentally during an examination for different, unrelated conditions, because symptoms are not clear and, especially in the beginning of the disease, often lacking. They can range from more general symptoms including fatigue, loss of appetite, loss of weight, fever, or anemia to more specific ones such as hematuria, lower back pain, or a mass on the side or lower back. Problematically, those symptoms are not indicative solely for kidney cancer. In case of diagnosis, it is crucial at which stage the cancer is detected **(Figure 1.1)**.

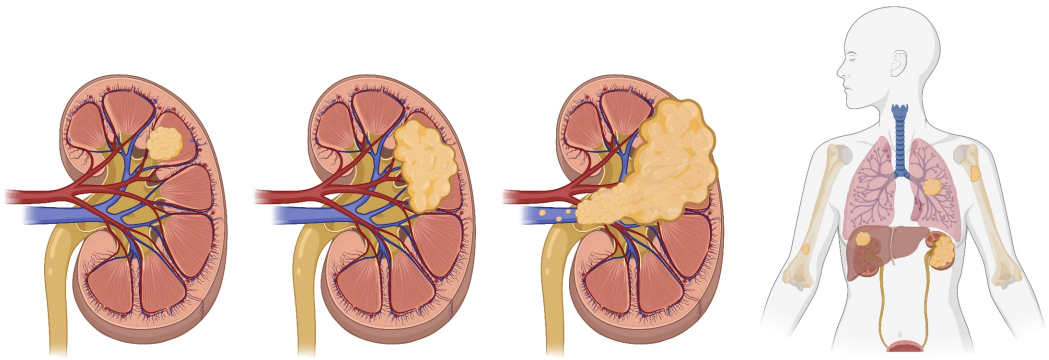

Figure 1.1| The different stages of kidney cancer. Stage I is defined by a small, localized tumor. In stage II the tumor is still located in the kidney, yet, it has increased in size. In stage III, the tumor has started growing into the surrounding tissue and in stage IV, the tumor continued growing and might have metastasized to nearby lymph nodes or distant organs such as lung, liver, or bone (American Society of Clinical Oncology 2021; Dudani et al. 2020) (created with BioRender.com).

The staging is based on the tumor-node-metastasis (TNM) system containing information on the size and extent of the main tumor (T), the spread to nearby lymph nodes (N), and the spread to distant sites (M), such as lung, bone, brain or liver. Whereas the overall 5-year survival rate for kidney cancer is 75%, the 5-year survival rate for the different stages differs drastically: for stage I and II it is 93%, for stage III 70% and for stage IV it drops down to 13% (**Table 1.1**) (American Society of Clinical Oncology 2021)**.**

Table 1.1| Stage, definition, TNM and 5-year survival rate of kidney cancer (American Society of Clinical Oncology 2021).

Stage		Definition	TNM	5-year survival rate
I		small (<7 cm), located solely in kidney	T1, N0, M0	93%
II		larger than 7 cm, located solely in kidney	T2, N0, M0	
III	**a**	started growing into renal vein, vena cava or tissue surround kidney (except adrenal gland or Gerota's fascia)	T3, N0, M0	70%
	b	tumor located outside kidney, spread to nearby lymph nodes, but not to distant lymph nodes, other organs or beyond Gerota's fascia	T3, N1, M0	
IV	**a**	tumor grows beyond Gerota's fascia, possibly into adrenal gland, might have spread to nearby lymph nodes, but not to distant lymph nodes or other organs	T4, any N, M0	13%
	b	any size of tumor, may have grown outside kidney, potentially spread to nearby lymph nodes and metastasized to distant lymph nodes and/or other organs	any T, any N, M1	

The standard of care therapy for kidney cancer in stage I to III is the removal of the primary tumor by partial or total nephrectomy. Patients who get diagnosed with stage IV with distant metastases receive immunotherapy (IT) in form of immune checkpoint inhibitors (ICI), alone or in combination with targeted therapy (TT) such as tyrosine kinase inhibitors (TKI) as a first line therapy. While (partial) nephrectomy in early stages is often curative, therapy options for patients which are not eligible for surgery are poor. In addition, some patients do not benefit from TT or IT. Therefore, these patients with terminal disease are left with the only option of palliation of their symptoms (American Society of Clinical Oncology 2021).

This highlights the urgency of early detection based on improved screening methods and the availability of appropriate biomarkers. Moreover, suitable therapies after diagnosis are

necessary. In order to find superior and more fitting biomarkers and therapies, a better understanding of the detailed mechanisms in the ccRCC etiology are inevitable.

1.1. Clear cell renal cell carcinoma

Kidney cancer is a neoplastic disease that is subdivided into several different forms, including renal cell carcinomas (RCC), transitional cell carcinomas, Wilms tumors and renal sarcomas. The most common form accounting for nine out of ten cases is RCC which is a heterogeneous disease consisting of three main histologically discriminable subtypes, namely clear cell RCC (ccRCC), papillary RCC (pRCC), which is further subdivided into type I and II, and chromophobe RCC (chRCC) (**Figure 1.2**).

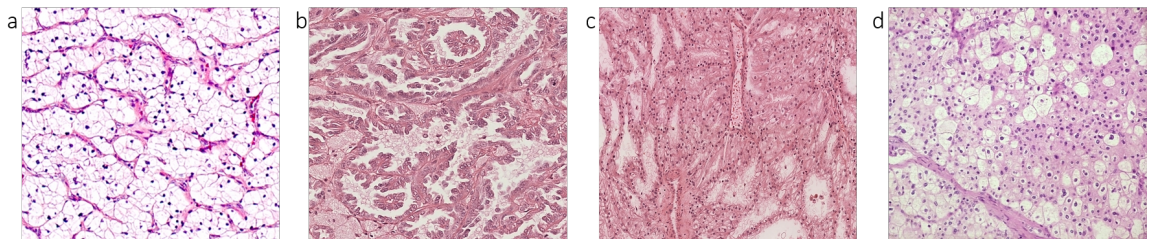

Figure 1.2| Representative pictures of the three main histological discriminable subtypes of RCC. The pictures depict examples of hematoxylin-eosin stained tumor tissues of RCC, namely (**a**) ccRCC, (**b**) pRCC type I, (**c**) pRCC type II and (**d**) chRCC.

CcRCC is the most common subtype making up 75% of all cases (Padala et al. 2020). It is a renal cortical tumor that arises from the proximal tubule cells. CcRCC is typically characterized by malignant epithelial cells with clear cytoplasm due to high amounts of lipids and glycogens. The cells are arranged in nests with intervening blood vessels (**Figure 1.2 a)** (Sirohi et al. 2018). Furthermore, ccRCC is characterized by loss of chromosome 3p which is accompanied by loss of genes that are located on that specific chromosomal segment (Zbar et al. 1987). Another feature of this tumor is its high heterogeneity which leads to varying therapy responses in patients. Moreover, the tumor microenvironment of ccRCC is highly immunosuppressive.

The importance of early detection, the lack of symptoms, the aggressiveness of the disease,

and the limitation of available therapies indicate the urgent need for valuable markers which are targetable.

1.1.1. Somatic mutations involved in ccRCC

Different subtypes of RCC are characterized by specific somatic mutations and chromosomal copy number alterations. The additional information helps to classify the subtypes not only by their histological and morphological phenotypes but also by their genetic profile. In addition, molecular differences within the subtypes can predict clinical outcome and treatment response rates (Manley and Hakimi 2016).

The earliest described chromosomal alteration in ccRCC was the loss of chromosome 3p (Zbar et al. 1987). It was found to be absent in more than 90% of patients. Chromosome 3p encodes the four genes, namely von Hippel Lindau (VHL), polybromo 1 (PBRM1), SET domain containing 2 (SETD2), and BRCA1 associated protein-1 (BAP1), which are most commonly mutated in ccRCC (The Cancer Genome Atlas Research Network 2013) (**Figure 1.3**).

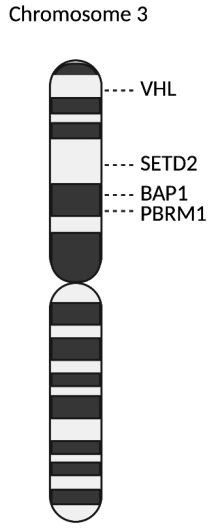

Figure 1.3| Illustration of chromosome 3 and the locus of the four most common mutated or lost genes in ccRCC. VHL (3p25.3), SETD2 (3p21.31), BAP1 (3p21.1) and PBRM1 (3p21.1) are all located in close proximity to each other and are affected by loss of chromosome 3p, which is found in more than 90% of all ccRCC patients (The Cancer Genome Atlas Research Network 2013) (created with BioRender.com).

1.1.1.1. VHL

The foundation of understanding ccRCC pathogenesis was set when the VHL gene was discovered in 1993 (Latif et al. 1993). Almost all ccRCC harbor a VHL alteration and/or chromosome 3p25 loss, which has been shown to be involved in both hereditary and sporadic ccRCC pathogenesis (Favazza et al. 2017; Linehan, Walther, and Zbar 2003). VHL is part of an E3 ubiquitin ligase complex that catalyzes the polyubiquitination of specific proteins which leads to their degradation via the proteasome. One such protein is hypoxia-inducible factor 1 (HIF-1), which consists of two subunits, namely alpha (HIF-1α) and beta (HIF-1β). While HIF-1α is rapidly degraded by the VHL E3 ubiquitin ligase complex under normoxic conditions, its degradation is inhibited under hypoxic conditions resulting in the stabilization and accumulation of HIF-1α (L. E. Huang et al. 1996). HIF-1α then forms heterodimers with HIF-1β which translocate to the nucleus, bind to hypoxia-response elements (HRE) and activate the transcription of target genes, such as phosphoglycerate (PGD) and lactate dehydrogenase A (LDHA), that help adapt and protect oxygen deprived tissues (C.-J. Hu et al. 2003).

Hence, the loss of VHL, induced by genetic or epigenetic mechanisms, prevents the degradation of HIF-1α and causes its accumulation. This then leads to the transcriptional activation of target genes not only under hypoxic but also under normoxic conditions. More than 800 direct HIF target genes have been described; some of which play a role in tumor development and progression (Gossage, Eisen, and Maher 2015; Jun et al. 2017).

Nevertheless, VHL loss alone is not sufficient to induce ccRCC tumorigenesis, rather, an accumulation of additional genetic and/or epigenetic changes is needed (Hsieh, Purdue, et al. 2017).

1.1.1.2. PBRM1

The second most common mutated gene in ccRCC is PBRM1, which is mutated in 40% of all cases (Varela et al. 2011). PBRM1 is located on chromosome 3p21.1, consequently, it is also affected by loss of the short arm of chromosome 3. PBRM1 encodes the protein BAF180 that is part of the chromatin remodeling switch/sucrose non-fermentable (SWI/SNF) complex. BAF180 is involved in numerous DNA repair mechanisms, including

DNA double-strand breaks (DSB)-induced silencing and repair, post-replication repair as well as in preventing genomic instability by promoting centromeric cohesion (Kakarougkas et al. 2014; Brownlee et al. 2014; Hopson and Thompson 2017). PBRM1 is considered a tumor suppressor gene, yet, its exact function in ccRCC remains unknown. Loss or silencing of PBRM1 was shown to impact cell cycle arrest and promote proliferation and migration in ccRCC (HongKai Wang et al. 2017, 1). Yet, this effect might be context dependent. Contrary, in cells with mutated HIF-1α, reduction or knockout of PBRM1 reduces cell proliferation suggesting promotion of tumorigenesis in this specific situation (Murakami et al. 2017) which underlines the complex situation within ccRCC pathogenesis.

Besides the mentioned genes some more genes which are located on chromosome 3p and are associated with ccRCC pathogenesis have been observed.

1.1.1.3. SETD2

SETD2 belongs to the most commonly mutated genes in ccRCC. The histone methyltransferase SETD2 can alter the trimethylation status of lysine 36 at histone 3 (H3K36) which promotes transcription and affects DNA damage repair mechanisms. Subsequently, loss of SETD2 has various effects ranging from genomic instability to aberrant transcriptional activity and can, therefore, lead to tumorigenesis (Rui Chen et al. 2020; J. M. Simon et al. 2014). Nevertheless, the underlying mechanism remains unknown. SETD2 mutations are associated with tumor aggressiveness, recurrence of the disease and reduced overall and progression-free survival (W. Liu et al. 2015; L. Liu et al. 2017; Ho et al. 2016). These observations, in addition with findings that SETD2 mutations are four times more likely in metastatic ccRCC, suggest a role in not only tumor development but also disease progression (Dalgliesh et al. 2010; Gerlinger et al. 2014; Hsieh, Chen, et al. 2017). Furthermore, SETD2 deficiency leads to decreased autophagy and poor prognosis in ccRCC patients which needs to be taken into account for potential therapy approaches (González-Rodríguez et al. 2020). Interestingly, SETD2 mutations seem to occur in clones that are already VHL-mutated which underlines SETD2's role in tumor progression (Y. Sato et al. 2013).

1.1.1.4. BAP1

The already described genes VHL, PBRM1 and SETD2 are all located within 43 Mb on chromosome 3p that is lost in 90% of all sporadic ccRCCs. Another gene that is located in that region and, hence, affected by loss of chromosome 3p is BAP1 (Peña-Llopis et al. 2013). In addition to chromosomal deletion inactivating mutations occur. One out of 10 ccRCCs harbors a BAP1 aberration (Guo et al. 2012; Duns et al. 2012). BAP1 is a member of the deubiquitinase (DUB) family of proteins, more specifically an ubiquitin carboxy-terminal hydrolase. BAP1 was shown to be involved in several tumor suppressive processes in different cancers, such as genome stability, chromatin modification, transcription factor regulation, regulation of gene transcription or repair of DNA DSB (Carbone et al. 2020). Deficiency of BAP1 was shown to be associated with increased activation of mechanistic target of rapamycin complex 1 (mTORC1), an important regulator of cell growth (Peña-Llopis et al. 2012). Further, BAP1 and PBRM1 showed a negative correlation suggesting that these mutations are mutually exclusive (Peña-Llopis et al. 2012; 2013).

While several somatic mutations and their effect on ccRCC tumorigenesis have been described, the exact genetic drivers and underlying mechanisms of ccRCC development are not fully deciphered. This lack of information challenges not only the prediction of clinical outcome but also the prediction of treatment responses.

1.1.2. Treatment options for clear cell renal cell carcinoma

To decide on appropriate therapies the extent of the disease must be considered including TNM stage, tumor size, grade, RCC subtype and molecular features. Localized renal cell carcinoma includes stages I, II and III, while advanced renal cell carcinoma includes stage IV. In most cases partial or radical nephrectomy for localized renal cell carcinoma is curative. After nephrectomy of localized advanced RCC with high risk of relapse, adjuvant therapy does not prolong disease-free survival (DFS) or overall survival (OS) (Motzer et al. 2021). However, in case of advanced disease, TT in combination with IT can improve OS (Bedke et al. 2021). The combination options for metastatic ccRCC patients include

pembrolizumab plus axitinib, lenvatinib plus pembrolizumab or nivolumab plus cabozantinib. Patients who cannot tolerate immune checkpoint inhibitors can receive an alternative combination consisting of two TT agents which include sunitinib or pazopanib (Bedke et al. 2021). Nevertheless, a considerable number of patients does not respond to these treatments due to intrinsic or adaptive resistance leaving them with no option than palliation at the moment.

1.2. Parkin in tumorigenesis

In order to find alternative or additional therapies for patients diagnosed with ccRCC the underlying molecular and mechanistic processes in the disease development need to be studied further. Besides the most common mutations, which were mentioned earlier, several other interesting genes have been described in ccRCC pathogenesis (Sanchez and Simon 2018; Yan et al. 2017). The gene PARK2, which codes for the protein Parkin, was first discovered in autosomal recessive juvenile Parkinson's disease (Kitada et al. 1998). However, since then evidence is growing that it may also serve as a tumor suppressor gene (Duan et al. 2019, 2; Lee et al. 2018, 2; Ni et al. 2017, 2; Poulogiannis et al. 2010; Veeriah et al. 2010, 2; Toma et al. 2013). In ccRCC the mRNA of the PARK2 is significantly down-regulated and associated with high-grade tumors, lymph node metastasis and reduced OS. Interestingly, the protein levels of Parkin are reduced, yet, no association with clinical outcome was observed (Toma et al. 2013). The exact mechanism for Parkin in ccRCC remains unknown. Different mechanisms for its tumor suppressive function have been discussed; e.g. Parkin expression was shown to be involved in cell cycle progression in colorectal cancers. Parkin is up-regulated upon epidermal growth factor (EGF) stimulation which can be suppressed by inhibiting the phosphoinositide 3-kinase (PI3K)-Akt-dependent pathway (Ikeuchi et al. 2009). Another study found that Parkin binds to microtubules leading to sensitization of breast cancer cells to drug-induced apoptosis (Hongxia Wang et al. 2009). Liu and colleagues could show that the ubiquitination of HIF-1α induces Parkin degradation and, consequently, inhibits migration and invasion of breast cancer cells (J. Liu et al. 2017). Furthermore, Parkin suppresses glycolysis by

ubiquitinating the pyruvate kinase M2 (PKM2) and, thus, diminishing its enzymatic activity suggesting an effect on tumor growth (K. Liu et al. 2016). Moreover, Parkin plays a role in mitophagy. It eliminates the accumulation of damaged mitochondria, mitochondrial DNA mutations and reactive oxygen species (ROS) (Bernardini, Lazarou, and Dewson 2017; J. Liu et al. 2018). These studies show that Parkin is involved in numerous mechanisms within the cell and that its downregulation can have serious consequences.

As an E3-ubiquitin-ligase Parkin selectively and specifically degrades polyubiquitinated proteins via the 26S proteasome (Trempe et al. 2013). Even though, several interaction partners of Parkin have been described, most of these studies focus on Parkin in the context of Parkinson's disease (Singh et al. 2018, 2). In cancer, the best studied process involving Parkin is the selective degradation of defective mitochondria, called mitophagy. This process regulates mitochondrial homeostasis and ROS production, which in turn, can affect cancer development (Bernardini, Lazarou, and Dewson 2017; Durcan and Fon 2015).

Unfortunately, due to its role as a tumor suppressor, Parkin is no ideal candidate for new therapy approaches, yet on the other hand, due to its function as an E3-ubiquitin-ligase proteins that accumulate in absence of Parkin may hold great promise for new therapies.

1.3. Ubiquitination

Parkin was described to play a role in a process, called ubiquitination, as an E3 ubiquitin ligase (Riley et al. 2013). Ubiquitination modifies proteins post-translationally via addition of ubiquitin (Ub). This eventually leads to the degradation of proteins and, thereby, controls cell homeostasis. Ub is a highly conserved protein made up of 76 amino acids. A cascade of enzymatic reactions covalently tags Ub to target proteins (Hershko and Ciechanover 1998; Pickart 2001; Deng et al. 2020).

The ubiquitin system consists of three main enzymes: E1, E2, and E3. They induce diverse biochemical reactions that are needed for Ub activation, Ub transfer and Ub ligation to the target protein. This multistep enzymatic reaction is initiated when Ub is activated by an E1 enzyme in an adenosine triphosphate (ATP)-dependent manner. A thioesther bond between

the carboxyl-terminus of Ub and the active site cysteine of E1 activates the Ub. Next, E1 delivers the activated Ub to an E2 enzyme and, lastly, the proper E3 ligase transfers the activated Ub to the target protein (Deng et al. 2020). After the transfer an iso-peptide bond is formed between the lysine ε-amino group of the target protein and the C-terminal of the Ub's carboxyl group. This step can be repeated multiple times to form polyubiquitin chains that lead to the specific detection and degradation of the protein via the 26S proteasome complex (Deng et al. 2020) **(Figure 1.4)**.

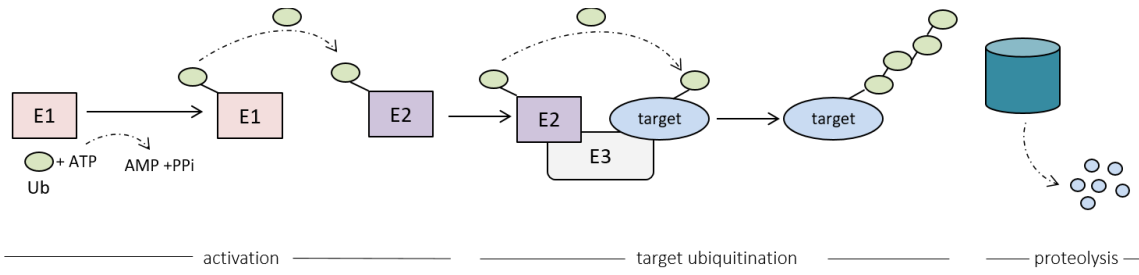

Figure 1.4| Simplified scheme of Parkin's ubiquitination process. Ubiquitination is initiated when Ub is activated by an E1 enzyme. The E1 enzyme uses ATP to adenylate and, subsequently, bind Ub **(activation)**. Next, the activated Ub is transferred to an E2 enzyme and an E3 ubiquitin ligase delivers the Ub to the target protein, where a polyubiquitin chain can be formed **(target ubiquitination)**. Lastly, the target protein is degraded. In case of conjugation to K48 or K11 the target protein is then degraded via the proteasome **(proteolysis)**.

Ub contains seven lysine acceptor sites. Depending on which lysine Ub gets attached to, the (poly)ubiquitinated protein has an effect on various biological processes, including signal transduction (H. Hu and Sun 2016), DNA repair (Ghosh and Saha 2012), transcriptional regulation (Mark and Rape 2021), and degradation. Polyubiquitin chains conjugated to the 48 lysine site (K48) or the 11 lysine site (K11) lead to degradation of the protein via the 26S proteasome complex (Hershko and Ciechanover 1998; Nakayama and Nakayama 2006; Dong Wang et al. 2017) **(Figure 1.4)**.

In humans only two E1 enzymes for Ub are known, namely, the canonical Ub activating enzyme 1 (UBE1) and the non-canonical Ub-like modifier-activating enzyme 6 (UBA6) (Haas et al. 1982; Pelzer et al. 2007). In contrast to the few E1 enzymes, humans contain

approximately 40 distinct E2 enzymes that carry a conserved Ub-binding catalytic domain of 150 amino acids, but, nevertheless, display extreme specificity in their interaction with E3 enzymes due to short N- and/or C-terminal extensions (Stewart et al. 2016). More than 600 E3 Ub ligases have been described in humans. Those can be classified into three major groups. Most E3s belong to the group of really interesting new gene (RING)-, followed by homologous to E6-associated protein C-terminus (HECT)-, and, the latest and smallest group, RING-in-between-RING (RBR) E3 ligases (Medvar et al. 2016; Dove et al. 2016). Ub transfer to the lysine on the target protein occurs either directly from the E2 enzyme as in the case for RING E3 ligases or via the formation of a thioester bond between Ub and a cysteine residue on the HECT E3 ligases. RBR E3s, also termed RING/HECT hybrid, represent a group that have both a canonical RING domain and a catalytic cysteine residue comparable to the HECT domain, therefore, serve as a hybrid between RING and HECT E3 ligases (George et al. 2018; Riley et al. 2013).

The PARK2 gene encodes the RBR E3 Ub ligase Parkin, which is made up of five domains: Ub-like (UBL), ring finger protein 0 (RING0), ring finger protein 1 (RING1), in-between RING (IBR) and ring finger protein 2 (RING2) domain (**Figure 1.5**).

Figure 1.5| Multi-domain protein Parkin. The Parkin protein is made up of the UBL domain at the N-terminal, followed by the RING0, RING1, IBR and the RING2 domain at the C-terminal.

Per se, Parkin is in an auto-inhibited state and has to undergo massive conformational change for activation. In the auto-inhibited state, RING1, where the E2 binding site is located, associates with a fragment called the repressor element of Parkin, which is located between IBR and RING2, and, thus, blocks the E2 binding site. Parkin's catalytic site, C431, located on the RING2 domain, is stalled due to the interaction of RING0 and RING2 hindering the E2 from transferring Ub (Trempe et al. 2013; Riley et al. 2013).

While no (E1) or only a few (E2) reports have been described for the involvement of

deregulated E1 and E2 enzymes in tumorigenesis, evidence is growing that in many cases deregulation of an E3 enzyme has an impact on cancer development (Nakayama and Nakayama 2006). Hence, E3 Ub ligases or their substrate proteins may be promising targets for new therapeutic approaches.

1.4. CDC28 protein kinase regulatory subunit 2 in tumorigenesis

CDC28 protein kinase regulatory subunit 2 (CKS2) is one of two members of the mammalian cyclin kinase subunit family. While the function of cyclin-dependent subunit 1 (CKS1) has been extensively researched in different cancers (Chai et al. 2019; Kang et al. 2019; Tsai et al. 2005; Westbrook et al. 2007), the role of CKS2 in cancer is poorly understood. Recently the role of CKS2 in cancer has gained interest. Huang and colleagues showed that overexpression of CKS2 leads to worsened prognosis and that CKS2 inhibition decreased proliferation and invasion in breast cancer cells (N. Huang et al. 2019, 2). Similar results were found in epithelial ovarian cancer. Again, CKS2 silencing suppressed proliferation, invasion and migration (J.-H. Xu, Wang, and Xu 2019). Further studies described the association between CKS2 expression and poor prognosis or cancer progression in different cancers including lung adenocarcinoma and bladder cancer (Xiao et al. 2020; Yu et al. 2015; R. Chen, Feng, and Xu 2011), yet, explanations for the underlying mechanism involved in the different cancers are scare. Most explanations describe a nuclear role and, consequently, involvement in cell cycle. CKS2 was shown to interact with deoxyuridine 5’-triphosphate nucleotidohydrolase (dUTPase) and regulate its nuclear localization (Gao et al. 2021). In addition, it binds to CDK2 which can result in overriding of the intra-S-phase checkpoint in replicative stress situations (Liberal et al. 2012). Recently a mitochondrial role for CKS2 has been described. CKS2 builds a complex with single stranded DNA binding protein 1 (SSBP1). This impacts mitochondrial DNA replication and energy supply of the cell which promotes resistance to chemotherapy and radiotherapy in cervical cancer (Jonsson et al. 2019). Interestingly, mitochondria and mitochondrial processes were described as promising targets for cancer therapy approaches (Dickerson, Jauregui, and Teng 2017). Therefore, further knowledge about the role of CKS2 in cancer may help find novel therapy agents.

1.5. Organoids in cancer research

One major barrier in developing new therapies remains the challenge of translating novel scientific findings into the clinical environment. While widely used cell lines are cost efficient, easy to handle and immortal, they may have undergone drastic genetic changes due to selective pressures of 2D culture conditions, thus, restricting the recapitulation of the patient's situation (Kapałczyńska et al. 2018). Animal models have improved cancer research immensely and closed the gap from bench to bedside further, nevertheless, the complex handling, high expenses and the limitation in recapitulating human pathological processes indicate the urgent need for an additional alternative tool for cancer research and therapy development (Yuki et al. 2020).

In recent years, organoids have gained increasing interest in the field of (cancer) research. Sato and colleagues showed in 2009 that a single leucine-rich repeat-containing G protein-coupled receptor 5 positive ($LGR5^{+}$) intestinal stem cell can induce epithelial organoids by being cultivated in a 3D matrix under conditions that mimic the *in vivo* situation (T. Sato et al. 2009). Since then many protocols for organoid cultures have been established (H. Chen et al. 2020; Frappart et al. 2020; Sachs et al. 2018). While in the beginning organoids were often generated from tissue-derived stem cells, recently, efforts have been made to generate organoids from patient-derived tumor tissues directly (Drost and Clevers 2018). One major drawback of the use of organoids in the development of novel or suitable therapy regimens is their lack of the native tumor microenvironment, which has an impact on therapy responses. In 2018, Neal and colleagues successfully developed patient-derived organoids (PDOs) using a special air-liquid interface (ALI) method (Neal et al. 2018). In addition to the recapitulation of the histological characteristics, they could show that the tumor microenvironment in their air-liquid interface patient-derived organoids (ALI PDOs) was retained, including immune and stromal cells. Furthermore, genetic profiling revealed identical mutations with the tumor of origin. Impressively, they were able to cultivate ALI PDOs from 100 different patients and 19 different tissue sites, including lung, pancreas, colon and kidney, which makes it a fascinating tool for testing and developing novel therapies for different malignancies (Neal et al. 2018).

1.6. Aims of this thesis

Evidence is growing that Parkin has tumor suppressive capacities and, thus, loss of Parkin can influence tumor development. However, the precise underlying mechanisms remain unknown. Especially in ccRCC studies focusing on Parkin are scarce.

Therefore, in the first part of this thesis I aimed to answer the following questions:

1. Do cells with and without Parkin expression differ in their phenotypic properties?

2. Are there underlying transcriptomic or proteomic differences in the cells which can explain the differences?

3. Is there a link between Parkin and CKS2 expression and clinicopathologial parameters?

Further, for the second part of this study I was interested in alternative tools for personalized therapies, because patient-derived tumor models for the development of new therapy approaches in ccRCC are still scarce. In order to translate novel scientific findings and therapy agents to the clinics, suitable tools that recapitulate the patient's situation more closely are urgently needed.

Therefore, in the second part of this thesis I aimed to answer the following questions:

1. Is it possible to cultivate fresh tumor material resected from patients *in vitro* and expand it?

2. Do the cultivated material and the derived organoids resemble the patients' histological situation and the molecular gene profile?

3. Is it possible to use this novel model system for therapy testing and development?

2. Materials and methods

2.1. Materials

2.1.1. Equipment

Product	Model/Serial number	Supplier
Adjustable pipettes (2.5 µl, 10 µl, 20 µl, 100 µl, 200 µl, 1000 µl)	Research® plus	Eppendorf AG, Hamburg, Germany
Agarose gel imaging system	GEL iX20 Crosslinker Fluo-Link/ CL1931203	Intas Science Imaging Instruments GmbH, Göttingen, Germany Biometra, Göttingen, Germany
Analyzer	BD LSRFortessa™	Becton Dickinson, Franklin Lakes, USA
Autostainer	Ventana BenchMark Ultra 480S	Roche Diagnostics, Basel, Switzerland Medac, Wedel, Germany
Balance	Kern 440-45N/WC063732 Mettler AC 100	Kern & Sohn GmbH, Balingen, Germany Mettler-Toledo, Gießen, Germany
Blot imaging system	ChemiDoc™ MP	Bio-Rad Laboratories, Hercules, USA
Blot transfer system	Mini Protean II Cell/32S/16254	Bio-Rad Laboratories, Hercules, USA
Cell culture hood	HSP 12/40178819	Kendro Laboratory Products, Hanau, Germany
Cell sorter	BD FACS Aria III	Becton Dickinson, Franklin Lakes, USA
Centrifuges	Mikro 200R Biofuge primo R	Andreas Hettich GmbH & Co. KG, Tuttlingen, Germany Thermo Fisher, Waltham, USA
Cell Freezing Container	CoolCell™ LX/CLS432002	Sigma-Aldrich, St. Louis, USA

Counting chamber	Neubauer improved	Marienfeld, Lauda-Königshofen, Germany
Gel electrophoresis chamber	BlueMarine™ 100	SERVA Electrophoresis GmbH, Heidelberg, Germany
Heating block	Thermomixer comfort/ 5355 23995	Eppendorf AG, Hamburg, Germany
HPLC system	Dionex Ultimate 3000 RSLC nano	Dionex GmbH, Idstein, Germany
Incubator	Hera cell	Thermo Fisher Scientific, Inc., Waltham, USA
Incubator for shaker	Certomat® H	Sartorius, Göttingen, Germany
Fractionator	Offgel fractionator	Agilent Technologies, Waldbronn, Germany
Heating magnetic stirrer	ARE	VELP Scientifica Srl, Usmate, Italy
Mass spectrometer	Orbitrap Fusion Lumos mass spectrometer	Thermo Fisher Scientific, Inc., Waltham, USA
Microscopes	BX50 Fluorescence Olympus BX50 light microscope	Olympus Corporation, Shinjuku, Japan
Microwave	-	Bosch
Orbital shaker	Braun Certomat® MO KS250basic	Sartorius, Göttingen Germany IKA Labortechnik, Staufen im Breisgau, Germany
pH electrode	WTW SenTix	Xylem Inc., Rye Brook, USA
pH meter	WTW inoLab® pH7110/ 18100381	Xylem Inc., Rye Brook, USA
Pipet-aid	pipetus®	Hirschmann Laborgeräte GmbH & Co. KG, Eberstadt, Germany
Power supply electrophoresis	PowerPac Basic/041BR28144 PowerPac 300/283BR10941	Bio-Rad Laboratories, Hercules, USA
Real-Time PCR system	ViiA 7	Thermo Fisher Scientific, Inc.,

		Waltham, USA
Rotator	RS-TR05/VF6K005653	Phoenix Instrument, Garbsen, Germany
SDS Electrophoresis System	XCell SureLock Mini-Cell	Thermo Fisher Scientific, Inc., Waltham, USA
Sequencer	HiSeq 2500 v4	Illumina, San Diego, USA
Spectrophotometer	NanoDrop™ 1000	Peqlab, Erlangen, Germany
Thermal cycler	GE4852T/BH19110079	HangZhou Bio-gener Technology CO., LTD, Hangzhou, China
Vacuum pump	Mini-membrane vacuum pump N811KN.18	KNF Neuberger, Inc., Balterswil TG, Switzerland
Vortex mixer	Vortex-Genie 2	Scientific Industries, Bohemia, USA
Water bath	Type 1008/ 10471994e	Gesellschaft für Labortechnik mbH, Burgwedel, Germany

2.1.2. Consumables

Product	Manufacturer
1.5 ml/2 ml reaction tubes	Sarstedt, Nümbrecht, Germany
5 ml Falcon® Round-bottom Tube with Cell-Strainer Cap	Corning, New York, USA
15 ml/50 ml centrifuge tubes	Sarstedt. Nümbrecht, Germany
Analytical column (C18)	Dr. Maisch HPLC GmbH, Ammerbuch, Germany
Axygen® CyclerSeal Sealing Film	Corning, New York, USA
Cell culture dishes and plates	Sarstedt, Nümbrecht, Germany
Cell Scraper with 2-Position Blade	Sarstedt, Nümbrecht, Germany
Corning® FluoroBlok™ Cell Culture Inserts	Corning, New York, USA
Cryotubes	Sarstedt, Nümbrecht, Germany
Disposable Serological Pipettes (5 ml, 10 ml, 25 ml)	Corning, New York, USA

Feather Disposable Scalpel	Feather, Osaka, Japan
Filtertips (10 µl, 100 µl, 200 µl, 1000 µl)	Greiner Bio-One, Frickenhausen, Germany
FluoroBlok™ Insert	Corning, New York, USA
FrameStar® 384 Well Skirted PCR Plate	4titude, Wotton, UK
MicroAmp® Fast Reaction Tubes	Thermo Fisher Scientific, Inc., Waltham, USA
Millicell Cell Culture Insert, 0.4 µm	Millipore, Burlington, USA
NuPAGE™ 4 to 12% Bis-Tris gel	Thermo Fisher Scientific, Inc., Waltham, USA
PES membrane	Pall Filtersystems GmbH, Crailsheim, Germany
Pipette tips (10 µl, 200 µl, 1000 µl)	Greiner Bio-One, Frickenhausen, Germany
Roti®-NC	Carl Roth, Karlsruhe, Germany
Sterile Single Use Vacuum Filter Units (Rapid Flow™) (0.2 µm)	Thermo Fisher Scientific, Inc., Waltham, USA
Superfrost slides	Menzel Gläser, Brunswick, Germany
Syringe filter (0.45 µm)	TPP Techno Plastic Products AG, Trasadingen, Switzerland
Tissue-Tek® Cryomold® (25×20×5 mm)	Sakura Finetek, Tokyo, Japan
Whatman™ Paper	GE Healthcare Life Sciences, Chalfont St Giles, UK

2.1.3. Materials

Product name	Company	Catalog no.	Final concentration
2.2.1. Cell culture			
2.2.1.1. Commercial cell lines			
786-O	ATCC, Manassas, USA	CRL-1932	-
0.25% Trypsin-EDTA	Thermo Fisher Scientific, Inc., Waltham, USA	25200056	-
Gibco® DMEM + GlutaMAX™ Medium	Thermo Fisher Scientific, Inc., Waltham, USA	31966021	-

Gibco® DPBS	Thermo Fisher Scientific, Inc., Waltham, USA	14190144	-
Gibco® Fetal Bovine Serum	Thermo Fisher Scientific, Inc., Waltham, USA	10270106	10%
Gibco® Pen Strep	Thermo Fisher Scientific, Inc., Waltham, USA	15140122	1%
Gibco® RPMI-1640 Medium	Thermo Fisher Scientific, Inc., Waltham, USA	21875034	-
293T	ATCC, Manassas, USA	ACS-4500	-
L Wnt-3A	ATCC, Manassas, USA	CRL-2647	-
RCC-MH	Cell lines service, Eppelheim, Germany	300237	-
R-Spondin 1	R&D Systems, Minneapolis, USA	3710-001-01	-
2.2.1.2. Primary cells			
B27-supplement	Thermo Fisher Scientific, Inc., Watham, USA	17504044	1X
Collagenase Type II	Thermo Fisher Scientific, Inc., Watham, USA	17101015	200 U/ml
FGF-basic (human recombinant)	PeproTech, Hamburg, Germany	100-18B	10 ng/ml
Gibco® DPBS	Thermo Fisher Scientific, Inc., Waltham, USA	14190144	-
Gibco® DMEM/F12 Medium	Thermo Fisher Scientific, Inc., Waltham, USA	11320033	-
Gibco® L-Glutamine	Thermo Fisher Scientific, Inc., Waltham, USA	25030081	4 mM
Gibco® MEM non Essential Amino Acids 100X	Thermo Fisher Scientific, Inc., Waltham, USA	11140035	1X
Gibco® Pen Strep	Thermo Fisher Scientific, Inc., Waltham, USA	15140122	2%
Gibco® RPMI-1640 Medium	Thermo Fisher Scientific, Inc., Waltham, USA	21875034	-
hrEGF	R&D Systems, Minneapolis, USA	236-EG	10 ng/ml
Hyaluronidase Type V	Sigma-Aldrich, St. Louis, USA		100 U/ml
Lipid Mixture 1	Sigma-Aldrich, St. Louis, USA	L0288	1X
***N*-Acetyl-Cysteine**	Acros Organics, Waltham, USA	160280250	1 mM

Roti®-CELL HEPES Solution	Carl Roth, Karlsruhe, Germany	9157.1	10 mM
2.2.1.3. ALI PDOs			
A83-01	Sigma-Aldrich, St. Louis, USA	SML0788	0.5 µM
B27 (without vitamin A)	Thermo Fisher Scientific, Inc., Waltham, USA	12587010	1 X
Cellmatrix Type I-A	FUJIFILM Wako Chemicals Europe, Neuss, Germany	637-00653	3 mg/ml
Collagenase Type 4	Rockland antibodies & assies	MB-121-0100	
CryoStor CS10	Stemcell Technologies, Vancouver, Canada	07930	-
EDTA	VWR International, Radnor, USA	E177-100ML	0.5 M
EGF	Sigma-Aldrich, St. Louis, USA	SRP3027	50 ng/ml
Gibco® Advanced DMEM/F12	Thermo Fisher Scientific, Inc., Waltham, USA	12634010	-
Gibco® Ham's F12 Nutrient Mix powder	Thermo Fisher Scientific, Inc., Waltham, USA	21700018	10X
Gibco® GlutaMAX Supplement	Thermo Fisher Scientific, Inc., Waltham, USA	35050061	1X
Gibco® Pen Strep	Thermo Fisher Scientific, Inc., Waltham, USA	15140122	1%
Human Noggin Recombinant Protein	Thermo Fisher Scientific, Inc., Waltham, USA	PHC1506	25 ng/ml
IL-2	PeproTech, Hamburg, Germany	200-02	600 U/ml
***N*-Acetyl-Cysteine**	Acros Organics, Waltham, USA	160280250	1 mM
Nicotinamide	Sigma-Aldrich, St. Louis, USA	N0636	10 mM
Normocin™	InvivoGen, San Diego, USA	ant-nr-1	1X
Recombinant human (Leu15-)gastrin	Sigma-Aldrich, St. Louis, USA	G9145	10 nM
Roti®-CELL HEPES Solution	Carl Roth, Karlsruhe, Germany	9157.1	200 mM
SB-202190	PeproTech, Hamburg, Germany		10 µM
Sodium bicarbonate ($NaHCO_{3)}$	Sigma-Aldrich, St. Louis, USA	S-7277	11.76 g/l / 1.1 g/L
Sodium hydroxide solution (NaOH)	Merck, Darmstadt, Germany	1.09137.1000	0.05 N

2.2.2. Plasmid cloning			
2.2.2.1. Sub-cloning			
2.2.2.1.1. Double-digest of plasmids of interest			
pRK5-HA-Parkin	Addgene, Watertown, USA	17613	-
PEGFP-parkin C431S	Addgene, Watertown, USA	45877	-
pLVX-EF1α-IRES-mCherry	gift from Prof. Dr. Hubert Schorle, Institute of Pathology, Department for Developmental Biology, University Hospital Bonn, Germany	631987	-
FastDigest Buffer (10X)	Thermo Fisher Scientific, Inc., Waltham, USA	B64	1X
FastDigest BamHI	Thermo Fisher Scientific, Inc., Waltham, USA	FD0054	-
FastDigest EcoRI	Thermo Fisher Scientific, Inc., Waltham, USA	FD0274	-
UltraPure™ DNase/RNase-free Distilled Water	Invitrogen, Waltham, USA	10977-035	-
2.2.2.1.2. Agarose gel electrophoresis			
1 kb DNA Ladder	New England BioLabs, Ipswich, USA	N3232L	-
Agarose Standard	Carl Roth, Karlsruhe, Germany	3810.3	1.5%
Ethidium Bromide Solution	Sigma-Aldrich, St. Louis, USA	46067	0.5 µg/ml
Quick-Load® Purple 100bp DNA Ladder	New England BioLabs, Ipswich, USA	N0551G	-
TAE buffer	Merck, Darmstadt, Germany		1X
2.2.2.1.3. DNA extraction from agarose gel and PCR clean-up			
Nucleospin® Gel and PCR Clean-Up	Macherey-Nagel, Düren, Germany	740609.50	-
UltraPure™ DNase/RNase-free Distilled Water	Invitrogen, Waltham, USA	10977-035	-
2.2.1.4. Ligation			
T4 DNA Ligase Buffer (10X)	Thermo Fisher Scientific, Inc., Waltham, USA	B69	1X
T4 DNA Ligase (5 U/µl)	Thermo Fisher Scientific, Inc., Waltham, USA	EL0012	5 U

UltraPure™ DNase/RNase-free Distilled Water	Invitrogen, Waltham, USA	10977-035	-
2.2.2.2. Bacterial transfection			
Agar-Agar	Carl Roth, Karlsruhe, Germany	1347.3	16 mg/ml
Ampicillin	Carl Roth, Karlsruhe, Germany	HP62.1	100 µg/ml
Kanamycin	Carl Roth, Karlsruhe, Germany	T832.2	50 µg/ml
One Shot™ TOP10F' Chemically Competent *E. coli*	Thermo Fisher Scientific, Inc., Waltham, USA	C303003	-
Sodium Chloride (NaCl)	PanReac AppliChem, Darmstadt Germany	141659.1214	5 mg/ml / 25 mg/ml
Trypton/Pepton aus Casein	Carl Roth, Karlsruhe, Germany	6681.3	10 mg/ml
Yeast extract	Merck, Darmstadt, Germany	113885	5/25 mg/ml
2.2.2.3. Plasmid isolation			
2-Propanol	Carl Roth, Karlsruhe, Germany	6752.4	100%
Ampicillin	Carl Roth, Karlsruhe, Germany	HP62.1	100 µg/ml
Ethanol absolute	PanReac AppliChem, Darmstadt, Germany	A3678	70%
Kanamycin	Carl Roth, Karlsruhe, Germany	T832.2	50 µg/ml
NucleoBond® Xtra Midi/Maxi	Macherey Nagel, Düren Germany	740410.50	-
UltraPure™ DNase/RNase-free Distilled Water	Invitrogen, Waltham, USA	10977-035	-
2.2.2.4. Plasmid DNA sequencing			
UltraPure™ DNase/RNase-free Distilled Water	Invitrogen, Waltham, USA	10977-035	-
2.2.3. Lentiviral production and cell transduction			
2.2.3.1. Virus production			
Gibco® DMEM + GlutaMAX™ Medium	Thermo Fisher Scientific, Inc., Waltham, USA	31966-021	-
Polyethyenimine (PEI)	Merck, Darmstadt, Germany	919012	10.4 µg/ml
PMD2.G	gift from Prof. Dr. Hubert Schorle, Institute of Pathology, Department for Developmental Biology, University Hospital Bonn, Germany	-	5.2 µg/ml

Poly-L-Lysine	Sigma-Aldrich, St. Louis, USA	A-005-C	0.1%
psPAX2	gift from Prof. Dr. Hubert Schorle, Institute of Pathology, Department for Developmental Biology, University Hospital Bonn, Germany	-	10 µl/ml
2.2.3.3. Transduction of cells			
Gibco® DPBS	Thermo Fisher Scientific, Inc., Waltham, USA	14190-144	-
Polybrene	Santa Cruz Biotechnology, Dallas, USA	sc-134220	8 µg/ml
2.2.3.4. Cell sorting			
0.25% Trypsin-EDTA	Thermo Fisher Scientific, Inc., Waltham, USA	25200-056	-
Gibco® DPBS	Thermo Fisher Scientific, Inc., Waltham, USA	14190-144	-
Gibco® Fetal Bovine Serum	Thermo Fisher Scientific, Inc., Waltham, USA	10270-106	10%
2.2.4. RNA extraction			
DNase I	Thermo Fisher Scientific, Inc., Waltham, USA	EN0521	1 U
Ethanol absolute	PanReac AppliChem, Darmstadt, Germany	A3678	100%
UltraPure™ DNase/RNase-free Distilled Water	Invitrogen, Waltham, USA	10977-035	-
Universal RNA Kit	Roboklon	E3598-02	-
2.2.5. qPCR analysis			
2.2.5.1. cDNA synthesis			
5X First-Strand Buffer	Thermo Fisher Scientific, Inc., Waltham, USA	18064022	1X
dNTP Mix	Thermo Fisher Scientific, Inc., Waltham, USA	18427013	0.5 mM each
DTT	Thermo Fisher Scientific, Inc., Waltham, USA	18064022	100 mM
oligo(dT) primer	Thermo Fisher Scientific, Inc., Waltham, USA	18418020	25 ng/µl

RNaseOUT™ Recombinant Ribonuclease Inhibitor	Thermo Fisher Scientific, Inc., Waltham, USA	10777019	40 U
SuperScript™ II Reverse Transcriptase	Thermo Fisher Scientific, Inc., Waltham, USA	18064022	200 U
2.2.5.2. qPCR			
iTaq™ Universal SYBR Green Supermix	Bio-Rad Laboratories, Hercules, USA	1725121	1X
UltraPure™ DNase/RNase-free Distilled Water	Invitrogen, Waltham, USA	10977-035	-
2.2.6. Immunoblotting			
2.2.6.1. Protein harvesting			
Gibco® DPBS	Thermo Fisher Scientific, Inc., Waltham, USA	14190-144	-
RIPA	Sigma-Aldrich, St. Louis, USA	R-0278	-
Halt™ Protease & Phosphatase Inhibitor Cocktail	Thermo Fisher Scientific, Inc., Waltham, USA	78440	1X
2.2.6.2. Protein concentration determination			
Pierce™ BCA Protein Assay	Thermo Fisher Scientific, Inc., Waltham, USA	23225	-
2.2.6.3. SDS-PAGE			
4X Laemmli Sample Buffer	Bio-Rad Laboratories, Hercules, USA	1610747	1X
NuPAGE™ MES SDS Running Buffer (20X)	Thermo Fisher Scientific, Inc., Waltham, USA	NP000202	1X
BlueStar Prestained Protein Marker	NIPPON Genetics EUROPE GmbH, Düren, Germany	MWP03	-
RIPA	Sigma-Aldrich, St. Louis, USA	R-0278	-
2.2.6.4. Western Blotting			
Methanol	Carl Roth, Karlsruhe, Germany	4627.6	10%
NuPAGE™ Transfer Buffer (20X)	Thermo Fisher Scientific, Inc., Waltham, USA	NP00061	1X

2.2.6.5. Immunodetection			
β-Actin antibody	Santa Cruz Biotechnology, Dallas, USA	sc-47778, clone: C4	dilution: 1:500
Hydrochloric acid	PanReac AppliChem, Darmstadt Germany	A5634	-
m-IgGκ BP-HRP	Santa Cruz Biotechnology, Dallas, USA	sc-516102	dilution: 1:5,000
Nonfat dried milk powder	PanReac AppliChem, Darmstadt Germany	A0830	5%
Parkin antibody	Santa Cruz Biotechnology, Dallas, USA	sc-32282, clone: PRK8	dilution: 1:200
Sodium Chloride	PanReac AppliChem, Darmstadt Germany	141659.1214	88 mg/ml
SuperSignal™ West Pico PLUS Chemiluminescent Substrate	Thermo Fisher Scientific, Inc., Waltham, USA	34579	-
TRIS	Carl Roth, Karlsruhe, Germany	0188.3	24 mg/ml
Tween® 20	PanReac AppliChem, Darmstadt Germany	A4974	0.1%
2.2.6.6. Membrane stripping			
Acetic acid 100%	Carl Roth, Karlsruhe, Germany	6755.1	-
Glycin	Carl Roth, Karlsruhe, Germany	3187.3	15 mg/ml
Sodium Chloride (NaCl)	PanReac AppliChem, Darmstadt Germany	141659.1214	29 mg/ml
2.2.7. Flow cytometry			
2.2.7.1. Cell cycle analysis			
DAPI	PanReac AppliChem, Darmstadt Germany	A4099	1 mg/ml
Ethanol absolute	PanReac AppliChem, Darmstadt, Germany	A3678	70%
Gibco® DPBS	Thermo Fisher Scientific, Inc., Waltham, USA	14190-144	-
Triton X-100	Sigma-Aldrich, St. Louis, USA	T8787	
Trypan Blue solution	Sigma-Aldrich, St. Louis, USA	T8154	0.2%

2.2.7.2. Annexin V Apoptosis analysis			
Annexin V-FITC Apoptosis Staining/Detection Kit	Abcam, Cambridge, United Kingdom	ab14085	-
DAPI	PanReac AppliChem, Darmstadt Germany	A4099	0.1 µg/ml
Gibco® DPBS	Thermo Fisher Scientific, Inc., Waltham, USA	14190-144	-
2.2.8. RNA sequencing			
2.2.8.1. 3'mRNA sequencing			
QuantSeq 3' mRNA-Seq Library Prep Kit FWD	Lexogen, Vienna, Austria	-	-
2.2.9. Transwell Boyden Chamber assay			
DAPI	PanReac AppliChem, Darmstadt Germany	A4099	2 µg/ml
Gibco® DPBS	Thermo Fisher Scientific, Inc., Waltham, USA	14190-144	-
Gibco® Fetal Bovine Serum	Thermo Fisher Scientific, Inc., Waltham, USA	10270-106	0.2% / 10%
Matrigel® Basement Membrane Matrix	Corning, New York, USA	354234	0.25 mg/ml
Methanol	Carl Roth, Karlsruhe, Germany	4627.6	-
Trypan Blue solution	Sigma-Aldrich, St. Louis, USA	T8154	0.2%
2.2.10. Protein quantification using mass spectrometry			
2.2.10.1. Peptide preparation			
Acrylamide	Sigma-Aldrich, St. Louis, USA	A9099	40 mM
Acetonitrile	Sigma-Aldrich, St. Louis, USA	34851	70%
Urea	Qiagen, Hilden, Germany	1018602	8 M
CHAPS	Sigma-Aldrich, St. Louis, USA	C-5070	4%
DTT	Sigma-Aldrich, St. Louis, USA	DTT-RO	1% / 20 mM
Halt™ Protease & Phosphatase Inhibitor Cocktail	Thermo Fisher Scientific, Inc., Waltham, USA	78440	1X

Formic Acid	Sigma-Aldrich, St. Louis, USA	00940	0.1%
Sodium deoxycholate	Sigma-Aldrich, St. Louis, USA	S1827	0.5%
Tetraethylammonium bromide	Sigma-Aldrich, St. Louis, USA	140023	20 mM
TMT11plex reagents	Thermo Fisher Scientific, Inc., Waltham, USA	A37724	-
Trifluoroacetic acid	Sigma-Aldrich, St. Louis, USA	76-05-1	2%
Trypsin	Sigma-Aldrich, St. Louis, USA	T2600000	-
Urea	Qiagen, Hilden, Germany	1018602	8 M
2.2.10.2. Liquid chromatography-mass spectrometry (LC-MS) measurements			
Acetonitrile	Sigma-Aldrich, St. Louis, USA	34851	90%
Formic Acid	Sigma-Aldrich, St. Louis, USA	00940	0.1%
2.2.11. CKS2 small interfering RNA (siRNA) knockdown			
AllStars Negative control siRNA (5 nmol)	Qiagen, Hilden, Germany	1022076	100 pmol
FlexiTube GeneSolution siRNA (1 nmol) CKS2	Qiagen, Hilden, Germany	1027416	100 pmol
Gibco® Opti-MEM™	Thermo Fisher Scientific, Inc., Waltham, USA	31985062	-
2.2.12. Tissue microarrays (TMA)			
CC1 solution	Roche Diagnostics	05279801001	-
CKS2 antibody	Abcam, Cambridge, United Kingdom	ab155078, clone: EPR7946(2)	dilution: 1:75
Dako EnVision HRP labelled polymer anti-rabbit	Dako Denmark, Glostrup, Denmark	K4003	ready-to-use
Dako liquid DAB+ substrate chromogen system	Dako Denmark, Glostrup, Denmark	K3468	ready-to-use
Formalin	Carl Roth, Karlsruhe, Germany	P733.3	≥37%
Parkin antibody	Santa Cruz Biotechnology, Dallas, USA	sc-32282, clone: PRK8	dilution: 1:50

Xylol	VWR International	28973.328	≥98%
2.2.13. Embedding of ALI PDOs			
Formalin	Carl Roth, Karlsruhe, Germany	P733.3	≥37%
Gibco® DPBS	Thermo Fisher Scientific, Inc., Waltham, USA	14190-144	-
Richard-Allan Scientific HistoGel™	Thermo Fisher Scientific, Inc., Waltham, USA	HG-4000-012	-
2.2.14. Immunohistochemistry			
CA9	Abcam, Cambridge, United Kingdom	ab253660 clone: EPR23055-5	1:8,000
CC1 solution	Roche Diagnostics	05279801001	-
CD8	Agilent Technologies, Santa Clara, USA	GA62361-2 clone: C8/144B	1:50
Ethanol	Berkel AHK, Ludwigshafen, Germany	1642M	100% to 0%
Granzyme B	Leica, Wetzlar, Germany	GRAN-B-L-CE clone: 11F1	1:50
Leucocyte Common Antigen	Agilent Technologies, Santa Clara, USA	M070101-2 clone: 2B11+PD7/26	1:2,000
PAX8 antibody	Cell Marque, Rocklin, USA	363M-17 clone: MRQ-50	1:100
PD-L1 antibody	Cell Signaling Technology, Danvers, USA	13684S clone: E1L3N	1:50
Vimentin antibody	Agilent Technologies, Santa Clara, USA	M072501-2 clone: V9	1:5,000
Xylol	VWR International, Radnor, USA	28973.328	≥98%

2.1.4. Buffers and solutions

Buffer/solution	Recipe
DAPI/Triton X-100 solution	0.1% Triton X-100 in 15 ml PBS, add 15 µl of DAPI (1 mg/ml)
4X Laemmli Sample Buffer	100 µl β-mercaptoethanol in 900 µl 4X Laemmli Sample Buffer
LB agar	5 g Trypton/Pepton, 2.5 g yeast extract, 2.5 g sodium chloride, 8 g Agar-Agar, fill up to 500 ml with distilled water
LB medium (5X)	25 g Trypton/Peptone, 12.5 g yeast extract, 12.5 g NaCl, fill up to 500 ml with distilled water
NuPAGE™ MES SDS Running Buffer (1X)	50 ml NuPAGE™ SDS Running Buffer, 950 ml distilled water
NuPAGE™ Transfer Buffer (1X)	50 ml NuPAGE™ SDS Running Buffer, 100 ml methanol, 850 ml distilled water
Protein lysis buffer for mass spectrometry	8 M Urea, 4% CHAPS, 1% DTT, 1X Halt™ Protease & Phosphatase Inhibitor Cocktail
Reconstitution buffer	1.1 g $NaHCO_3$, 2 ml 1N NaOH, 10 ml HEPES in 38 ml distilled water
Stripping buffer	0.45 g Glycin, 0.87 g NaCl, dissolve in 25 ml distilled water, adjust pH to 2.8 with acetic acid, fill up to 30 ml
TBS	24 g TRIS, 88 g NaCl, dissolve in 900 ml distilled water, adjust pH to 7.6 with HCL, fill up to 1 l
Type I collagen solution with supplements	100 ml 10X Ham's F12, 100 ml reconstitution buffer, 800 ml Cellmatrix Type I-A

2.1.5. Media

Medium	Recipe
10X Ham's F12	106.26 g Ham's F12 Nutrient Mix, powder, 11.76g $NaHCO_3$, fill up to 1 l with distilled water
ADMEM/F12	25 ml Basic medium, 12.5 ml L-Wnt3A conditioned medium, 12.5 ml R-spondin 1 conditioned medium, 2 µl A83-01, 16.5 µl, SB-202190, 25 µl hEGF, 6.25 µl Human Noggin Recombinant Protein, 100 µl Normocin, 50 µl IL-2
Basic medium	500 ml ADMEM/F12, 5 ml Pen/Strep, 5 ml GlutaMAX supplement, 500 µl HEPES, 10 ml B27 supplement (without vitamin A), 100 mg *N*-Acetyl-Cysteine, 20 µl recombinant human (Leu15-)gastrin, 6 mg Nicotinamide
DMEM-GlutaMAX™ plus supplements	DMEM-GlutaMAX™, 10% FCS, 1% Pen Strep
Low serum medium	RPMI-1640, 0.2% FCS
RPMI-1640 plus supplements	RMPI-1640, 10% FCS, 1 % Pen Strep
SRM medium	DMEM/F12, 5% FBS, 1% Pen Strep, 10 ng/ml hrEGF, 10 ng/ml FGF-basic, 1X B27-supplement, 1X Lipid Mixture 1, 1mM *N*-Acetyl-Cysteine, 4 mM L-Glutamine, 1X Non-essential amino acids, 10 mM HEPES

2.1.6. Oligonucleotides

Gene	Sequence (5'→ 3')
2.2.2.4. Plasmid DNA sequencing	
EF1α forward	TCAAGCCTCAGACAGTGGTTC
IRES reverse	CCTCACATTGCCAAAAGACG
2.2.5.2. qPCR	
PARK2 forward	TAGCTTTGCACCTGATCGC
PARK2 reverse	CCACACAAGGCAGGGAGTAG
CKS2 forward	GCTCTTCGCGCTCTCGTTTCATTT
CKS2 reverse	CTCTGGGTAACATAACATGCCGGT
TBP forward	GCCGAATATAATCCCAAGCG
TBP reverse	TGGACTGTTCTTCACTCTTGGC
β-Actin forward	AGAGCTACGAGCTGCCTGAC
β-Actin reverse	AGCACTGTGTTGGCGTACAG
2.2.11. CKS2 small interfering RNA (siRNA) knockdown	
FlexiTube GeneSolution siRNA CKS2	AAGTTTGTATGTTGCATTTAA CTCAGTTAAATGCAACTGCAA TAGGTTACTGTAAGATGTTTA CTGTAAGATGTTTAAGATAAA

2.1.7 Software

Name	Purpose	Source
Adobe Illustrator CS2	vector based graphics software	www.adobe.com
ApE- A plasmid Editor	plasmid editor software	www.jorgensen.biology.utah.edu
BioRender	graphics software	www.biorender.com
CaseViewer	digital microscopy application	www.3dhistech.com
Fiji	image analysis software	www.imagej.net
FinchTV	chromatogram viewer, editor and analyzer	www.finchtv.software.informer.com
FlowJo™	flow-cytometry data analysis software	www.flowjo.com
GraphPad Prism	statistical analysis and figure creating software	www.graphpad.com
iTerm	terminal emulator for MacOS	www.iterm2.com
LibreOffice	word processing and editing software	www.libreoffice.org
R	statistical computing and graphics software	www.r-project.org
Sublime Text	text editor for code	www.sublimetext.com
Zotero	reference management software	www.zotero.org

2.2. Methods

2.2.1. Cell culture

2.2.1.1. Commercial cell lines

786-O (American Type Culture Collection (ATCC)) and RCC-MH (Cell Lines Service (CLS)) cells were maintained in Gibco® RPMI-1640 (Thermo Fisher Scientific, Inc.) and 293T (ATCC) cells were cultured in Gibco® DMEM-GlutaMAX™ (Thermo Fisher Scientific, Inc.). All media were supplemented with 10% Gibco® Fetal Bovine Serum (FBS) (Thermo Fisher Scientific, Inc.) and 1% Gibco® Pen Strep (Thermo Fisher Scientific, Inc.). 293T cells were maintained in Gibco® DMEM GlutaMAX™ (Thermo Fisher Scientific, Inc.) at 37 degree Celsius (°C) in a humidified incubator (5% CO_2, 95% humidity). Cells were ordered from the Global Bioresource Center ATCC and CLS. 786-O cells were authenticated by multiplex human cell line authentication test (MCA) (Multiplexion GmbH). Cells were regularly passaged and checked for mycoplasma contamination. They were passaged twice a week at a 1:15 ratio for 786-O and 293T and at a 1:3 ratio for RCC-MH cells.

Conditioned medium was produced by culturing L Wnt-3A cells (ATCC) in Gibco® DMEM-GlutaMAX™ (Thermo Fisher Scientific, Inc.) supplemented with 10% FBS (Thermo Fisher Scientific, Inc.) and 1% Gibco® Pen Strep (Thermo Fisher Scientific, Inc.). Cells were plated in 150 mm tissue culture dishes in 15 ml medium. After four days, the medium was removed and sterile filtered using Nalgene™ Rapid-Flow™ Sterile Single Use Vacuum Filter Units (0.2 µm) (Thermo Fisher Scientific, Inc.). New medium was added and the cells were cultured for three more days. Again, the medium was removed and sterile filtered and mixed 1:1 with the first batch from the fourth day. Conditioned medium was stored at 4°C short term or frozen and stored at -20°C long term.

R-Spondin 1-conditioned medium was produced by plating the cells in 150 mm culture dishes in Gibco® Advanced DMEM/F12 (Thermo Fisher Scientific, Inc.). The cells were then cultured for ten days. After ten days, the medium was collected, centrifuged at 3,000 rpm for 15 minutes (min) at 4°C and sterile filtered using Nalgene™ Rapid-Flow™ Sterile Single Use Vacuum Filter Units (0.2 µm) (Thermo Fisher Scientific, Inc.). Conditioned medium was stored at 4°C short term or -20°C long term.

2.2.1.2. Primary cells

Primary cells were cultivated as described before (Adrian Georg Simon et al. 2020; Esser et al. in press). In detail, a piece of the freshly resected tissue from patients undergoing partial or complete nephrectomy in the Department of Urology of the University Hospital Bonn, Germany, between October and December 2017, was obtained. The tumors were classified according to UICC 2017 and the tumor grade was determined according to ISUP 2016. After receiving the tissue, it was minced and digested at 37°C under constant shaking in pre-warmed Gibco® RPMI-1640 (Thermo Fisher Scientific, Inc.) containing 200 U/ml Collagenase type II (Thermo Fisher Scientific, Inc.), 100 U/ml Hyaluronidase Type V (Sigma-Aldrich) and 2% Pen Strep (Thermo Fisher Scientific, Inc.). After 2 hours (h), the digested cell suspension was filtered, the cells were washed with Gibco® Dulbecco's Balanced Salt Solution (DPBS) (Thermo Fisher Scientific, Inc.), centrifuged and plated in a specific serum-reduced medium (SRM) comprised of Gibco® DMEM/F12 medium (Thermo Fisher Scientific, Inc.) and multiple supplements, which are described in detail in **Table 2.5**.

2.2.1.3. ALI PDOs

ALI PDOs were cultivated as described before (Esser et al. 2020). Tissues from freshly resected tumor biopsies were cut thoroughly on ice, washed three times with Gibco® Advanced DMEM/F12 (ADMEM/F12) (Thermo Fisher Scientific, Inc.) containing 1X Normocin (InvivoGen). Subsequently, the minced tissue pieces were resuspended in 1 ml Cellmatrix Type I-A (FUJIFILM Wako Chemicals Europe) containing 10X Ham's F12 (Gibco® Ham's F-12 Nutrient Mix powder, Thermo Fisher Scientific, Inc.) and reconstitution buffer **(Table 2.4)** in a ratio of 8:1:1, respectively. Next, the fragment-collagen solution was added on top of a Millicell Cell Culture Insert (0.4 µm) (Millipore), which was previously coated with 1 ml of the mentioned collagen I solution containing 10X Ham's F12 and reconstitution buffer. The insert was placed into a regular 6-well plate and left to solidify for 30 min in a 37°C humidified incubator (5% CO_2, 95% humidity). After solidification, 1 ml of ADMEM/F12 supplemented with 50% L-Wnt3A and R-

Spondin 1 conditioned medium with 1 mM Roti®-CELL HEPES (Thermo Fisher Scientific, Inc.), 1X GlutaMAX Supplement (Thermo Fisher Scientific, Inc.), 10 mM Nicotinamide (Sigma-Aldrich), 1 mM *N*-Acetyl-Cysteine (Acros Organics), 1X B27 (without vitamin A) (Thermo Fisher Scientific, Inc.), 0,5 µM A83-01 (Sigma-Aldrich), 1X Pen Strep (Thermo Fisher Scientific, Inc.), 10 nM Gastrin (Sigma-Aldrich), 10 µM SB-202190 (PeproTech), 50 ng/ml EGF (Sigma-Aldrich), 25 ng/ml Human Noggin Recombinant Protein (Thermo Fisher Scientific, Inc.), 1X Normocin and 600 U/ml IL-2 (PeproTech) were added **(Table 2.5)**. Passaging of ALI PDOs was performed by adding 200 U/m1 Collagenase Type 4 (Rockland antibodies & assays) to the insert and incubating the insert for 30 min at 37°C until the collagen was dissociated. Next, three washing steps with DPBS (Thermo Fisher Scientific, Inc.) and EDTA (VWR International) were conducted to inhibit the activity of the Collagenase Type 4. ALI PDOs were taken up by 1 ml Type I collagen solution as described above and replated at desired mass density into new air-liquid interface collagen gels. Cryopreservation was performed by dissociating the Cellmatrix Type I-A as described above, washing with DPBS and resuspension in CryoStor CS10 (Stemcell Technologies) before being placed into a Corning® CoolCell™ LX Cell Freezing Container (Sigma-Aldrich) in a -80°C freezer. After one week the samples were transferred to liquid nitrogen tanks.

2.2.2. Plasmid cloning by sub-cloning

2.2.2.1. Double-digest of plasmids of interest

PARK2 and PARK2-C431S lentiviral plasmids were generated by sub-cloning the human PARK2 wild type (WT) gene (from plasmid pRK5-HA-Parkin; addgene #17613) or PARK2 harboring the C431S mutation (from pEGFP-parkin C431S; addgene #45877) into the restriction enzyme sites FastDigest EcoRI (Thermo Fisher Scientific, Inc.) and FastDigest BamHI (Thermo Fisher Scientific, Inc.) of plasmid pLVX-EF1α-IRES-mCherry (the plasmid was a gift from Prof. Dr. Hubert Schorle, Institute of Pathology, Department of Developmental Biology, University Hospital Bonn, Germany). For the double-digest the following reaction was set up:

Table 2.1| Set-up of the double-digest reaction.

Component	Input
DNA (1 µg/µl)	1 µl
10x Buffer	2 µl
each restriction enzyme	1 µl
UltraPure™ DNase/RNase-free Distilled Water	15 µl

The mixture was incubated for 15 min at 37°C and stopped by heat-inactivation at 80°C for 5 min.

2.2.2.2. Agarose gel electrophoresis

Next, the product fragments were separated on an agarose gel according to their sizes. 1.5 g Agarose Standard (Carl Roth) was dissolved in 100 ml 1x TAE buffer (Merck) and heated in a microwave until the agarose was dissolved. After 5 µl of Ethidium Bromide Solution (Sigma-Aldrich) were added, gels were poured into electrophoresis chambers and left to solidify at room temperature (RT). Next, samples were loaded into the lanes of the gel and the gel was run at 70 volt (V) for 30 to 60 min. 6 µl of 1kb DNA Ladder (New England BioLabs) or Quick-Load® Purple 100bp DNA Ladder (New England BioLabs) were used as a standard. Gels were imaged using Agarose gel imaging system GEL iX20 (Intas Science Imaging Instruments). In case, of DNA extraction from the gel Crosslinker Fluo-Link (Biometra) was used for imaging and it was ensured that UV exposure was minimized to avoid damage of the DNA.

2.2.2.3. DNA extraction from agarose gel and PCR clean-up

DNA extraction was done according to the Nucleospin® Gel and PCR Clean-up kit (Macherey-Nagel) according the manufacturer's protocol. The DNA fragment of interest was excised from the gel using a clean scalpel (Feather.) The excised sample was placed in a 1.5 ml tube and Buffer NTI was added to dissolve the remaining agarose gel. Sample was

placed into a NucleoSpin® Gel and PCR Clean-up column (Macherey-Nagel), centrifuged at 11,000 g for 30 seconds (s) and the flow-through was discarded. Next, the membrane was washed using Buffer NT3, centrifuged at 11,000 g for 30 s and subsequently dried by discarding the flow-through and centrifuging the sample once more at 11,000 g for 1 min. Lastly, the DNA was eluted using 20 µl UltraPure™ DNase/RNase-free Distilled Water (Invitrogen).

In case of PCR clean-up, the sample was directly added to Buffer NTI without previous gel separation and the steps of the protocol were followed as described before. DNA concentration was measured by NanoDrop™ 1000 (Peqlab) according to the manufacturer's recommendation. Purity was assessed by measuring the ratio of absorbance at 260 nanometer (nm) and 280 nm (A260/280) and at 260 nm and 230 nm (A260/230). A value of 1.8 for A260/280 was considered pure for DNA. A260/230 ratios between 2 to 2.2 were considered free of contamination.

2.2.2.4. Ligation

The cleaned-up DNA fragment was ligated into the cleaned-up plasmid by setting up the following reagents in a microcentrifuge tube on ice:

Table 2.2| Set-up of the ligation reaction.

Component	Input
T4 DNA Ligase Buffer (10X)	2 µl
Vector DNA (200 ng) (3:1)	1.87 µl
Insert DNA (103.8 ng)	0.77 µl
UltraPure™ DNase/RNase-free Distilled Water	14.36 µl
T4 DNA Ligase	1 µl

The reaction was gently mixed and briefly centrifuged. Next, it was incubated for 10 min at RT, heat-inactivated at 65°C for 10 min and chilled on ice.

2.2.2.5. Bacterial transformation

Bacterial transformation was conducted by thawing chemically competent *Escherichia coli (E. coli)* One Shot™ TOP10F' (Thermo Fisher Scientific, Inc.) bacteria on ice and, subsequently, 1 µl plasmid DNA was added to the competent bacterial cells and mixed carefully. Next, the mixture was incubated on ice for 30 min and heat-shocked for 45 s at 42 °C before being placed on ice for 3 min. 500 µl 1X lysogeny broth (LB)-media was added to the competent bacterial cells and incubated for 45 min at 37°C under vigorous shaking. 50 µl of the competent bacterial cell mixture were spread to LB-agar plates containing the appropriate selection antibiotic and incubated upside-down overnight (ON) at 37°C.

2.2.2.6. Plasmid isolation

Single colonies were picked and transferred to 1X LB medium containing the appropriate selection antibiotic. Next, the suspension was incubated at 37°C for 6-8 h (Mini Prep) or ON (Midi Prep) while shaking. The next day, plasmid DNA was extracted using the NucleoBond® Xtra Midi/Maxi Kit (Macherey-Nagel) according to the manufacturer's instructions. In short, bacterial cultures were centrifuged at 6,000 g for 15 min at 4°C. Afterwards, Buffer NEU was added and mixed until cultures turned colorless. Lysates were loaded on the NucleoBond® Xtra Column Filter and washed with Buffer EQU, followed by a washing step with Buffer WASH. Next, DNA was eluted and precipitated by addition of isopropanol, centrifuged at 15,000 g for 30 min at 4°C. Then 70% ethanol was added, centrifuged again at 15,000 g for 5 min at RT and air-dried. Lastly, the dried pellet was reconstituted with UltraPure™ DNase/RNase-free Distilled Water (Invitrogen) and the DNA concentration was determined using a NanoDrop™ 1000 (Peqlab) according to the manufacturer's recommendation.

2.2.2.7. Plasmid DNA sequencing

The isolated DNA was sequenced to confirm the correct gene sequence. Plasmid DNA was diluted with UltraPure™ DNase/RNase-free Distilled Water (Invitrogen) to achieve a concentration between 80-100 ng/µl. 5 µl of DNA were mixed with 5 µl of the corresponding sequencing primer (5 µM). Samples were sequenced by Sanger sequencing (GATC Services, Eurofins, Cologne, Germany) using EF1α forward and IRES reverse primers (**Table 2.6; Supplementary figure 8.1**). The sequenced DNA was viewed with Finch TV and aligned to the wild-type sequence of PARK2, which was retrieved from the National Center for Biotechnology Information (NCBI) (NCBI Resource Coordinators 2018), using the plasmid editor software, ApE.

2.2.3. Lentiviral production and cell transduction

2.2.3.1. Virus production

Lentiviral particles were produced by co-transfecting 293T cells (ATCC) with the lentiviral backbone plasmid of interest, the packaging plasmid psPAX2 and the envelope plasmid pMD2.G (the packaging and envelope plasmids were both gifts from Prof. Dr. Hubert Schorle, Institute of Pathology, Department for Developmental Biology, University Hospital Bonn, Germany). Before transfection, plates were coated with Poly-L-Lysine (Sigma-Aldrich) and 293T cells were plated. The next day, the following lentiviral target mix was set up:

Table 2.3| Set-up of the lentiviral target mix.

Component	Input per 6 well	Final concentration
Gibco® DMEM + GlutaMAX™ Medium (serum free)	26 µl	
pMD2.G (lentiviral helper plasmid)	126 ng	5.2 µg/ml
psPAX2 (lentiviral helper plasmid	272 ng	10.4 µg/ml
lentiviral target plasmid	544 ng	20.9 µg/ml

Next, 7.8 µl of polyethylenimine (PEI) (Merck) transfection reagent was added, vortexed and incubated for 10 min at RT. After the incubation, the transfection mixture was added directly to the cultured cells, the plate was gently shaken and returned to the incubator (37°C, 5% CO_2, 95% humidity).

2.2.3.2. Virus harvesting

48 h after transfection cells showed expression of mCherry and a rounder phenotype. For harvesting, media containing the viral supernatant was collected and passed through a 0.45 µm syringe filter (TPP Techno Plastic Products AG). Next, aliquots were prepared and stored at -80°C.

2.2.3.3. Transduction of cells

Cells, which were to be transduced, were plated at 60% confluency. The next day, the medium of the cells was replaced by medium containing 10% FBS (Thermo Fisher Scientific, Inc.) and 8 µg/ml polybrene (Santa Cruz Biotechnology) and one vial (100 µl) of thawed lentivirus was added. The cells were placed in the incubator (37°C, 5% CO_2, 95% humidity). 24 h later the medium was aspirated, cells were washed once with DPBS (Thermo Fisher Scientific, Inc.) and fresh medium was added. One day later, medium was aspirated again, cells were washed once more with DPBS (Thermo Fisher Scientific, Inc.) and fresh medium was added. After that, the cells were ready for further selection.

2.2.3.4. Cell sorting

After successful transduction, the positive clones were sorted for mCherry by fluorescence-activated cell sorting (FACS) and, subsequently, expanded. For that, cells were washed with DPBS (Thermo Fisher Scientific, Inc.) and trypsinized. 0.25% Trypsin (Thermo Fisher Scientific, Inc.) was inhibited by FBS (Thermo Fisher Scientific, Inc.) and cells were centrifuged at 1,500 g for 5 min at RT. Cells were washed once with DPBS (Thermo

Fisher Scientific, Inc.), spun down and resuspended in DPBS with 10% FBS before passing them through a Cell-Strainer Cap of a 5ml Falcon® Round-bottom Tube (Corning). Cells were placed on ice until being processed by the Flow Cytometry Core Facility of the University Hospital Bonn, Germany. Cell sorting was performed on a BD FACS Aria III.

2.2.4. RNA Extraction

RNA was extracted with the Universal RNA Kit (Roboklon) according to the manufacturer's instructions. In brief, cells were lysed in the dish, transferred to a homogenization spin-column and centrifuged at 11,000 g. 100% cold Ethanol was added, mixed, and the samples were applied to the RNA binding spin-column. Next, the column was washed three times with the washing buffer supplied by the manufacturer and an on-column DNase digestion step was performed in between the washing steps as recommended by the manufacturer. RNA was eluted by addition of UltraPure™ DNase/RNase-free Distilled Water (Invitrogen). The concentration was quantified by NanoDrop™ 1000 (Peqlab) and the quality was checked by observing the A260/280 ratio and the A260/230 ratio. A 260/280 ratio of 2 was considered pure for RNA. A 260/230 ratio ranging from 2 to 2.2 was considered to be free of contamination.

2.2.5. qPCR analysis

2.2.5.1. cDNA snythesis

The extracted RNA was reverse transcribed with SuperScript™ II Reverse Transcriptase (Thermo Fisher Scientific, Inc.) according to the manufacturer's instructions. The following components were mixed together:

Table 2.4| Set-up of the cDNA synthesis- first step.

Component	Input
dNTP Mix (10 mM each)	1 µl
oligo(dT) primer (500 µg/ml)	1 µl
RNA (1 µg/ µl)	1 µl
UltraPure™ DNase/RNase-free Distilled Water	9 µl

After mixing the components together, they were heated to 65°C for 5 min and quick chilled on ice. Next, the following components were added:

Table 2.5| Set-up of the cDNA synthesis- second step.

Component	Input
5X First Strand Buffer	4 µl
0.1 M DTT	2 µl
RnaseOUT (40 U/µl)	1 µl

Again, the components were mixed and, subsequently, incubated at 42°C for 2 min. Lastly, 200 U of SuperScript™ II Reverse Transcriptase were added, incubated at 42°C for 50 min and heat-inactivated at 70°C for 15 min.

2.2.5.2. qPCR

For quantitative PCR (qPCR) analysis, iTaq Universal SYBR Green Supermix (Bio-Rad Laboratories), target-specific primers and 5 ng of cDNA template were combined in a 384-well-plate in technical triplicates (**Table 2.13**). Before analysis, the plates were sealed with Axygen® CyclerSeal Sealing Film (Corning) and shortly spun-down.

Table 2.6| Set-up of the qPCR reaction mixture.

Component	Input
cDNA (5 ng)	1 µl
Primer forward (10 µM)	0.25 µl
Primer reverse (10 µM)	0.25 µl
iTaq Universal SYBR Green Supermix (2x)	5 µl
UltraPure™ DNase/RNase-free Distilled Water	3.5 µl

The samples were analyzed on a ViiA 7 Real-Time PCR system (Thermo Fisher Scientific, Inc.) using the following program:

Table 2.7| Conditions of the qPCR program.

Stage	Input
Hold stage	50°C, 2 min; 95°C, 10 min
PCR stage	(95°C, 15 s; 63°C, 2 s; 60°C, 1 min) x 40 cycles
Melt curve stage	95°C, 15 s; 60°C, 1 min; 95°C, 15 s

To ensure primer specificity and amplification of a single product, a melt curve analysis was included in the qPCR program. Data were normalized to the housekeeping genes TBP and β-actin according to the ΔΔCT method and differences between the genes were displayed relative to the control sample ($2^{-\Delta\Delta CT}$) (Livak and Schmittgen 2001). Control samples were either wild-type cells or non-malignant tissue. The primer sequences for the qPCR are listed in **2.1.6. Oligonucleotides**.

2.2.6. Immunoblotting

2.2.6.1. Protein harvesting

Cells were lysed directly in the cell culture dishes. First, cells were washed with ice-cold DPBS (Thermo Fisher Scientific, Inc.). Next, RIPA buffer (Sigma-Aldrich) supplemented with 1X Halt™ Protease & Phosphatase Inhibitor Cocktail (Thermo Fisher Scientific, Inc.) was added to the wells. Using a Cell Scraper (Sarstedt) the cell lysates were detached from the culture dishes, transferred to microcentrifuge tubes and kept on ice for 30 min. Next, centrifugation at 14,000 g for 20 min at 4 °C was performed. The supernatant was transferred to a new microcentrifuge tube and protein concentration was determined by the bicinchonic acid (BCA) Assay.

2.2.6.2. Protein concentration determination (BCA Assay)

Protein concentration was measured with the Pierce™ BCA Protein Assay Kit (Thermo Fisher Scientific, Inc.) according to the manufacturer's instructions for 96-well microplates. In short, a serial dilution of the standard ranging from 10 µg/µl to 0.625 µg/µl was prepared and 5 µl were pipetted into each well. 50 parts of BCA reagent A and 1 part of BCA reagent B were mixed and 102 µl were added to each well. The plate was incubated for 30 min at 37°C and the results were read-out.

2.2.6.3. SDS-PAGE

Protein separation was performed according to standard protocols. 20 to 30 µg of protein was separated on a NuPAGE™ 4 to 12% Bis-Tris gel (Thermo Fisher Scientific, Inc.). Proteins were diluted with RIPA buffer to obtain the desired concentration. Next, Laemmli Sample Buffer (Bio-Rad Laboratories) was added to each sample and the samples were denatured at 95°C for 5 min before loading. In order to verify the sizes of the proteins, 6 µl of BlueStar Prestained Protein Marker (NIPPON Genetics EUROPE GmbH) was used. NuPAGE™ MES SDS Running Buffer (20X) (Thermo Fisher Scientific, Inc.) was diluted to 1X and gels were run at 70 V for 15 to 20 min and at 120 V until the proteins were separated accordingly.

2.2.6.4. Western Blotting

After SDS-PAGE, proteins were transferred to a PVDF membrane. PVDF membranes were activated with methanol before use. For that, membranes were placed into methanol for 1 min at RT and, subsequently, placed into 1X NuPAGE™ Transfer Buffer (Thermo Fisher Scientific, Inc.) **(2.1.4. Buffers and solutions)**. Gel, PVDF membrane, sponges and Whatman™ Paper (GE Healthcare Life Sciences) were assembled into the transfer cassette according to the following order:

red side-sponge-2X Whatman paper-membrane-gel-2X Whatman paper-sponge-grey side

Bubbles between the gel and membrane were removed by applying pressure to the sandwich. The sandwich was placed in the Mini-PROTEAN® II Cell blotting chamber (Bio-Rad Laboratories) and proteins were blotted for 30 min to 1 h at 70 V. To avoid overheating of the proteins, the transfer chamber was placed into a box containing ice.

2.2.6.5. Immunodetection

Membranes were blocked with 5% nonfat dried milk powder (PanReac AppliChem) in TBS-T (Tris-buffered saline with 0.1% Tween® 20 (PanReac Applichem)) for 1 h at RT. Next, membranes were incubated with the desired primary antibody ON at 4°C on a rotator. The next day, the membranes were washed three times with TBS-T for 5 min at RT on a shaker and incubated with the appropriate horseradish peroxidase (HRP)-conjugated secondary antibody for 1 h at RT. Again, the membranes were washed with TBS-T (3×5 min) on a shaker at RT and developed with SuperSignal™ West Pico PLUS Chemiluminescent Substrate (Thermo Fisher Scientific, Inc.). For that, equal parts of the luminol/enhancer solution and the peroxide solution were mixed together, added to the membranes and incubated for 5 min at RT. The membranes were removed from the solution and excess reagent was drained. Chemiluminescent signals were detected using the Blot imaging System Chemi Doc MP (Bio-Rad Laboratories) and quantified using the open source image processing package Fiji (Schindelin et al. 2012).

The following antibodies were used for immunoblotting: Parkin (1:200, Santa Cruz Biotechnology, sc-32282, clone: PRK8); β-Actin (1:500, Santa Cruz Biotechnology, sc-47778, clone: C4); m-IgGk BP-HRP (1:5,000, Santa Cruz Biotechnology, sc-516102).

2.2.6.6. Membrane stripping

Due to similar sizes of the protein of interest and the loading control, primary and secondary antibodies needed to be removed by stripping the membrane. For that, the membrane was washed in TBS-T and incubated in Stripping Buffer **(2.1.4. Buffers and solutions)** for 1 h at RT on a shaker. After incubation, the membrane was blocked again and immunodetection was performed as described before **(2.2.6.5. Immunodetection)**.

2.2.7. Flow cytometry

2.2.7.1. Cell cycle analysis

To analyze the cell cycle, cells were harvested by washing with DPBS (Thermo Fisher Scientific, Inc.) and trypsinization. After centrifugation, cells were washed in DPBS (Thermo Fisher Scientific, Inc.) once more. Next, ice-cold 70% Ethanol absolute (PanReac AppliChem) was added dropwise to fix the cells. Afterwards, the cells were incubated at 4°C ON. The next day, cells were centrifuged and stained with DAPI/Triton X-100 solution (**2.1.4. Buffers and solutions**) and incubated for 20 min in the dark before being analyzed on a BD LSRFortessa™. Acquired data were analyzed using the FlowJo™ software.

2.2.7.2. Annexin V Apoptosis Assay

Annexin V staining was performed with the Annexin V-FITC Apoptosis Staining/Detection Kit (Abcam) according to the manufacturer's instructions. In short, cells were harvested and washed with DPBS (Thermo Fisher Scientific, Inc.). Next, they were counted; 1×10^5 cells were resuspended in 500 µl 1X Annexin V Binding Buffer and incubated with

Annexin V-FITC for 15 min at RT. In order to quantify dead cells, DAPI staining (0.1 µg/ml) was included in the Annexin-V FITC staining step. After staining, cells were analyzed on a BD LSRFortessa™ and data were analyzed using FlowJo™ software.

2.2.8. RNA sequencing

2.2.8.1. 3'mRNA sequencing

RNA was extracted as described above (**2.2.4. RNA Extraction)**. Library preparation was performed by the Next Generation Sequencing (NGS) Core Facility of the University Hospital Bonn, Germany, using the QuantSeq 3' mRNA-Seq Library Prep Kit FWD (Lexogen) according to the manufacturer's instructions. After library prepartion, the samples were analyzed by a HiSeq 2500 v4 sequencer (Illumina) in high output mode (1×50 bp single reads).

2.2.8.2. Data analysis

The obtained raw single-read sequencing results were processed as described before (Esser et al. 2020; in press). First, the sequences were mapped to the human genome (GRCh38) with hisat2-2.1.0 (Kim et al. 2019). Next, the mapped reads were processed using samtools (Li et al. 2009) and reads were quantified with the Subread package featureCounts (Liao, Smyth, and Shi 2014). Statistical analysis for the read counts was conducted with the Bioconductor software package DESeq2 (Michael Love 2017). For each group the differentially expressed genes were calculated with p-values by applying multiple testing corrections. False discovery rate (FDR) was calculated by the Bonferroni correction method and a FDR cutoff of 0.05 was accepted as significant. Next, LFC shrinkage was performed with the apeglm method (Zhu, Ibrahim, and Love 2019). The Principle Component Analysis (PCA) and Volcano plots were generated using the packages ggplot2 (Wickham 2016) and Enhanced Volcano (Blighe 2018). The differentially expressed genes were further analyzed using the Hallmark gene set collection (Molecular Signature Database, Broad Institute). A list with pre-ranked differentially expressed genes was called

into the Gene Set Enrichment Analysis (GSEA) software. Default settings were applied to analyze for enriched hallmark gene sets (Subramanian et al. 2005). The data sets used for this analysis can be found in the online repository Sequence Read Archive (SRA) under the following accession numbers: PRJNA758615 (data set for the first part of this thesis) and PRJNA634836 (data set for the second part of this thesis) (https://www.ncbi.nlm.nih.gov/sra).

2.2.9. Transwell Boyden Chamber migration and invasion assays

Cells were starved ON in low serum medium (0.2% FBS). The next day, cells were counted and 30,000 cells were plated in 200 µl low serum medium on top of a FluoroBlok™ insert (Corning). 600 µl of complete growth medium (10% FBS) was placed into the bottom part (**Figure 2.1 a**).

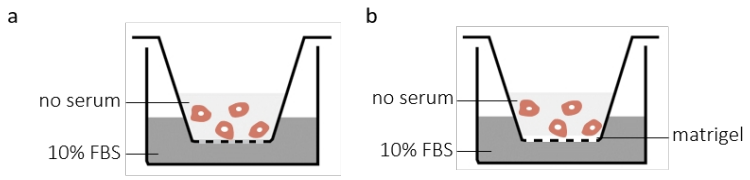

Figure 2.1| Set-up of the Transwell Boyden Chamber migration and invasion assay. (a) Cells are plated on top of a FluoroBlok™ insert in low serum medium. Complete growth medium is added in the lower chamber as an attractant for migration. (b) FluoroBlok™ (Corning) inserts are coated with Matrigel® Basement Membrane Matrix (Corning) before plating the cells in low serum medium and adding full growth medium as an attractant for invasion.

Cells were placed in an incubator (37°C, 5% CO_2, 95% humidity) for 16 h. After incubation, the medium was aspirated. The inserts were placed in 750 µl of 100% Methanol (Carl Roth) containing 1.5 µl DAPI (PanReac AppliChem) (1 mg/ml) and incubated for 15 min at RT. Next, the DAPI-methanol suspension was removed, washed twice with DPBS (Thermo Fisher Scientific, Inc.) and pictures were taken on an Olympus

BX50 fluorescence microscope (Olympus Corporation) (5 pictures per insert to cover the bulk of the migrated cells). For the invasion assay, the procedure was slightly changed by coating the inserts with 0.25 mg/ml Matrigel® Basement Membrane Matrix (Corning) before plating the cells (**Figure 2.1 b**). For that, the Matrigel® Basement Membrane Matrix (Corning) was applied to the insert and the cells were incubated for 3 h in an incubator (37°C, 5% CO_2, 95% humidity). Before plating the cells, the coated inserts were placed in the hood and left to dry. The cells were then incubated for 48 h and analyzed as described above for the migration assay.

2.2.10. Protein quantification using mass spectrometry

2.2.10.1. Peptide preparation

Protein was harvested from cells by adding the following buffer: 8 M Urea (Qiagen), 4% CHAPS (Sigma-Aldrich), 1% DTT (Sigma-Aldrich) and 1% Halt™ Protease & Phosphatase Inhibitor Cocktail (Thermo Fisher Scientific, Inc.). Cells were scraped, incubated on ice for 30 min and subsequently sonicated for 5 min at 30 s intervals. Afterward, samples were placed on ice for 5 min and centrifuged for 20 min at 13,000 g. Samples were given to the Mass Spectrometry Core Facility of the University Hospital Bonn, Germany, and processed as previously described (Esser et al. in press).

In detail, the obtained cell lysates were processed by in solution preparation on centrifugal filter units modified from published studies (León et al. 2013; Masuda, Tomita, and Ishihama 2008; Manza et al. 2005; Wiśniewski et al. 2009). 30 µg of protein were used for loading. Proteins were loaded onto centrifugal filter units with a 10 kDa cutoff modified polyethersulfone (PES) membrane (Pall Filtersystems GmbH) and reduced with 20 mM DTT at 55°C for 30 min. Thiol group alkylation was achieved by addition of 40 mM acrylamide for 30 min at RT. Buffer was exchanged and to a total volume of 50 µl, 250 ng trypsin (Sigma-Aldrich) were added in 20 mM triethylammonium bicarbonate (TEAB) (Sigma-Aldrich) with 0.5% sodium deoxycholate (SDC) (Sigma-Aldrich). Samples were digested for 10 h at 37°C. After collection of peptides (10,000xg for 5 min at RT), trifluoroacetic acid (2% final) (Sigma-Aldrich) was used to precipitate SDC. By applying

phase transfer with equal volume of ethyl acetate the remaining SDC was removed. After drying the peptides in a vacuum concentrator, they were again dissolved in 20 mM TEAB and isobaric TMT11plex reagents (Thermo Fisher Scientific, Inc., Inc.) were used for labeling. Peptides were redissolved and pooled and subsequently desalted on Oasis HLB cartridges (Waters GmbH). Next, the eluates containing 70% acetonitrile (Sigma-Aldrich) and 0.1% formic acid (Sigma-Aldrich) were dried. The eluates were then fractionated to twelve fractions by isoelectric point using an Offgel fractionator (Agilent Technologies). The fractionated peptides were dried before being stored at -20°C.

2.2.10.2. Liquid chromatography- mass spectrometry (LC-MS) measurements

Peptides were separated on a Dionex Ultimate 3000 RSLCnano HPLC system (Dionex GmbH) as previously described (Esser et al. in press). Operation of the autosampler was performed in µl-pickup mode and 0.1% formic acid (FA) (Sigma-Aldrich) (solvent A) was used to dissolve peptides before 1 µg (nominal) were injected onto a C18 analytical column (300 mm length, 75 µm inner diameter, ReproSil-Pur 120 C18-AQ, 1.9 µm (Dr. Maisch HPLC GmbH)). Next, separation of peptides was achieved by a linear gradient from 2 to 35% of solvent B, which consisted of 90% acetonitrile (Sigma-Aldrich) and 0.1% FA, within 120 min at 300 nanoliter per min. NanoHPLC and Orbitrap Fusion Lumos mass spectrometer (Thermo Fisher Scientific, Inc.) were coupled online and every 3 s peptide ions between 330 and 1,500 mass-to-charge ratio (m/z) were scanned in the Orbitrap detector with a resolution of 1.2×10^5 (maximum fill time 50 ms, automatic gain control target 4×10^5). As an internal calibration polysiloxane (445.12002 m/z) was used (typical mass error ≤1.5 parts per million). Next, to identify the peptides they were exposed to collision induced dissociation (CID) in a top-speed method (CID: 0.7 Dalton (Da) isolation, threshold intensity 5,000, normalized energy 35%). The fragments were then analyzed in the linear ion trap with target 1×10^4 and maximum fill time 35 ms, turbo mode and repeated analysis was excluded for 25 s for fragmented peptide ions. Lastly, to detect reporter ions in the Orbitrap analyzer (resolution 50,000, maximum fill time 86 ms, target 1×10^5) the top 8 fragment ions were chosen for synchronous precursor selection and fragmented with higher energy CID (1.4 Da isolation, 65% collision energy).

2.2.10.3. Proteomics data analysis

R environment (R version 4.0) (R Development Core Team 2021) was used for statistical analyses of the peptide-spectrum match (PSM) level data by means of an in-house developed workflow as described before (Esser et al. in press). One sample from 786-O^{PARK2} and 786-O was removed directly at the beginning because of extreme amount of missing values. The removed samples corresponded to tandem mass tag (TMT) channels 127N (786-O) and 128C (786-O^{PARK2}) **(Supplementary figure 8.2)**. Filtering was applied prior to statistical analysis for non-unique peptides and single-shot proteins, meaning that proteins which were identified or quantified by only one peptide were filtered out. Taking all available fractions into consideration, only the ones with the least number of missing values per PSM and across all TMT channels were chosen. If there was a case with more than one fraction available per PSM, the one with the highest average intensity across all channels was selected. After filtering was applied, the PSM-level data were variance-stabilized and transformed via the Bioconductor VSN package (Huber et al. 2002). Next, using the Tukey's median polish method the data were aggregated to protein-level abundances. Lastly, statistics were performed by the R package limma (Ritchie et al. 2015) and p-values were adjusted for multiple testing and FDR were calculated via the Benjamini-Hochberg method. Proteins with $|\log_2 FC| > 1$ were picked for further analysis.

2.2.11. CKS2 small interfering RNA (siRNA) knockdown

Cells were transfected with 100 pmol of FlexiTube GeneSolution siRNA CKS2 (sequences are noted in **2.1.6. Oligonucleotides**) or AllStars Negative Control siRNA (scramble) (Qiagen, proprietary sequence). For that Lipofectamine 2000 (Thermo Fisher Scientific, Inc.) and Gibco® Opti-MEM (Thermo Fisher Scientific, Inc.) were mixed together and incubated for 5 min at RT. After the incubation, it was added to the FlexiTube GeneSolution siRNA and incubated for 20 min at RT. Next, the mixture was carefully added to the cells. After 4 to 6 h the medium was replaced by regular growth medium. 24 to 48 h post-transfection further experiments were conducted.

2.2.12. Tissue microarrays (TMA)

TMAs were constructed as described before (Esser et al. in press).

After fixing ccRCC and non-neoplastic tissue in formalin (Carl Roth) and embedding it in paraffin, the material was used to construct the TMA. First, hematoxylin and eosin (HE) stained sections from tumor and non-malignant tissue were examined under a microscope and representative areas from each tissue were identified. Next, the selected areas were transferred from FFPE blocks to TMA blocks by punching two malignant and two non-malignant areas with a diameter of 1 mm for each case. Afterward, sections of 2 µm were cut from each TMA, mounted on Superfrost slides (Menzel Gläser). Before antigen-retrieval, slides were deparaffinized with xylol (VWR International) and gradually rehydrated in a series of decreasing ethanol concentrations. Antigen retrival was performed by placing the slides in cell conditioning 1 (CC1) solution (Roche Diagnostics; pH8) for 20 min. Staining of Parkin (1:50; Santa Cruz Biotechnology; clone: PRK8) was performed on a Ventana BenchMark Ultra Autostainer (Roche Diagnostics). For CKS2 (1:75; abcam; clone: EPR7946(2)), the staining was performed manually and incubated ON at 4°C. Detection occurred by incubation with an anti-rabbit secondary antibody (Dako Envision HRP labeled polymer; ready-to-use; Dako Denmark) and liquid diaminobenzidin (DAB)+ substrate chromogen system (Dako Denmark) was used for immunohistochemical staining. Counterstaining with HE was conducted for 30 s at RT before mounting the slides. Stainings were evaluated under an Olympus BX50 light microscope (Olympus Corporation) blind to clinical parameters such as clinical outcome, clinical and pathological stage. Intensities for the staining were graded for cytoplasmic and nuclear stainings of tumor cells or non-malignant cells. For intensities a 4-tier grading system was applied: 0: negative; 1: weakly positive; 2: moderately positive; 3: strongly positive. Parkin showed cytoplasmic staining and patients were separated into two groups based on their Parkin expression: cases with Parkin expression of grade 0 and 1 were considered for low Parkin expression and cases with grade 2 and 3 of Parkin expression were considered for high Parkin expression. CKS2 showed cytoplasmic and nuclear staining to similar degrees. These were also separated into two groups: low CKS2 expression (grade 1 and 2, similar to the non-malignant tissue) and high CKS2 expression (grade 3). Negative tumor cases were

not noticed. Staining intensities and grading system are displayed in **Supplementary figure 8.3**.

2.2.13. Embedding of ALI PDOs

In order to perform HE stainings of ALI PDOs, the ALI PDOs needed to be embedded first. For that, the grown ALI PDOs were removed from the Millicell Cell Culture Insert (Millipore) with the help of a disposable scalpel (Feather) and fixed in formalin (Carl Roth) for 30 min. Next, the fixed ALI PDOs were removed from formalin and three washing steps with DPBS (Thermo Fisher Scientific, Inc.) were performed. Meanwhile, Richard-Allan Scientific HistoGel™ (Thermo Fisher Scientific, Inc.) was liquified by heating to 65°C and cooling down to 55°C, which ensures that the gel solidifies more quickly after it is applied to the sample. The fixed ALI PDOs were placed in Tissue-Tek® Cryomold® (Sakura Finetek) and 1 ml liquified HistoGel™ was added. Samples were placed in the fridge at 4°C to solidify before being embedded in paraffin. HE staining was then performed according to standardized protocols of our routine laboratory.

2.2.14. Immunohistochemistry

IHC stainings were performed to standardized protocols of our routine laboratory. In detail, sections from FFPE blocks were cut and mounted to Superfrost slides (Menzel Gläser). Next, sections were deparaffinized with xylol (VWR International) and gradually rehydrated in descending concentrations of ethanol (Berkel AHK). Antigen retrieval was performed in CC1 solution (Roche Diagnostics) for 20 min at pH 8. Afterward, the slides were stained using an Autostainer 480S (Medac). The following antibodies were used for IHC: PAX8 (1:100; Cell Marque; clone: MRQ-50), vimentin (1:5,000; Agilent Technologies; clone: V9), PD-L1 (1:50; Cell Signaling Technology; clone: E1L3N), CA9 (1:8,000; Abcam; clone: EPR 23055-5), CD8 (1:50; Agilent Technologies; clone: C8/144B), Leucocyte Common Antigen (LCA) (1:2000; Agilent Technologies; clone: 2B11+PD7/26), Granzyme B (1:50; Leica; clone: 11F1).

2.2.15. Therapy testing

Therapy testing was performed as described before (Esser et al. 2020).
ALI PDOs were taken in culture and cultivated one week prior to treatment start. For each patient three inserts were used. One insert was treated with the TKI cabozantinib at at concentration of 2.5 µM, one insert with the ICI nivolumab at a concentration of 10 µg/ml and the third insert was kept as a control and only medium was changed. Every three days, the medium with the appropriate therapy was renewed. One week after beginning of the experiment, the ALI PDOs were embedded as described in **2.2.13** and stained with HE to visualize the degree of necrosis for analysis. In order to measure viable cells in contrast to the total area, slides were digitalized with a Mirax scanner (Zeiss), pictures of the digitalized scans were taken using the CaseViewer software and subsequently analyzed by Fiji (Schindelin et al. 2012). A 4-tier grading system was applied: for no necrotic tumor areas no response was indicated: "-", for up to 1/3 of necrotic tumor areas a weak response was indicated: "+", for up to 2/3 of necrotic tumor areas a moderate response was indicated: "++" and for more than 2/3 of necrotic tumor areas a strong response: "+++" was indicated.

2.2.16. Patient data

2.2.16.1. TMA

TMA from formalin-fixed paraffin embedded material from 241 patients who underwent partial or radical nephrectomy between 1992 to 2004 for renal tumors in the Department of Urology, Charité University Medicine Berlin, Germany, were included in the study (EA1/134/12). The studies were approved by the Ethics Committee of the University Hospital Bonn, Germany (EK 233/20). The mean age of the patients was 60.8 years ranging from 30-86 years and the median of the follow-up was 102.5 months ranging from 0-177 months. The remaining clinico-pathological characteristics of the patients are summarized in **Table 2.8.**

Table 2.8| Clinico-pathological data of patients included in the TMA. Table re-used from (Esser et al. in press).

Parameter	Number
Sex	
male	168
female	94
pT stage	
pT1	153
pT2	18
pT3	88
pT4	3
Grading	
G1	48
G2	144
G3	49
G4	21
Total	**n=262**

2.2.16.2. Primary cell cultures

Tissues for primary cell cultures were obtained from patients undergoing complete or partial nephrectomy in the Department of Urology, University Hospital Bonn, Germany, between October and December 2017. The Ethics Committee of the University Hospital Bonn, Germany, approved the cultivation and further analysis of the primary cells (EK 219/17) and all patients provided consent for use in future research. The mean age of the patients was 67 years ranging from 50-87 years. The remaining clinico-pathological characteristics are displayed in **Table 2.9**.

Table 2.9| Clinico-pathological data of patients from which the samples for the primary cell cultures were obtained. Table re-used from (Esser et al. 2020).

Parameter	Number
Sex	
male	4
female	3
pT stage	
pT1	4
pT2	3
Grading	
G1	1
G2	3
G3	3
Total	**n=7**

2.2.16.3. qPCR analysis of patients' mRNA levels

The material for the qPCR analysis was obtained from patients, which underwent complete or partial nephrectomy in the Department of Urology, University Hospital Bonn, Germany, between January 2008 and August 2016. The Ethics Committee of the University Hospital Bonn, Germany, approved the cultivation and further analysis of the primary cells (EK 219/17) and all patients provided written informed consent. The mean age of the patients was 65.41 years ranging from 42-85 years. The remaining clinico-pathological characteristics are displayed in **Table 2.10**.

Table 2.10| Clinico-pathological data of patients which were included in the qPCR analysis.

Parameter	Number
Sex	
male	40
female	23
pT stage	
pT1	36
pT2	6
pT3	21
Grading	
G1	5
G2	42
G3	15
G4	1
Total	**n=63**

2.2.16.4. ALI PDOs

Prior to tumor resection, the patients' consent was obtained from the patients undergoing surgery. Tumor tissue was obtained from treatment-naïve patients, who underwent partial or radical nephrectomy between 2019 and 2020 in the Department of Urology, University Hospital Bonn, Germany. The experiments were approved by the Ethics Committee of University Hospital Bonn, Germany (417/17 and 96/19). Tumor tissue was obtained from treatment-naïve patients, who underwent partial or radical nephrectomy between 2019 and 2020 in the Department of Urology, University Hospital Bonn, Germany. Pathological evaluation confirmed the malignancy of the samples. The clinico-pathological parameters for the patients of which tumor tissues were resected are displayed in **Figure 6.1** and **Supplementary table 8.7**.

2.2.17. Statistics

Data were analyzed using either GraphPad Prism version 8.2.0. or within the R environment version 4.0 (R Development Core Team 2021). To conduct statistical analysis for paired samples Wilcoxon test was performed in GraphPad Prism. Multiple comparisons were analyzed by Kruskal-Wallis test with Dunn's test as a post hoc analysis using GraphPad Prism.

The Kaplan Meier plots (followed by log-rank test), Cox proportional hazards regression model, and Pearson's and Spearman's correlation analysis were conducted and generated in the R environment using the packages survminer (Kassambara, Kosinski, and Biecek 2021), survival (Therneau 2020) and ggplot2 (Wickham 2016). Data are presented as mean ± SEM. A p-value of <0.05 was considered significant.

3. Results I

The underlying mechanism of Parkin downregulation and its accompanied effects on tumorigenesis in ccRCC remains unknown. As mentioned previously, the investigation *in vitro* in commercial ccRCC cell lines or primary cells is unfeasible due to the lack of Parkin expression. In addition, Parkin seems to be downregulated upon cultivation highlighting the potential advantage of Parkin deficient cells compared to cells which express Parkin. This, however, restricted the investigation of Parkin deficiency and its effect on malignancy in a patient derived setting. Thus, I overexpressed the Parkin gene, PARK2, in commercial cell lines in order to conduct functional assays and research possible interaction partners of Parkin in ccRCC.

3.1. PARK2 mRNA levels are decreased in tumor tissue and cultivated cells

Parkin is down-regulated in many cancers (J. Liu et al. 2018; Lee et al. 2018; Toma et al. 2013; Ni et al. 2017). In order to verify these findings in ccRCC, I analyzed PARK2 mRNA expression in 63 patients. Even though in some cases the Parkin gene, PARK2, was up-regulated in ccRCC tissue in contrast to non-malignant tissue, in most patients PARK2 was significantly down-regulated (**Figure 3.1 a**), which is in agreement with literature (Toma et al. 2013).

Unfortunately, most cell lines do not express Parkin, therefore, we cultivated seven ccRCC patient samples and established tumor primary cells (Adrian Georg Simon et al. 2020). We aimed to establish primary cells which show a similar Parkin expression as their corresponding tumor tissue. Ultimately, we measured the PARK2 mRNA levels in contrast to non-malignant tissue. In most patients PARK2 was down-regulated in the tumor tissue in contrast to non-malignant tissue as expected. Interestingly, cultivated primary cells showed lower expression of PARK2 (**Figure 3.1 b**) suggesting a selective pressure in favor of cells lacking Parkin. Thus, the cultivated primary cells are unfortunately limited in their use for thorough characterization of Parkin.

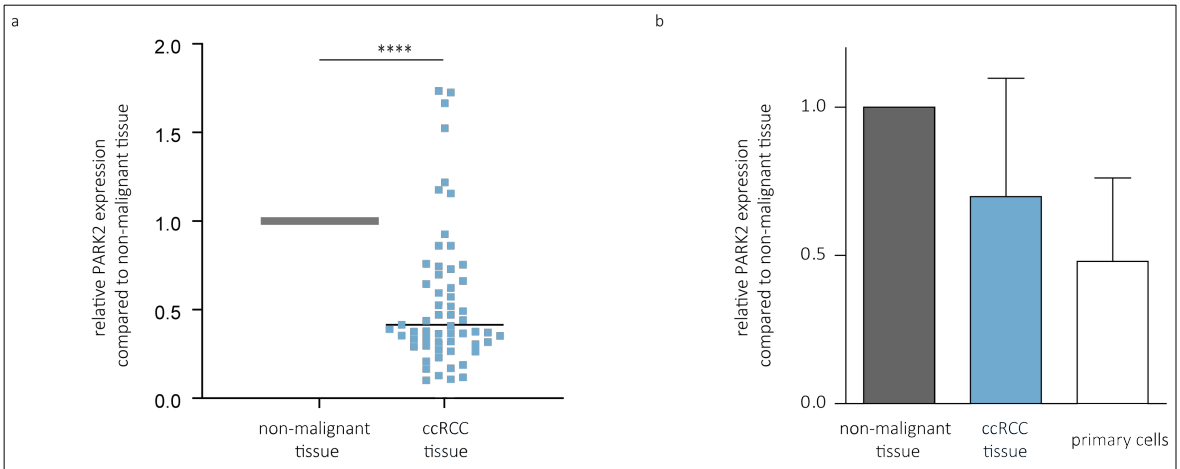

Figure 3.1| PARK2 mRNA is decreased in tumor tissue and cultivated cells. (a) qPCR analysis of PARK2 revealed lower PARK2 levels in tumor tissue of ccRCC patients compared to non-malignant tissue (n=63). Wilcoxon test was calculated; p**** <0.0001. **(b)** PARK2 mRNA levels in original tissue and primary cells were compared to non-malignant tissue by qPCR analysis. Tumor tissue showed decreased PARK2 mRNA levels compared to non-malignant tissue. PARK2 was reduced even more when cells were cultivated (n=7). Data are mean±SEM. Figure re-used from (Esser et al. in press).

3.2. PARK2 overexpression reduces migration and invasion *in vitro*

Commercial ccRCC cell lines and established primary cells do not express Parkin to a sufficient level, hence, I stably overexpressed PARK2 in the ccRCC cell lines 786-O (786-O^{PARK2}) via lentiviral transduction and subsequently selected them by flow cytometry. The Parkin gene, PARK2, was introduced into a pLVX-EF1α-IRES-mCherry vector (pLVX-EF1α-IRES-PARK2-mCherry) and transduced into 786-O cells (786-O^{PARK2}). As a control, I transduced the 786-O cells with only the empty vector (pLVX-EF1α-IRES-mCherry) (EV; 786-O^{EV}) as well (**Figure 3.2 a**). To validate the overexpression of PARK2 in the generated 786-O cells, I performed qPCR analyses. The results showed a significantly higher mRNA expression of PARK2 in 786-O^{PARK2} cells. The relative mRNA expression of 786-O^{PARK2} was more than 3000 higher compared to 786-O and 786-O^{EV} **(Figure 3.2 b)**. As expected, no difference was observed between 786-O and the control 786-O^{EV} (**Figure 3.2**

b). At times protein and mRNA levels are poorly correlated since mRNA expression differences are not always retained on the protein level (Edfors et al. 2016). Thus, I investigated the protein expression by immunoblotting. Immunodetection showed a clear signal in the transduced cells (786-O^{PARK2}) (**Figure 3.2 b**). The relative densities showed a strong increase of Parkin expression in 786-O^{PARK2} cells compared to WT. Again, no difference between WT and control was observed (**Figure 3.2 c**).

Parkin was reported to play a role in tumor progression and metastasis (Ni et al. 2017; J. Liu et al. 2017). However, for ccRCC no studies have been performed so far. Therefore, I conducted functional assays to observe the effect of Parkin expression on the phenotype. I investigated the cell cycle and apoptosis by flow cytometry as well as migrative and invasive capacities *in vitro* by the Transwell Boyden Chamber assay. While PARK2 overexpression had no effect on the cell cycle (**Supplementary figure 8.4 a**) nor apoptosis (**Supplementary figure 8.4 b**), differences in the migrative and invasive behavior were revealed between WT and PARK2 overexpressing cells. In contrast to 786-O and 786-O^{EV}, 786-O^{PARK2} cells showed a significant lower migration, which was reduced by more than 50% (**Figure 3.2 d**). Next, I examined the invasive capacity of the cells *in vitro* by coating the Transwell Boyden Chambers with matrigel, which imitates the extracellular matrix that tumor cells need to invade in order to colonize surrounding and foreign tissues. The overexpression of PARK2 reduced the cell's invasive behavior significantly. While I did not observe any difference between 786-O and 786-O^{EV}, 786-O^{PARK2} cells were significantly less invasive. Only 5% of cells with Parkin expression showed invasive behavior compared to more than 25% of cells lacking Parkin (**Figure 3.2 e)**. In order to find explanations for the phenotypic differences, I conducted 3' mRNA sequencing. However, the only significant differently expressed gene between 786-O or 786-O^{EV} and 786-O^{PARK2} was PARK2 (FDR<0.05, |log2FC| > 2) (**Supplementary figure 8.5, Supplementary table 8.1; Supplementary table 8.2**). Comparison of the transcriptomic profile of WT and control cells showed no difference **(Supplementary figure 8.5; Supplementary table 8.3)**. These findings indicate that PARK2 overexpression does not affect the transcriptomic profile of the cells, therefore, the reasons for the phenotypic observations remain unknown (Esser et al. in press).

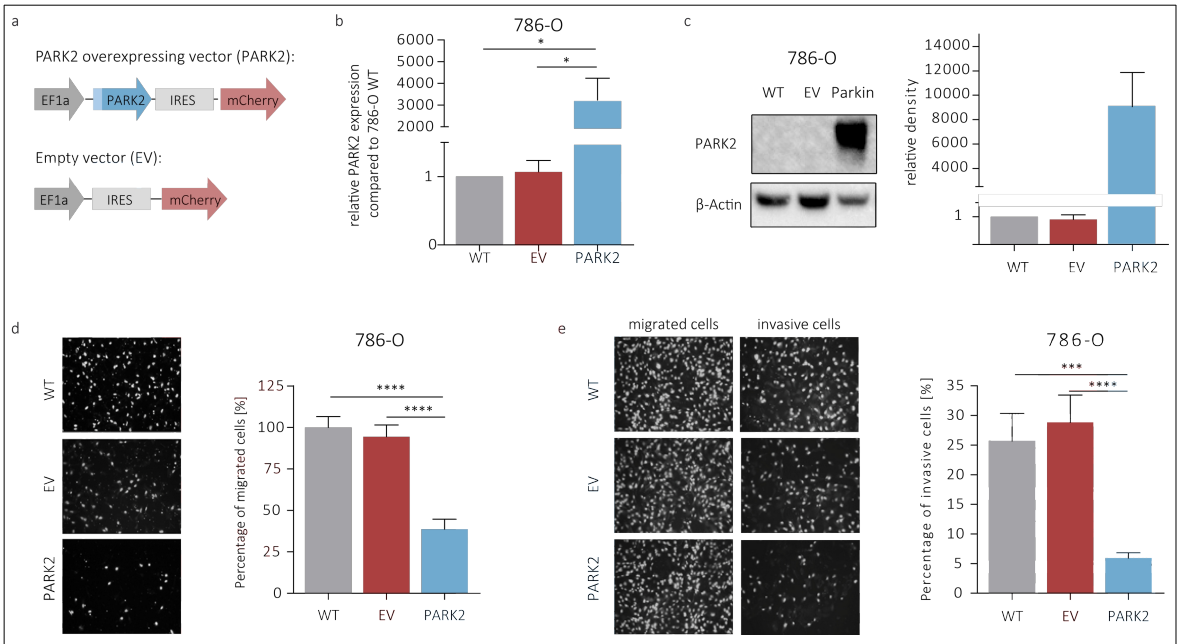

Figure 3.2| PARK2 overexpression reduces migration and invasion *in vitro*. (a) Cells were generated by transduction of a lentiviral vector with or without the gene of interest (PARK2) under an EF1α promoter and separated to mCherry by IRES. **(b)** PARK2 mRNA levels were assessed by qPCR analysis and indicated higher mRNA levels in transduced cells. The experiment was conducted in triplicates and TBP and β-Actin served as housekeeping genes. Kruskal-Wallis test was calculated with Dunn's test as a post hoc test; p* <0.05. **(c)** The protein levels of Parkin in the different cells was assessed by immunoblotting. β-Actin served as a loading control. Relative densities were measured in Fiji. **(d)** Transwell Boyden Chamber migration assays were performed to reveal differences in migration (n=3). Kruskal-Wallis test was calculated with Dunn's test as a post hoc test; p**** <0.0001. **(e)** Overexpression of the PARK2 gene caused a reduction in invasion compared to control cells (n=3). Kruskal-Wallis test was calculated with Dunn's test as a post hoc test; p**** <0.0001, p*** <0.001. Data are mean±SEM. Figure re-used from (Esser et al. in press).

3.3. LC-MS reveals low levels of CKS2 in the presence of Parkin

One of Parkin's best described roles is that it functions as an E3 ubiquitin ligase which specifically sequesters and marks proteins for degradation (Shimura et al. 2000). Therefore, LC-MS was performed to identify a potential shift in the proteome upon expression of Parkin. When comparing 786-O and the control 786-O^{EV}, 4 proteins with different protein levels (|log2FC| >1) were found, namely Histidine Rich Glycoprotein (HRG), Keratin 16 (KRT16), different Histone proteins such as Histone H2A type-c (HIST2H2AC), Histone H2A type 3 (H2AW), Histone H2A type 2-B (H2AC21) and Histone H2AX (H2AX) (**Supplementary table 8.4**). 43 proteins showed a different protein abundance when comparing WT and 786-O^{PARK2} cells (**Supplementary table 8.5**) and 38 between the control 786-O^{EV} and 786-O^{PARK2} (**Supplementary table 8.6; Figure 3.3 a**). Only two proteins, namely Ubiquitin-Conjugating Enzyme E2 Z (UBE2Z) and Oxysterol Binding Protein Like 10 (OSBPL10) showed significance with a FDR score lower than 0.05. Due to Parkin's role as a E3 ubiquitin ligase, I focused on proteins that were up-regulated in absence of Parkin which was the case for 29 proteins in both conditions (786-O and 786-O^{EV}). I further selected the proteins by investigating if they are considered unfavorable prognostic markers in ccRCC (Uhlen et al. 2017) (Human Protein Atlas accessed from http://www.proteinatlas.org) and if they have been linked to a migrative phenotype in the literature (N. Huang et al. 2019; J.-H. Xu, Wang, and Xu 2019; Yu et al. 2015). Among those proteins was CKS2, which is under the top 20 most up-regulated proteins in 786-O^{EV} cells compared to 786-O^{PARK2} **(Supplementary table 8.6)**. CKS2 showed no significance, however, its adjusted p-value was comparable to that of Parkin **(Figure 3.3 a)**. The profile plots display the relative abundance of the identified Parkin and CKS2 peptides presented for each replicate. While no difference in the protein abundance is observed in 786-O and 786-O^{EV} cells (mean abundance of approximately 4.5), Parkin abundance increased in cells that were transduced with the overexpressing plasmid (mean abundance of approximately 6.5) (**Figure 3.3 b**). When comparing CKS2 levels, no difference is observed between 786-O and 786-O^{EV} cells (mean abundance of approximately 6.5), while CKS2 levels decrease when Parkin is expressed (mean abundance approximately 5.5) (**Figure 3.3 c**).

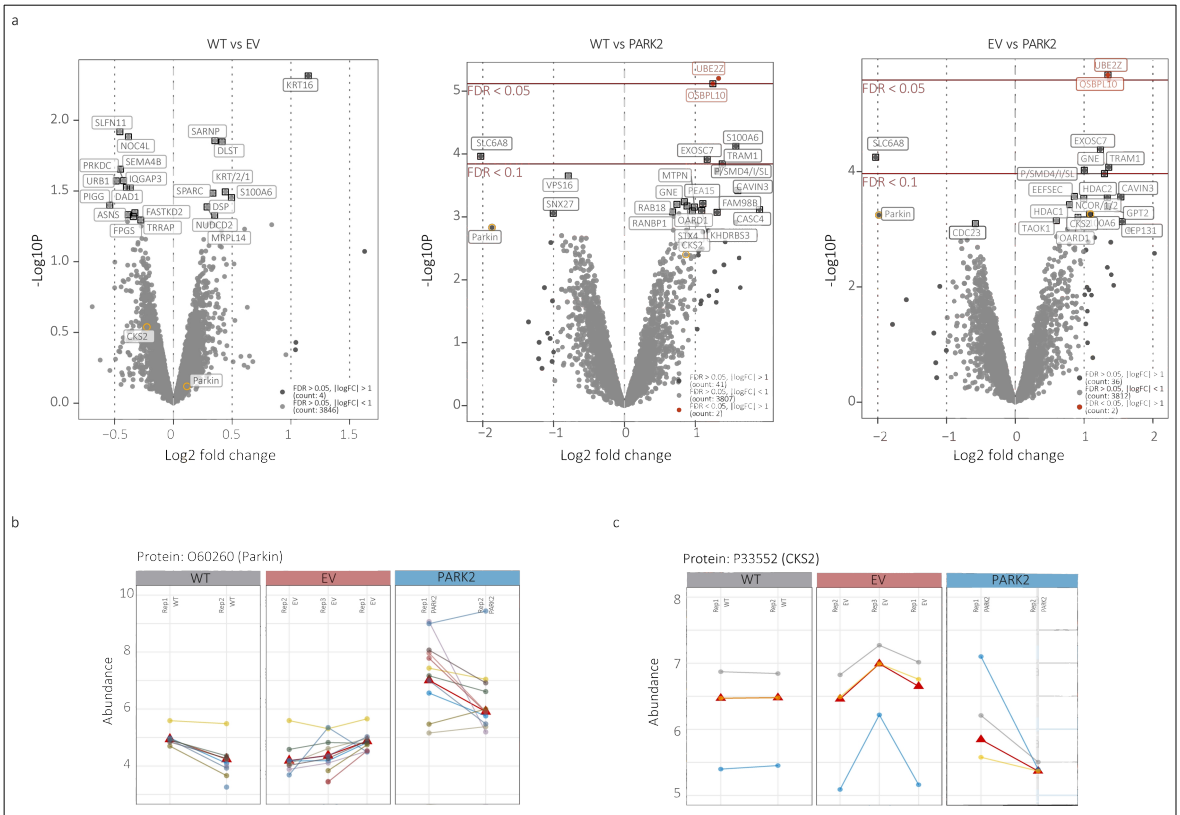

Figure 3.3| LC-MS reveals low levels of CKS2 in presence of Parkin. (a) Volcano plots illustrate the expression of the different proteins in the generated 786-O cells. While only slight differences in protein levels were observed for 786-O and 786-O^{EV} (|log2FC| > 1, count: 4), bigger differences could be noted when comparing 786-O (|log2FC| > 1, count: 43 (2 with FDR < 0.05)) or 786-O^{EV} (|log2FC| > 1, count: 38 (2 with FDR < 0.05)) with 786-O^{PARK2} cells. **(b)** Profile plots illustrate that the abundance of Parkin peptides was increased in 786-O^{PARK2}. **(c)** CKS2 peptide abundance was decreased in 786-O^{PARK2}. Figure re-used from (Esser et al. in press).

3.4. The migratory capacity is unchanged to wild-type cells when mutating PARK2's catalytic site, but decreased when silencing CKS2

Parkin is involved in several different cellular mechanisms (Bernardini, Lazarou, and Dewson 2017; Hongxia Wang et al. 2009; Riley et al. 2013; Singh et al. 2018). In order to investigate if CKS2 levels are altered due to Parkin's activity as an E3 ubiquitin ligase, I introduced a mutation in the catalytic site of Parkin. Mutating the putative cysteine to serine at amino acid 431 of Parkin has been reported to abolish Parkin's E3 ubiquitin ligase function (Wenzel et al. 2011). Cells were generated by transduction with lentiviral vectors containing the PARK2 C431S mutation (786-O^{C431S} and RCC-MH^{C431S}) (**Figure 3.4 a**). PARK2 and CKS2 mRNA levels were measured by qPCR and, as expected, PARK2 levels were higher in PARK2 overexpressed cells and cells harboring the C431S mutation (**Figure 3.4 b**). PARK2 mRNA expression was the highest in 786-O^{PARK2} cells. In 786-O^{C431S} the relative mRNA expression was more than 2000 higher compared to WT and control cells (786-O^{EV}) indicating that the transduction of these cells was successful as well. RCC-MH cells showed a comparable upregulation of PARK2 in cells being transduced with either the PARK2-plasmid or the C431S-plasmid. However, since I was interested in the E3 function of Parkin and its accompanied degradation of proteins, I checked if there are differences on the mRNA level of CKS2 which would have disproved my hypothesis. qPCR analysis of CKS2 revealed that the mRNA expression was not altered by introduction of PARK2 or the catalytic-mutant C431S (**Figure 3.4 c**). This shows that altered levels of Parkin have no effect on the gene expression of CKS2, which was revealed before by RNA sequencing results, too **(Supplementary table 8.1; Supplementary table 8.2)**. Furthermore, the defect of the catalytic site of Parkin and its accompanied loss of its E3 ligase function does not alter CKS2 expression on the mRNA level **(Figure 3.4 c)**.

To assess the effect of the C431S mutation in PARK2 on migration, I repeated the Transwell Boyden Chamber assay. In addition to 786-O^{PARK2}, I included RCC-MH cells, which have been transduced with the different plasmids (RCC-MH^{EV}, RCC-MH^{PARK2} and RCC-MH^{C431S}). As previously seen in 786-O^{PARK2} cells, RCC-MH cells showed a decrease

in migration when Parkin was expressed. Expression of the ligase deficient C431S mutation did not elicit an effect on cell migration in both cell lines (786-O and RCC-MH), hence, the cells showed no decrease in migration. In fact, the migrative capacity was comparable to the controls (**Figure 3.4 d**). This suggests that the E3 ligase activity of Parkin may be responsible for the decreased levels in migration. Since LC-MS revealed lower CKS2 protein levels upon overexpression of Parkin, I hypothesized that silencing of CKS2 by siRNA could cause similar effects. Thus, I knocked down CKS2 in WT and control cells **(Figure 3.4 e)**. Knockdown of CKS2 in cells lacking Parkin caused a similar migration level compared to 786-O^{PARK2} and RCC-MH^{PARK2} cells **(Figure 3.4 f; Figure 3.4 g)**. Silencing of CKS2 in 786-O^{PARK2} and RCC-MH^{PARK2} cells resulted in a decrease of migration compared to PARK2 overexpressed cells transfected with scramble siRNA, although this was not significant **(Figure 3.4 g)**. This suggests that CKS2 may not solely be regulated by Parkin, instead other signal cues may be responsible for the migrative behavior of the cells (Esser et al. in press).

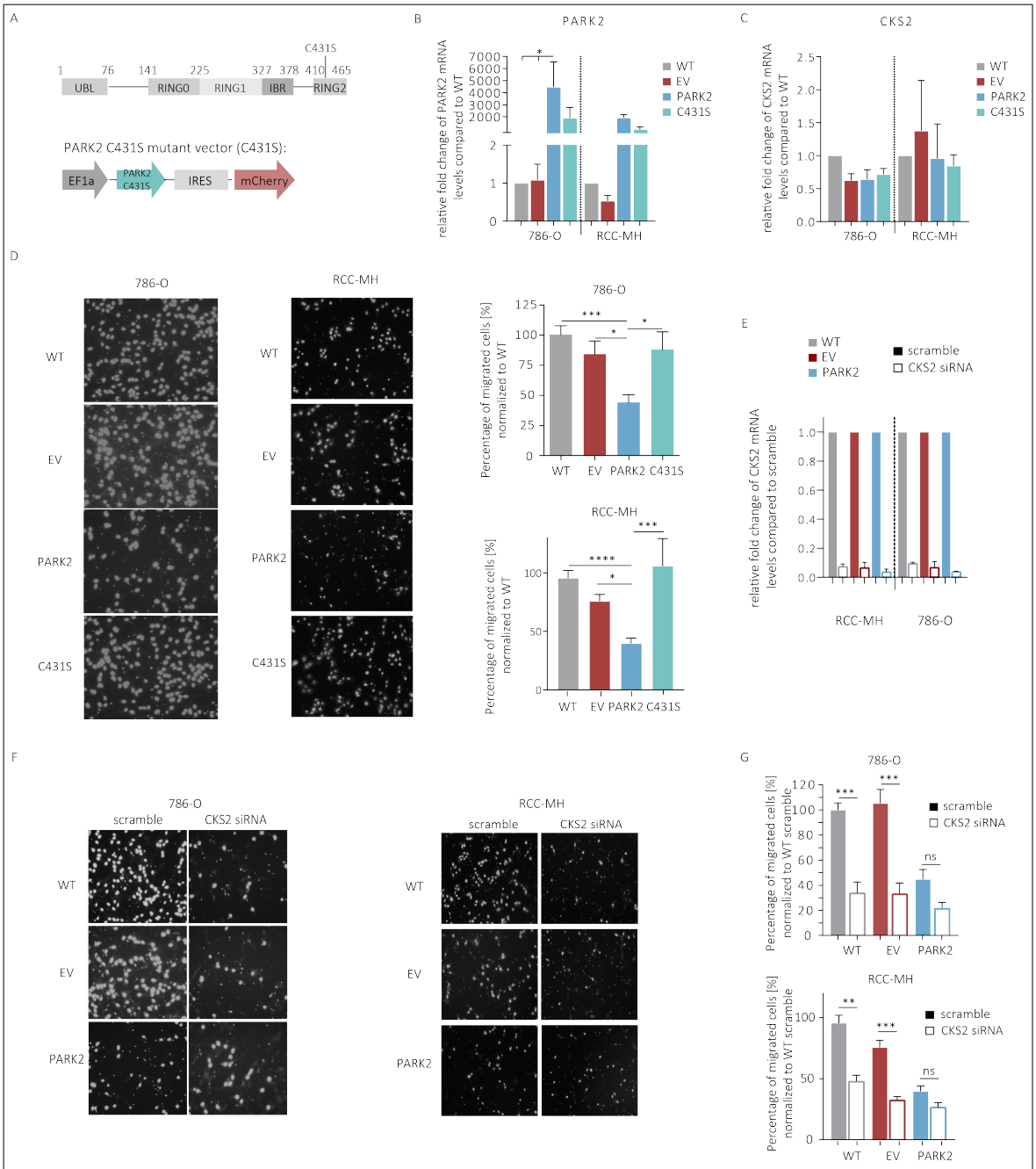

Figure 3.4| The migratory capacity is unchanged to wild-type cells when mutating PARK2's catalytic site, but decreased when silencing CKS2. (a) The PARK2 gene with the mutation in the catalytic site and the plasmid used for generating the PARK2 C431S mutant cells. **(b)** qPCR was performed to examine PARK2 levels. The experiment was conducted in triplicates and TBP and ß-Actin were used as housekeeping genes. Kruskal-Wallis test was calculated with Dunn's test as a post hoc test; p* <0.05. **(c)** qPCR analysis of CKS2 revealed no difference between the generated ccRCC cell lines. (Figure description continues on next page.)

Figure 3.4 (continued)| (d) Transwell Boyden Chamber migration assays were repeated, including the mutant ccRCC cell lines 786-O^{C431S} and RCC-MH^{C431S} (n=3). Kruskal-Wallis test was calculated with Dunn's test as post hoc test; p**** <0.0001, p*** <0.001, p* <0.05. **(e)** CKS2 levels were assessed after knockdown with siRNA. The experiment was conducted in triplicates. TBP and β-Actin served as housekeeping genes. **(f)** Pictures of the different cell lines after termination of the migration assay. Migrated cells were counted with Fiji. **(g)** Migrative capacity of the cells was assessed after knockdown of CKS2 (n=2). Significance was calculated by Kruskal-Wallis test and Dunn's test; p*** <0.001, p** <0.01, ns = not significant. Data are mean±SEM. Figure modified from (Esser et al. in press).

3.5. High CKS2 levels show association with poor survival and higher grading in patients

Since I demonstrated that CKS2 levels impact the migrative and invasive behavior, I was next interested in the effect of CKS2 levels on patient survival. For that a TMA with ccRCC samples of 262 patients was prepared to analyze the survival probability and correlation between different parameters (**Table 2.8**). Kaplan Meier curves indicated a significant better survival for patients with low CKS2 expression (p=0.001). The median survival for patients with high CKS2 expression was 40 months, whereas patients with low CKS2 expression did not reach median survival even after 150 months (**Figure 3.5 a**).

Patients with high levels of Parkin showed a tendency of better survival, yet, it was not significant (p=0.45) (**Figure 3.5 b**). Cox proportional hazards regression analysis revealed a highly significant better survival for patients with low CKS2 protein levels (p=0.0246), low grading (grade 1 or 2) (p=0.034), and low pT staging (stage 1 or 2) (p<0.001). Patients with high Parkin protein levels had a tendency towards better survival, yet this was not significant (p-value=0.652) (**Figure 3.5 c**). In order to analyze the statistic relationship between different parameters, namely CKS2, Parkin, and pT stage, I performed Pearson's correlation. CKS2 and pT showed a tendency towards a positive correlation (r=0.077), however, no significance was observed (p-value=0.224). A significant weak negative

correlation between Parkin and pT could be observed (r=-0.126, p-value=0.046) (**Figure 3.5 d**). Grading and CKS2 levels were analyzed by Spearman's correlation analysis and correlated weakly positive with a rho of 0.159 and a p-value of 0.0124 **(Figure 3.5 e)**. Grading and Parkin expression showed no correlation (rho=-0.064; p-value=0.315) **(Figure 3.5 e)**. Pearson's correlation analysis between Parkin and CKS2 showed no correlation (r=0.063, p-value=0.309) (**Figure 3.5 f**).

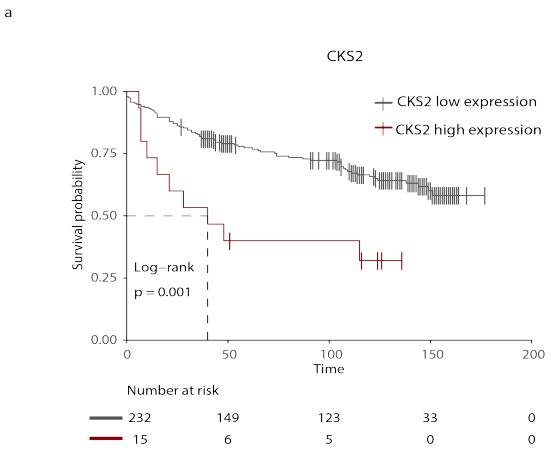

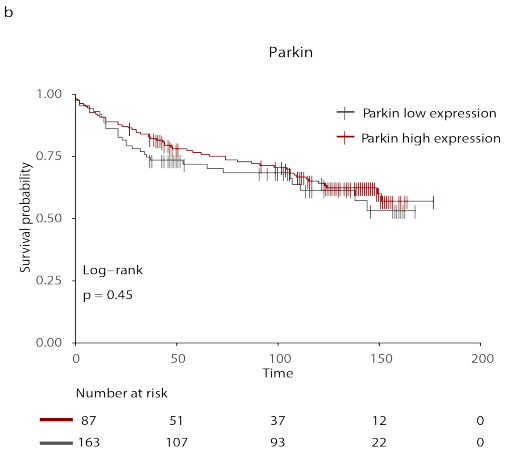

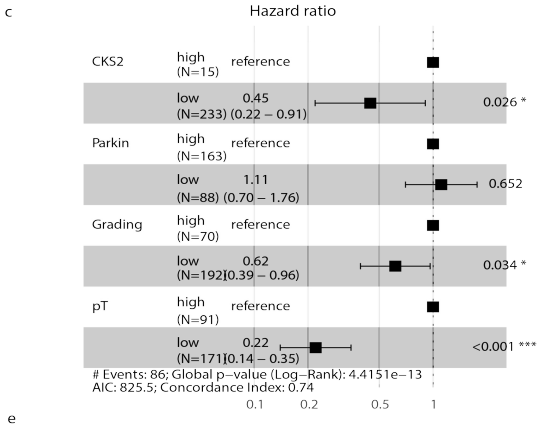

d

CKS2		
pT	Pearson's r	0.07748843
	p-value	0.224
	95% CI	-0.04753756, 0.20012387
	t-stat	1.219
	df	246
Parkin		
pT	Pearson's r	-0.1259917
	p-value	**0.04614**
	95% CI	-0.245973676, -0.002206968
	t-stat	-2.0041
	df	249

e

CKS2		
Grading	Spearman's rho	0.1586622
	p-value	**0.01235**
Parkin		
Grading	Spearman's rho	-0.06371953
	p-value	0.3147

f

Parkin		
CKS2	Pearson's r	0.06341729
	p-value	0.3093
	95% CI	-0.05892689
	t-stat	1.0187
	df	257

Figure 3.5| High CKS2 levels show association with poor survival and higher grading in patients. (a) Kaplan Meier curves represent the survival probability of CKS2 expression levels for different time points in months. Patients with high CKS2 levels show decreased survival. Significance was assessed with log-rank test (p=0.001). Number at risk indicates the number of patients which are still alive at given time point (n=247). **(b)** Kaplan Meier curve of Parkin levels shows a tendency for better survival for patients with high Parkin levels, yet it is not significant (log-rank test: p=0.45) (n=250). **(c)** Cox proportional hazard ratio indicates the association between survival and different parameters, namely CKS2 expression, Parkin expression, grading, and pT. (Figure description continues on next page.)

Figure 3.5 (continued)| (d) Pearson's correlation analysis depict relationship between CKS2 and pT as well as between Parkin and pT. Table includes Pearson's r, significance (p-value), 95% confidence interval (CI), t-statistic (t-stat), and degree of freedom (df). **(e)** Spearman's correlation of CKS2 or Parkin and grading is shown in the table depicted in the figure. **(f)** The table shows Pearson's correlation of CKS2 and Parkin including Pearson's r, p-value, 95% CI, t-statistic, and df. Figure re-used from (Esser et al. 2021).

4. Results II

Organoids have recently emerged as a great tool for cancer research. In addition to addressing questions in basic research, their potential for translational applications shows great promise to advance treatment options towards more personalized cancer therapies. Nevertheless, therapy testing in organoids is restricted by the lack of microenvironmental factors. Co-cultivation of organoids with exogenous immune cells can only recapitulate the patient's complex situation to a certain point. Thus, many therapies which were successful in *in vitro* studies failed in the clinical setting. This challenges novel approaches in patient-derived model systems. Therefore, I aimed to establish and characterize ALI PDOs which were derived from ccRCC tissues (Esser et al. 2020).

4.1. Establishment of a patient-derived kidney tumor ALI PDO biobank

Neal and colleagues established a protocol which describes the cultivation of PDOs in an ALI system that maintains the complex structure of the tissue of origin (Neal et al. 2018). To obtain ALI PDOs, the tumor tissue is resected from the patient. Next, it is fragmented into small pieces and the tissue pieces are reconstituted in a collagen I matrix which is plated on top of an insert, that has previously been coated with the same collagen I matrix. The insert is then placed into a culture plate and submerged in a special culture medium containing several additives and growth factors **(Figure 4.1 a)**.

Based on this protocol, I established 42 ALI PDOs which were derived from different renal tumors that have been surgically resected before. In this study, I included the most common subtypes of RCC, namely ccRCC and pRCC. 26 out of 42 samples were confirmed as ccRCC, five as pRCC. In addition, eight upper urinary tract urothelial carcinomas were confirmed and included, because at times they occur in the renal pelvis. Lastly, three oncocytomas were taken into culture **(Figure 4.1 b; Supplementary table 8.7)**. Overall, the success rate of ALI PDO establishment from tumor tissue was 72%. For ccRCC tissues, 77% (20/26) were successfully taken into culture and I was able to establish ALI PDOs, which could be passaged and cultivated for more than 30 days. 80% (4/5) of the pRCCs were successfully cultivated as ALI PDOs and 88% (7/8) of the upper

urinary tract urothelial carcioma. In addition, ALI PDOs of one of the three oncocytomas, which is a benign renal tumor, were effectively established. Unfortunately, I failed to cultivate the single case of the chRCC, a rare RCC subtype. The clinico-pathological characteristics of the patients from which the ccRCC tumors were resected are shown in **figure 4.1 c**. The tissues were obtained from 20 male and six female patients with an age range of 33 to 87 years. Furthermore, 18 of the tumors were organ-confined (T1-T2) and the remaining eight were non-organ-confined (T3-T4). Most of the tumors were graded as G2 (13 tumors), whereas the others were equally distributed between G1, G3 and G4, namely five as G1, five as G3 and three as G4 **(Figure 4.1 c)**.

Microscopically, the majority of the ALI PDOs appear as roundish, dense structures **(Figure 4.1 d)**, and only a small amount showed cystic organoid structures. Size and form of the ALI PDOs vary as well as the expansion rates. Generally, ALI PDOs were passaged every three to four weeks in a splitting ratio of 1:3. Cryopreservation and recovery of the ALI PDOs was possible as described by Neal and colleagues (Neal et al. 2018).

After successful establishment and analysis of the growth characteristics, I sought to further characterize the ccRCC ALI PDOs, which make up the majority of the cultivated cases. Further characterization included histological staining and RNA sequencing to validate the ALI PDOs as a suitable platform for studying personalized cancer therapy (Esser et al. 2020).

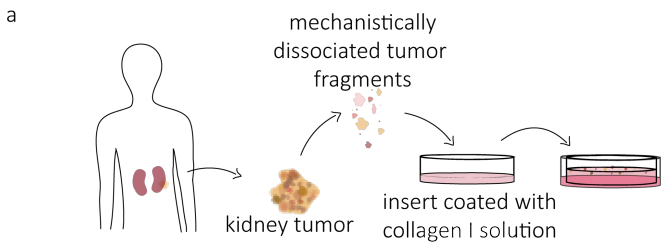

c

ccRCC	number
sex	
m	20
f	6
T stage	
organ-confined (T1-T2)	18
non-organ-confined (T3-T4)	8
grading	
G1	5
G2	13
G3	5
G4	3

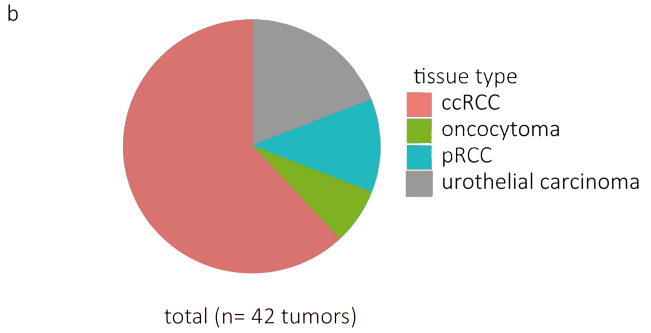

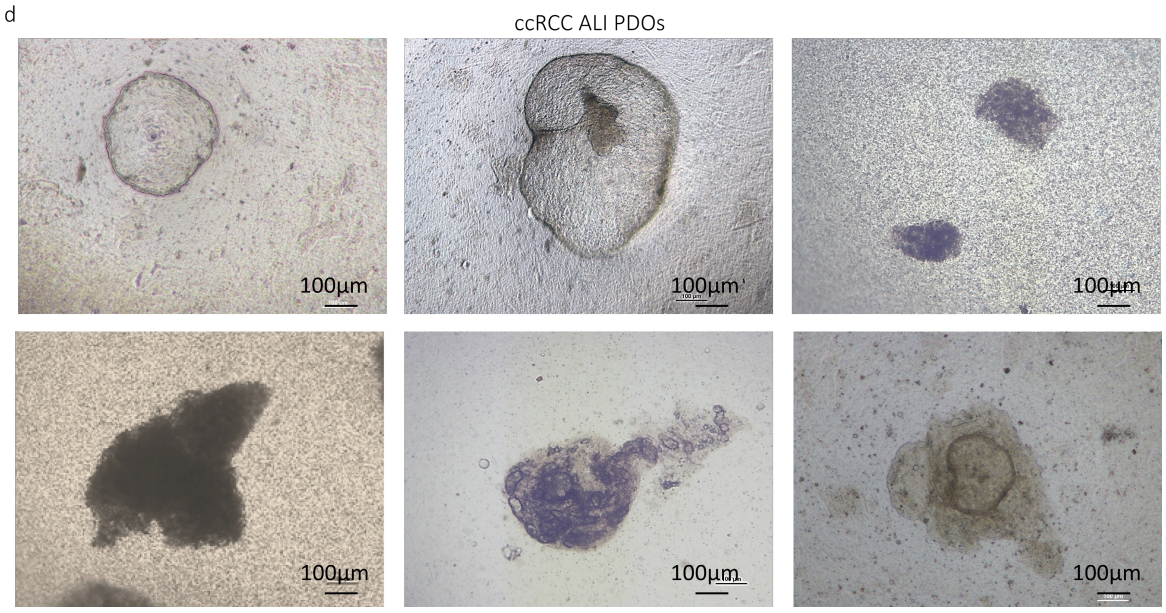

Figure 4.1| Establishment of a patient-derived kidney tumor ALI PDO biobank. (a) Resected tumor tissue was cultivated by mechanistic fragmentation and subsequent uptake in a collagen I solution. Ultimately, the fragmented kidney tissue was plated in a previously coated insert, placed in a cell culture dish and submerged in a special culture medium. **(b)** 42 kidney tissue types were cultivated, including 26 ccRCCs, five pRCCs, eight urothelial carcinomas and three oncocytomas. **(c)** Clinico-pathological characteristics of the cultured ccRCC ALI PDOs, including sex, T stage and grading. **(d)** Pictures of the cultivated kidney PDOs taken at 5X with a light microscope. Figure re-used from (Esser et al. 2020).

4.2. Kidney tumor ALI PDOs resemble tumor of origin histologically

After successfully cultivating the tumor tissues *in vitro*, I next wondered if the histology of the ALI PDOs resembles that of the original tumor. In order to verify the similarity between the tumor of origin and the established ALI PDOs IHC stainings were performed which can give conclusions about the typical histological characteristics. HE staining revealed that the tumor histology of the ALI PDOs resembled the complex histological structure of the tissue of origin in ccRCC, pRCC and also urothelial carcinoma. ccRCC cultures showed the typical nests of epithelial cells with clear cytoplasm and distinct cell membrane. Although the vascular tissue was missing, as expected. pRCC ALI PDOs resembled the tumor of origin with its characteristic single layer of cells with basophilic cytoplasm. Urothelial carcinoma ALI PDOs showed papillary features similar to the tumor tissue they were derived from **(Figure 4.2)**. The growth pattern of the ALI PDOs was solid in the majority of the cases **(Figure 4.2)**. In two cases, the ALI PDOs showed a cystic phenotype (Esser et al. 2020).

After successful validation of the histological characteristics, I was eager to find out if common tissue markers are still present in the ALI PDOs and, therefore, add validation to this novel model system.

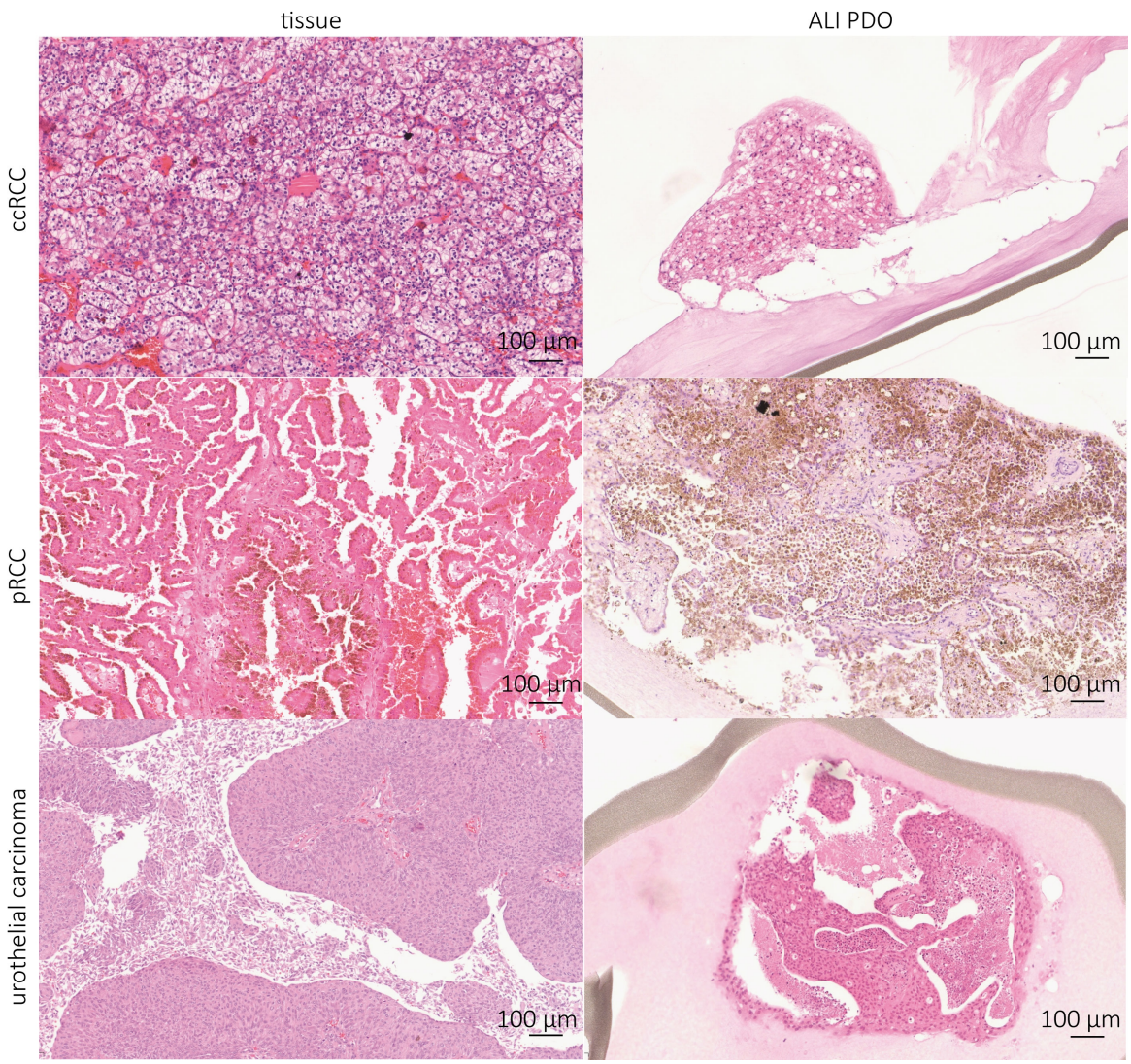

Figure 4.2| Kidney tumor ALI PDOs resemble tumor of origin histologically. IHC stainings were prepared to compare ALI PDOs with their derived tumor tissue. ccRCC, pRCC and urothelial carcinoma ALI PDOs showed the same tissue characteristics as their matched tissues. Pictures were taken at 10X magnification. Figure re-used from (Esser et al. 2020).

For that, further IHC analyses were performed. ccRCC ALI PDOs showed positivity for paired box 8 (PAX8), a marker of renal epithelial origin, additionally, verifying the resemblance of the cultured samples and the tissue of origin. Carbonic anhydrase 9 (CA9) is a characteristic marker for ccRCC. The established ALI PDOs showed positive staining for CA9. Moreover, ALI PDOs were analyzed for vimentin in order to verify the presence

of stromal cells. The staining showed a strong positivity of the cultivated tissues for vimentin. Next, I was intrigued to find out if immune cells are retained in the ALI PDOs. LCA is a marker of leucocytes. One huge advantage of the ALI PDOs towards regular organoids is the additional retention of the microenvironment including immune cells (Neal et al. 2018). IHC of LCA staining revealed positive cells proving the presence of immune cells **(Figure 4.3)**. These results provide evidence that the complex tissue architecture, phenotype and cellular composition of the primary tumors were maintained (Esser et al. 2020).

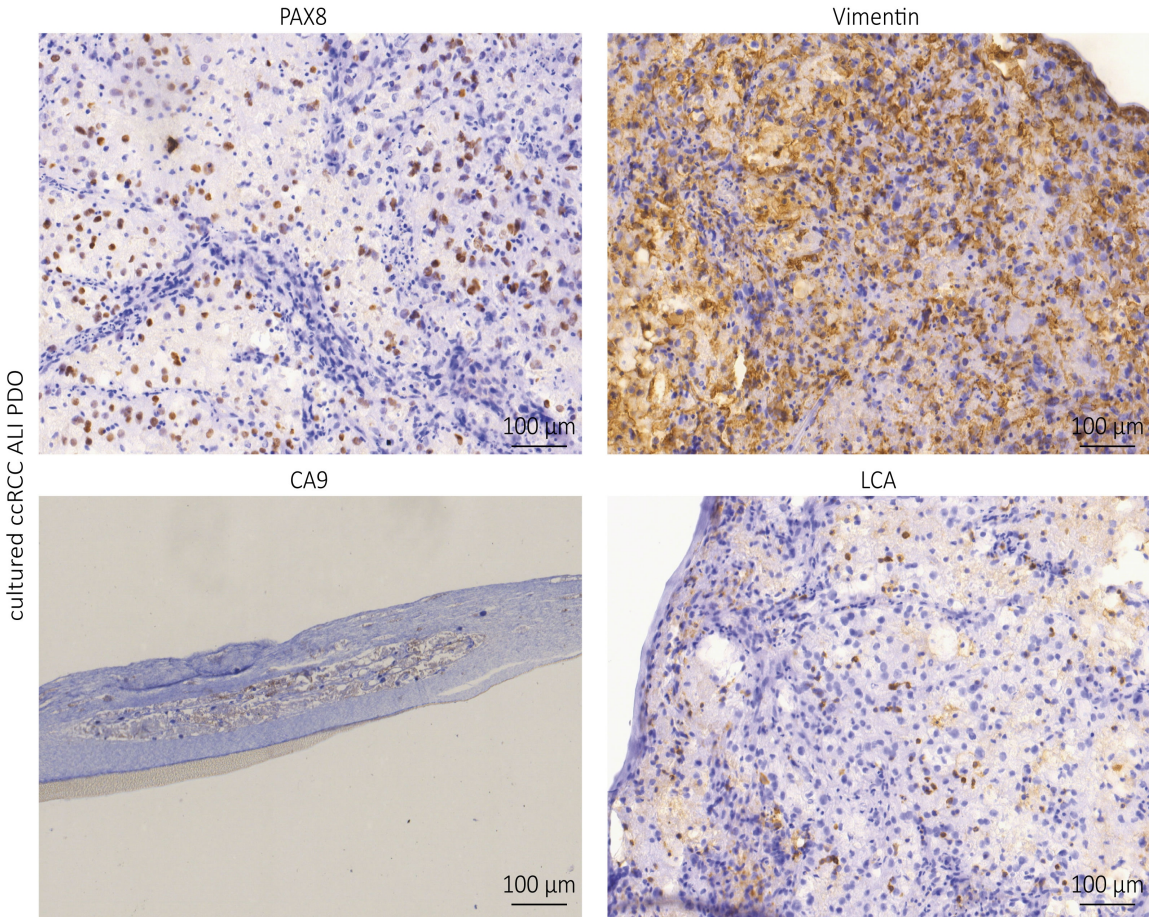

Figure 4.3| Immunohistochemistry staining of cultured ccRCC ALI PDOs. ALI PDOs show positivity for PAX8, Vimentin, CA9 and LCA. Pictures were taken at 20X magnification. Figure re-used from (Esser et al. 2020).

4.3. Examination of immune cells and immune checkpoint proteins validates ALI PDOs as a suitable model

As of now treatment options for ccRCC are surgery, TKI and ICI. Although, some patients show great responses towards those therapies, others do not respond at all (Rini, Campbell, and Escudier 2009; Motzer et al. 2018; 2019). Thus, I wondered if the presence of the immune checkpoint proteins programmed death protein 1 (PD-1) and programmed death ligand 1 (PD-L1) in the tumors of origin can give hints about therapy responses towards ICI. In order to answer that questions, IHC of PD-1 and PD-L1 were performed and positive cells were manually counted under a light microscope. While the expression of PD-1 ranged from 0 to 80% on the immune cells, the expression of PD-L1 on the tumor cells ranged from 0 to 5%. In five cases, the immune cells in the primary tumors showed PD-1 staining. Three of them showed less than 10% PD-1 staining on the immune cells and the remaining two showed positivity in 20% (ALI PDO 9) and 80% (ALI PDO8) of the immune cells. However, all tumor cells in the original tissues were absent of PD-L1, except for two. 1% of immune cells in ALI PDO 7 and 5% of tumor cells in ALI PDO 9 expressed PD-L1 **(Table 4.1)**. Next, the presence of CD8-positive cytotoxic T cells was examined **(Table 4.1)**. The presence of cytotoxic T cells in the tumor tissue varied substantially. While one primary tissue contained more than 100 CD8+ cells per high power field (HPF) (ALI PDO 9), the remaining tissues showed a range from 2 to 90 CD8+ T cells per HPF **(Table 4.1)**. Next, the original tissues were analyzed for the cytotoxic immune cell marker granzyme B **(Table 4.1)**. The majority of the primary tissues was negative for granzyme B, but in three tumor tissues individual cells stained positive for this marker, which could indicate the presence of cytotoxic active CD8+ T cells **(Table 4.1)**. To confirm if CD8 and granzyme B staining is preserved in the ALI PDOs, IHC stainings were performed and showed positivity for the markers of interest **(Figure 4.4)**. These results proof the presence of cytotoxic immune cells in ALI PDOs, which implies that the ALI PDOs are a proper tool for testing ICI targeting the PD-1/PD-L1 axis (Esser et al. 2020).

Table 4.1| Primary tissues from which the ALI PDOs were derived from were stained and examined for CD8, granzyme B, PD-1 and PD-L1 positivity to draw conclusions on therapy response. Table modified from (Esser et al. 2020).

ALI PDO (primary tumor tissue)	**CD8**	**Granzyme B**	**PD-1**	**PD-L1**
1	80/HPF	negative	5% immune cells	negative
2	35/HPF	individual cells	3% immune cells	negative
4	25/HPF	negative	negative	negative
5	20/HPF	negative	negative	negative
7	90/HPF	individual cells	5% immune cells	1% immune cells
8	70/HPF	individual cells	80% immune cells	negative
9	>100/HPF	negative	20% immune cells	5% tumor cells
10	2/HPF	negative	negative	negative

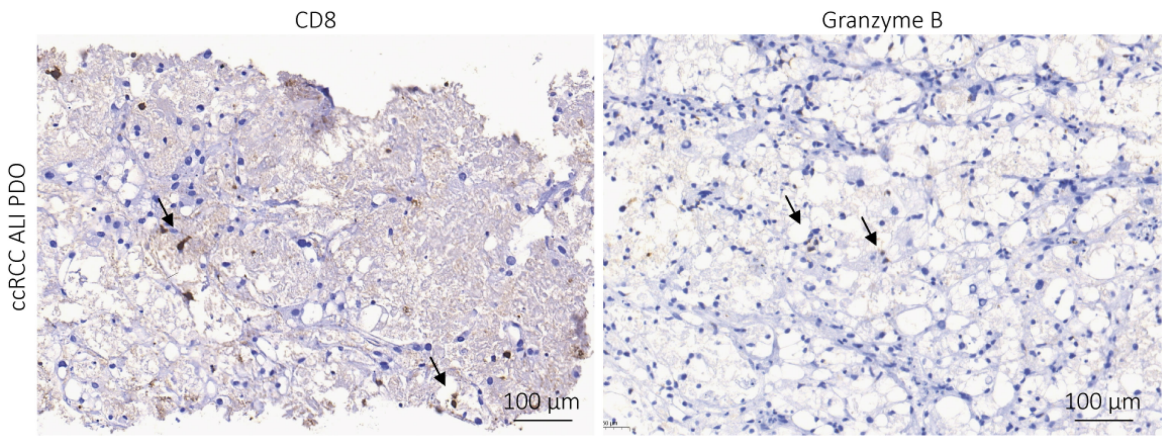

Figure 4.4| Immune cells are preserved in ALI PDOs. IHC stainings of CD8 and granzyme B of the ALI PDOs was performed to validate the presence of immune cells. Asterisks indicate positive stained cells. Pictures were taken at 20X magnification. Figure re-used from (Esser et al. 2020).

4.4. RNA sequencing demonstrates close molecular relationship of ALI PDOs and tissue of origin

After verifying the similarity of the histological structures and the presence of immune cell subtypes, I was eager to investigate the molecular profiles of the ALI PDOs in contrast to their matching tumors. Thus, isolated total RNA from the cultured ALI PDOs was analyzed by 3' mRNA sequencing. Analysis revealed that only 418 genes with a FDR<0.05 and | log2FC(2)| were differently expressed when comparing the ALI PDOs to their matched tumors. Out of these 418 genes, 161 genes were up-regulated and 257 were down-regulated. First, I wanted to visualize the samples' close relationship of their genetic profiles. This was achieved by performing PCA. The PCA shows that the different ALI PDOs and the tumors of origin cluster together, respectively. Furthermore, the genetic profiles of ccRCC and pRCC subtypes are in close proximity **(Figure 4.5 a)**. To illustrate the differently expressed genes in more detail, a volcano plot was generated **(Figure 4.5 b)**. When exploring the down-regulated genes in the ALI PDOs, it was found that hemoglobin genes which are expressed in blood cells are strongly down-regulated. The hemoglobin genes, namely hemoglobin subunit beta (HBB) and hemoglobin subunit alpha (HBA),

were highlighted in the volcano plot **(Figure 4.5 b)**. This finding was no surprise since the ALI PDOs lack vascularization and, thus, no blood circulation occurs. Therefore, irrespective of these findings, the genetic profiles did not vary to a high degree which supports the close molecular similarity of the generated ALI PDOs and their matched tumors (Esser et al. 2020). Next, I used the Hallmark gene set collection (Molecular Signature Database, Broad Institute) and analyzed the differently expressed genes via GSEA. GSEA revealed an up-regulation of 5 gene sets (FDR<0.05) **(Supplementary table 8.8)** and a down-regulation of 4 gene sets (FDR<0.05) (**Supplementary table 8.9)**. The five up-regulated gene sets with FDR<0.05 were: Allograft rejection, MTORC1 signaling, ROS pathway, MYC targets V1 and complement. The four down-regulated gene sets with FDR<0.05 were: KRAS signaling down, WNT beta catenin signaling, pancreas beta cells, and hedgehog signaling. In the top 20 up-regulated gene sets, the gene sets inflammatory response **(Figure 4.5 c)** and IL-2 STAT5 pathway **(Figure 4.5 d; Supplementary table 8.8)** were also included. Yet, the FDR for the enrichment of the inflammatory response was 0.102 and for the IL-2 STAT5 pathway 0.213, respectively. Moreover, the normalized enrichment scores (NES) were quite moderate with values of 1.39 for inflammatory response and 1.18 for IL-2 STAT5 pathway **(Figure 4.5 c; Figure 4.5 d; Supplementary table 8.8**). The genes which are part of the hallmark inflammatory response and the hallmark IL-2 STAT 5 pathway are highlighted in the depicted volcano plot in **Figure 4.5 b** (Esser et al. 2020).

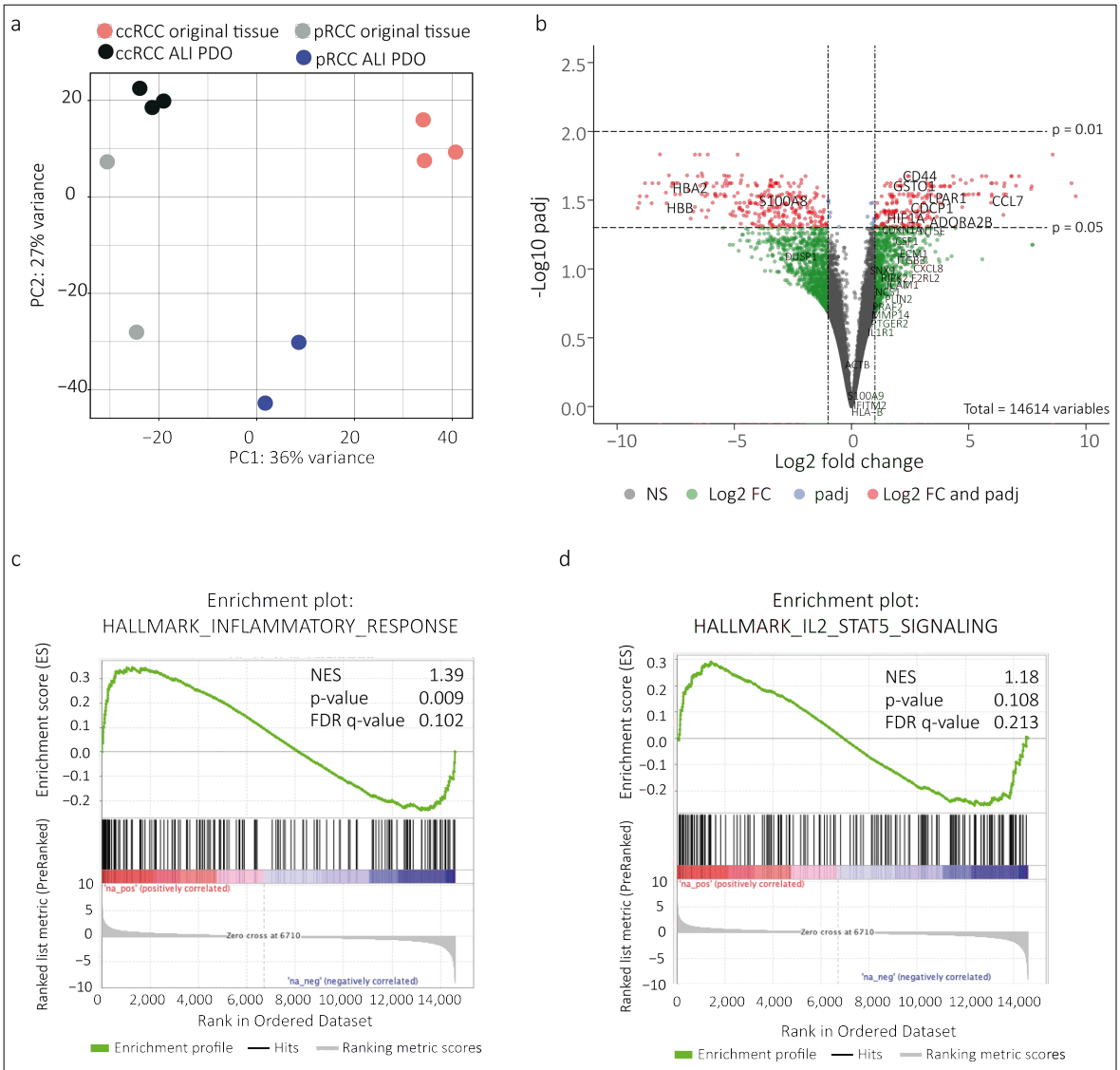

Figure 4.5| RNA sequencing demonstrates close molecular relationship of ALI PDOs and tissue of origin. (a) The close molecular relationship of the samples' gene expression profiles was projected onto the first two principal components in a PCA plot. **(b)** Volcano plot displaying the differentially expressed genes. Genes of interest, which are associated with inflammatory response and IL-2 STAT 5 signaling, are indicated in the up-regulated genes, genes expressed in blood are indicated in the down-regulated genes. **(c)** Genes correlated with inflammatory response were up-regulated. **(d)** Genes correlated with IL-2 STAT5 signaling were up-regulated. NES= normalized enrichment score. Figure re-used from (Esser et al. 2020).

4.5. Treatment shows different response rates for individual ALI PDOs

After verifying the histological and molecular resemblance including the presence of cytotoxic immune cells in the ALI PDOs compared to their matched tumors, I wondered if ALI PDOs are a suitable model system for therapy testing. For that, ten ALI PDOs were treated for one week either with the TKI cabozantinib (2.5 µM) or the anti-PD-1 ICI nivolumab (10 µg/ml). After termination of the experiment, the treated patient ALI PDOs were analyzed for viable cell areas compared to the control group and differences in response rates were observed **(Figure 4.6)** (Esser et al. 2020).

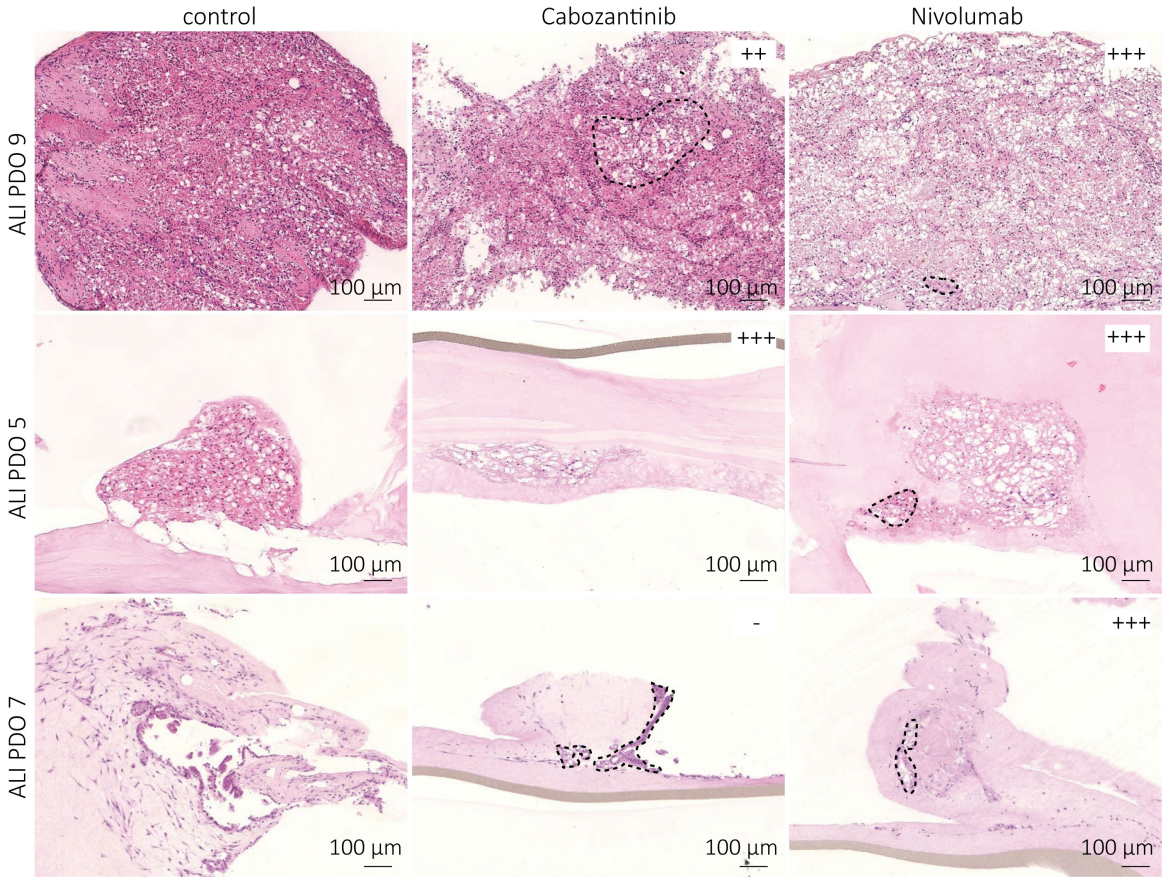

Figure 4.6| Treated ALI PDOs show drastically different responses. ALI PDOs were treated with 2.5 µM cabozantinib or 10 µg/ml nivolumab for one week, embedded and HE stained. ALI PDO 9 showed a stronger response towards nivolumab, ALI PDO 5 showed a similar response towards cabozantinib and nivolumab, ALI PDO 7 responded only to nivolumab. Dashed lines indicate areas of viable cells in treated ALI PDOs. Figure re-used from (Esser et al. 2020).

No substantial decrease in viability was observed in the untreated control group. While some ALI PDOs responded to both therapies, cabozantinib and nivolumab indicated by a similar degree of necrosis (ALI PDO 1, 5, 6), others responded only to nivolumab (ALI PDO 7), or not at all (ALI PDO 10). In most cases, one of the therapies was more efficient than the other (**Table 4.2**). Interestingly, when evaluating which ALI PDOs responded towards nivolumab, it appears that the response is dependent on the amount of CD8+ cells in the matched tumor tissue **(Table 4.1)** (Esser et al. 2020). ALI PDOs, which responded well to nivolumab had a high amount of CD8+ cells per HPF in its corresponding tissue. Three out of four ALI PDOs which showed a strong response towards nivolumab had more than 70 CD8+ cells per HPF (ALI PDO 7, 8, 9), while the remaining one had 35 CD8+ cells per HPF (ALI PDO 2) (**Table 4.1; Table 4.2**). In the majority of the cases, if ALI PDOs responded to a therapy, their response was better towards nivolumab. In two cases, they responded equally well towards cabozantinib and nivolumab (ALI PDO 5, 6). ALI PDO 4 was the only case which showed a better response towards the TKI cabozantinib than the ICI nivolumab **(Table 4.2)**.

Summarizing it can be stated that the ALI PDOs responded to the different types of therapies, namely the TT agent cabozantinib and the IT agent nivolumab (Esser et al. 2020). This suggests the established ALI PDO cultures as a suitable tool for personalized therapy testing.

Table 4.2| The response rate of the ALI PDOs was determined by measuring the area of necrotic cells in comparison to the whole area of the ALI PDO with Fiji. "-": no response, "+": weak response (up to 1/3 of necrotic areas), "++": medium response (up to 2/3 of necrotic areas), "+++": strong response more than 2/3 of necrotic areas). Table re-used from (Esser et al. 2020).

ALI PDO	Treatment	Response
1	control	-
	cabozantinib	+
	nivolumab	++
2	control	-
	cabozantinib	++
	nivolumab	+++
3	control	-
	cabozantinib	++
	nivolumab	+++
4	control	-
	cabozantinib	+++
	nivolumab	++
5	control	-
	cabozantinib	++
	nivolumab	++
	control	-

6		
	cabozantinib	++
	nivolumab	++
7	control	-
	cabozantinib	-
	nivolumab	+++
8	control	-
	cabozantinib	++
	nivolumab	+++
9	control	-
	cabozantinib	++
	nivolumab	+++
10	control	-
	cabozantinib	-
	nivolumab	-

5. Discussion

In the first part of this thesis, I analyzed the effect of Parkin deficiency on ccRCC pathogenesis. While many studies have described that PARK2 and the protein Parkin, which it encodes, are down-regulated in several cancer entities, its effect on ccRCC tumorigenesis remains unknown.

Here, I found that PARK2 overexpression induces anti-migrative and anti-invasive behavior in ccRCC cells. Furthermore, Parkin seems to influence CKS2 protein levels via its E3 ubiquitin ligase activity. I show that by silencing CKS2 it is possible to reduce migration to a degree similar to cells overexpressing PARK2. Moreover, CKS2 is correlated with patient prognosis and tumor grading. Consequently, these results propose CKS2 as a potential, interesting biomarker candidate and a suitable therapeutic target (Esser et al. in press).

5.1. PARK2 expression analysis in patients and cultured cells

While RCC incidence rates have reached a plateau and death rates have been decreasing in the last years, kidney cancer still accounts for almost 5% of all diagnosed cancers worldwide (Ferlay et al. 2020). The discovery of possible tumor driving mutations has shed some light on the pathogenesis and possible therapy options. However, the extreme heterogeneity and immunosuppressive feature of ccRCC remains a challenge.

Down-regulation or absence of PARK2 due to mutation, loss of heterozygosity or promoter hypermethylation is associated with worse prognosis in numerous cancer entities (L. Xu et al. 2014). PARK2 was also described to be down-regulated in ccRCC patients compared to non-malignant tissue. In addition, down-regulation of Parkin protein levels were associated with aggressive disease and poor clinical outcome (Toma et al. 2013).

Several studies have investigated the diverse functions of Parkin in different cancers (J. Liu et al. 2017; Hongxia Wang et al. 2009; Ikeuchi et al. 2009; Lee et al. 2018), however, extensive knowledge about the biological function of Parkin in ccRCC is still lacking. This is the first study that thoroughly investigates the effect of Parkin deficiency in ccRCC. Unfortunately, the ccRCC cell lines that I wanted to use do not express Parkin. In addition,

primary cells which closely recapitulate the molecular profile of the tissue they derived from could provide an additional model system to test my hypothesis in a more patient related context. Unfortunately, our group found that almost all ccRCC primary cells lose any PARK2 expression upon cultivation. This observation suggests a selective pressure in favor of cells lacking Parkin (Esser et al. in press). Moreover, it is tempting to speculate if Parkin deficient cells are therefore also more aggressive. Yet, the deficiency of Parkin in ccRCC primary cell lines makes it an inappropriate tool for studying the effects of Parkin (Esser et al. in press). In addition, primary cells are limited in their passaging capacities restricting them in studies for thorough characterization of cellular functions.

5.2. Characterization of the phenotypic features of the generated cell lines

Due to the absence of Parkin in ccRCC cell lines, I transduced the ccRCC cell lines 786-O and RCC-MH with a pLVX-EF1α-PARK2-IRES-mCherry vector to constantly overexpress PARK2 and enable detailed investigations. There are ongoing debates if RCC cell lines are truly of ccRCC character. 786-O is most commonly used in ccRCC research because it displays many features that are characteristic for the ccRCC subtype, including VHL mutation and altered HIF and vascular endothelial growth factor (VEGF) pathways. Moreover, injection into nude mice induces clear cell tumors (Brodaczewska et al. 2016). Hence, this cell line serves as a great tool for ccRCC research. In addition, I used RCC-MH. RCC-MH is a cell line derived from the kidney clear cell carcinoma of a 59 year old female patient which grows in an adherent, monolayer and is phenotypically comparable to the 786-O cell line.

In 2011, Hanahan and Weinberg redefined the six formerly known hallmarks of cancers, comprising the multistep process that is required for human tumor development, to eight hallmarks. Underlying these hallmarks are genome instability and inflammation. The hallmarks consist of different cellular capacities, such as evading growth suppressors, resisting cell death, enabling replicative immortality, sustaining proliferative signaling, inducing angiogenesis, activating invasion and metastasis and the two recently emerging hallmarks which are reprogramming of energy metabolism and evading immune destructing (Hanahan and Weinberg 2000; 2011).

In order, to investigate the effect of Parkin expression on the phenotypic features of cancer, I conducted functional assays, including cell cycle analysis, apoptosis assay and migration and invasion assays.

Yeo and colleagues found that restoration of Parkin in glioma cells promoted G_1 cell cycle arrest affecting the proliferation rate (Yeo et al. 2012). Furthermore, it was shown that Parkin promotes cancer cell apoptosis via mitochondrial depolarization (Carroll, Hollville, and Martin 2014). However, in my established cell lines I did not see a difference in the different phases of the cell cycle nor apoptosis.

Moreover, Parkin has been shown to inhibit breast cancer progression (J. Liu et al. 2017) and its inactivation has been described with lymph node metastasis in nasopharyngeal carcinoma (Ni et al. 2017). Tumor cells need to acquire several mechanistic changes in order to initiate metastasis, travel to distant tissues and invade foreign organs which ultimately leads to the formation of a metastatic tumor (Massagué and Obenauf 2016). The poor prognosis of patients with ccRCC goes along with metastatic occurrence (American Society of Clinical Oncology 2021). As of now, the prognosis for metastasized ccRCC is devastating. Finding new genes which are responsible for the initiation of metastasis and the process of migration and invasion could enable new diagnostic and therapeutic options that prolong survival. Since Parkin has been described as a tumor suppressor gene, that is frequently down-regulated in many cancers, it is an unsuitable therapeutic target (J. Liu et al. 2018). However, proteins that increase due to Parkin loss and promote tumorigenesis might serve as an interesting option in treating patients.

The obtained results from my study show a higher migrative and invasive capacity *in vitro* for wild-type cells and control cells containing an empty pLVX-EF1α-IRES-mCherry vector. The Transwell Boyden Chamber assay is a suitable tool to investigate directed migration towards a stimulant in a controlled manner (Justus et al. 2014). Liu and colleagues showed that the metastatic phenotype was linked to Parkin's function as an E3 ubiquitin ligase. In their study they reported that Parkin efficiently ubiquitinated HIF-1α at lysine 477 (K477) which led to its degradation. Moreover, silencing of Parkin in breast cancer cells increased migration and invasion *in vitro* and significantly promoted lung metastasis *in vivo* (J. Liu et al. 2017). Interestingly, Parkin deficiency in melanoma cells suppressed migration by inhibiting Mitofusin 2 (MFN2) ubiquitination. However,

malignant melanoma and metastatic malignant melanoma tissue analysis revealed, as expected, high levels of MFN2 but, contradictory, also high levels of Parkin (Lee et al. 2018). These findings indicate that Parkin expression might have different effects at different stages of tumor progression. Further, this discrepancy highlights the contradiction within the biology of Parkin and the many different roles within the cell and, therefore, the various effects on tumor pathogenesis. Hence, the precise function of Parkin under certain conditions needs to be further investigated to find the exact target proteins which are ubiquitinated by Parkin in the specific cancer type. In addition, the complex and tightly controlled mechanisms of Parkin in different situations remain to be solved.

In order to explore if the higher metastatic features *in vitro* are provoked by molecular differences between the cells, I conducted 3'mRNA sequencing. Cells need to undergo several molecular changes to be able to leave the primary tumor, invade the surrounding tissue and enter the bloodstream without undergoing anoikis, a term describing the induction of apoptosis due to the detachment from the extracellular matrix. This is achieved by acquiring several cellular changes, including migrative and invasive properties, which are collectively known as epithelial-mesenchymal transition (EMT) (Guan 2015). Surprisingly, 3'mRNA sequencing revealed no difference in the genetic profile. The only significant gene was the Parkin gene, PARK2, confirming the overexpression but leaving the explanation for the higher malignant capacities open (Esser et al. in press).

5.3. Finding of target proteins that are responsible for the phenotype

Therefore, I wondered if the observed phenotype can be linked to Parkin's described role as an E3 ubiquitin ligase. I hypothesized that the loss of Parkin is accompanied by the accumulation of proteins which promote malignancy such as migration and invasion (Esser et al. in press).

To check my hypothesis, LC-MS was performed. In the LC-MS results several proteins were increased in absence of Parkin. The only significantly (FDR <0.05) up-regulated proteins in WT and control cells were UBE2Z, also known as UBA6-specific E2 enzyme 1

(USE1), and OSBPL10. UBE2Z is an E2 ubiquitin conjugating enzyme that is involved in the second step of the ubiquitination process (Aichem et al. 2010). Not many studies about UBE2Z in cancer have been conducted. UBE2Z has been described to be associated with hepatocellular carcinoma and to be part of an energy-metabolic based gene signature correlating with clinical outcome in esophagus carcinoma (Shi et al. 2020; W. Zheng et al. 2021). Interestingly, UBE2Z is up-regulated in renal cancer compared to non-malignant tissue (Gu et al. 2007). Recently, Roverato and colleagues found that Parkin binds to UBE2Z and serves as an E3 ligase for the cytokine inducible modifier HLA-F adjacent transcript 10 (FAT10) *in vitro* (Roverato et al. 2021). Next to ubiquitination, FAT10ylation is a second process, which targets proteins for degradation by the proteasome independent of ubiquitin. In contrast to ubiquitination, a single FAT10 molecule is sufficient to bind to the 26S proteasome and induce degradation via the proteasome. Moreover, contradictory to the ubiquitination pathway, FAT10 is not recycled and reused, rather, it is assumed that it gets degraded along with its target protein (Schmidtke, Aichem, and Groettrup 2014).

Due to its function as an E2 conjugating enzyme its unlikely that UBE2Z gets degraded by the E3 ligase Parkin. Moreover, its involvement with Parkin in the FAT10ylation process suggests that lack of Parkin decreases FAT10ylation. This could explain the accumulation of UBE2Z since the degradation process is disrupted only at the E3 ligation step. Yet, UBE2Z might still get activated and target proteins. Therefore, it would be interesting to research if activation of UBE2Z leads to the stabilization of another protein which then induces malignancy.

The second significant protein was OSBPL10. In cancer, circular RNA of OSBPL10 has been described as an oncogenic factor in gastric and cervical cancer (S. Wang et al. 2019; Yang et al. 2020). However, OSBPL10 is considered a favorable prognostic marker in ccRCC disagreeing with our phenotypic findings and making it unattractive for further investigations (Uhlen et al. 2017). Hence, I did not follow up on this protein.

Surprisingly, Parkin did not show significance in the LC-MS results. Yet, I showed that mRNA and protein are highly up-regulated in cells transduced with the overexpressing vector. Therefore, proteins showing a similar adjusted p-value as Parkin may also be considered true (Esser et al. in press).

To narrow down promising proteins, I investigated which proteins are considered

unfavorable prognostic markers in ccRCC (Uhlen et al. 2017). Moreover, I went back to literature to look into the most interesting proteins that have been described with our observed phenotype. One protein that stood out was CKS2. CKS2 was higher in cells with no Parkin expression indicating that Parkin might regulate CKS2 levels which then cause a less aggressive phenotype (Esser et al. in press). CKS2 is highly expressed in many tumors and associated with metastasis (N. Huang et al. 2019; J.-H. Xu, Wang, and Xu 2019; Yu et al. 2015). It binds to the catalytic subunit of cyclin dependent kinases and is responsible for cell cycle progression (Spruck et al. 2003). Besides its involvement in cell cycle, CKS2 has been described to play a role in mitochondrial function in cervical cancer. CKS2 forms a complex with SSBP1 and influences mitochondrial DNA (mtDNA) replication which controls the energy supply of the cell and, subsequently, the aggressiveness of the cell (Jonsson et al. 2019). On the other hand, Parkin monitors mitochondrial quality control by selectively degrading defective mitochondria (Durcan and Fon 2015). It can be speculated that the loss of Parkin leads to an increase of CKS2 which may result in increased energy supply of the cell and decreased degradation of defective mitochondria effecting a higher aggressiveness of the cell.

Thus, the opposing expression levels of Parkin and CKS2 as well as their role in mitochondrial function and tumor aggressiveness hint towards a possible, interesting link between those two proteins which needs to be further investigated.

5.4. Investigation of Parkin's E3 ligase activity on CKS2 levels and phenotype

CKS2 levels are higher in cells lacking Parkin. Hence, I assumed that this effect is due to the loss of Parkin and its accompanied loss of the E3 ubiquitin ligase activity. In order to analyze the effect of Parkin's E3 ubiquitin ligase activity on CKS2 levels, I introduced a mutation into the catalytic site of Parkin. Cysteine was replaced by serine at amino acid 431. Mutating the catalytic site C431 in the RING2 domain leads to the abolishment of Parkin's E3 ligase activity (Trempe et al. 2013; Riley et al. 2013).

I showed that inactivation of the E3 ligase activity has no effect on mRNA levels of Parkin and CKS2 compared to WT as expected. In a recent study, Zheng and Hunter found that

mitochondrial translocation of Parkin is abolished when the catalytic cysteine is mutated to serine. Furthermore, this leads to trapping of ubiquitin (X. Zheng and Hunter 2013). In addition, Sarraf and colleagues examined the targets of Parkin ubiquitination upon mitochondrial depolarization and discovered that the associations between Parkin and its targets are abolished when introducing the C431S mutation (Sarraf et al. 2013). Unfortunately, CKS2 was not among the detected targets, however, the analysis was conducted using the colorectal carcinoma cell line HCT116, which might explain the differences. Furthermore, we did not conduct a specific ubiquitination assay but a general LC-MS analysis which only answers the question of differences in the proteomic profiles. Therefore, it cannot be excluded that the decreased levels of CKS2 in the LC-MS analysis are due to different posttranslational mechanisms.

Accordingly, I conducted further experiments with the introduced mutated catalytic site C431S. My results show that even though PARK2 mRNA expression was increased in cells tranduced with PARK2 and PARK2(C431S), migrative capacities of C431S harboring cells were similar to WT and control. This suggests that the catalytic site of Parkin regulates proteins that are responsible for migration *in vitro* and, hence, that loss of Parkin's E3 ubiquitin ligase activity results in a more aggressive phenotype (Esser et al. in press). Nevertheless, this did not reveal any clues about the involvement of CKS2 in the more aggressive behavior of ccRCC. Therefore, I wondered if the higher migration can be inhibited by reducing CKS2 levels. It was previously shown that silencing of CKS2 led to a strong increase of caspase-3 activity and an increase of Bax expression in gastric cancer cells as well as in cholangiocarcinoma cells indicating that the interference with CKS2 results in the induction of apoptosis in the mentioned cancer cells (Tanaka et al. 2011; Shen et al. 2013). Shen and colleagues further reported that knockdown of CKS2 causes G_2 cell cycle arrest which is induced by the reduction of cyclin A and cyclin B1 expression. Thus, overexpression of CKS2 advances cholangiocarcinoma progression (Shen et al. 2013). Although, previous studies have investigated the effect of CKS2 inhibition on migration in different cancer types (Hua et al. 2016; You, Lin, and Zhang 2015), no studies have been conducted in ccRCC.

Therefore, I knocked-down CKS2 and performed a migration assay for approximately 16 hours in order to ensure that the migrative differences are not due to differences in the

proliferative or apoptotic rate. In addition, it was ensured that cells looked alike upon beginning of the experiment. I observed that silencing of CKS2 in wild-type and control cells reduced migration to a similar amount as the introduction of wild-type Parkin. This supports the hypothesis that CKS2 is regulated by the E3 ubiquitin ligase Parkin. Further, it supports the hypothesis that high levels of Parkin lead to a less migrative phenotype modulated by the decrease in CKS2 expression. In addition, the possibility of reversing the observed phenotype by silencing CKS2 emphasizes the great promise CKS2 may hold as a therapeutic target for different types of cancer with high levels of CKS2.

5.5. The effect of CKS2 and Parkin expression on the prognosis of patients

Many studies about CKS2 have investigated the association between CKS2 expression and clinicopathological parameters (You, Lin, and Zhang 2015; Xiao et al. 2020; R. Chen, Feng, and Xu 2011; J.-H. Xu, Wang, and Xu 2019; N. Huang et al. 2019; J. Wang et al. 2014). Yu and colleagues showed that increased CKS2 levels are associated with poor prognosis, enhanced TNM stage and larger tumor size in colorectal cancer patients. Additionally, it was found that CKS2 is a promising prognostic indicator (Yu et al. 2015). Similar results were obtained in a study exploring lung adenocarcinoma. CKS2 up-regulation was associated with poor prognosis and larger tumor size (Xiao et al. 2020). In breast cancer it was found that CKS2 mRNA and protein levels are increased in cancer tissue compared to the adjacent non-malignant tissue. CKS2 overexpression was associated with larger tumor size, lack of progesterone receptor expression, poor tumor differentiation and worse overall survival (J. Wang et al. 2014). All these studies hint towards CKS2 as a potential prognostic indicator.

In my study, high CKS2 expression was significantly associated with lower survival, whereas for Parkin no significance was observed. A trend towards better survival for patients with high Parkin expression could be obtained. However, the expression levels for Parkin in general were lower compared to CKS2. While for CKS2 there was a high variability in the staining intensity of the different patient samples in the TMAs, for Parkin most samples showed no or really low expression and only some showed a decent

expression. Cox proportional hazard regression model analysis showed that patients with high CKS2 levels, high grading and high pT stage are more likely to die. CKS2 expression was even more significant compared to grading showing the great prognostic potential of CKS2. Again, for Parkin there was only a tendency. Patients with high Parkin levels are less likely to die, which was not significant. The same has been observed before in a different subtype of RCC. While high PARK2 mRNA levels were associated with better survival, protein expression was not associated with overall survival in pRCC (Adrian G. Simon et al. 2020). In addition, it was described before that Parkin protein expression was significantly downregulated in ccRCC, yet, no correlation to clinicopathological parameters was observed (Toma et al. 2013). Letessier and colleagues investigated the impact of Parkin protein deficiency on the prognosis of breast cancer patients and noted no difference in prognosis. However, they found that in some cases the 5´- or the 3´ region of PARK2 was lost and that these alterations were associated with reduced metastasis-free survival. Yet, the alteration in the PARK2 gene had no effect on the protein expression (Letessier et al. 2007). These findings show that the protein expression of Parkin cannot solely be taken into account for prognosis estimation, in fact, genetic variances and accompanied mechanistic alterations may play a bigger role. It would be interesting to examine my patient samples for potential genetic variances and especially for loss of the 3' region. Loss of the 3' region may go along with loss of the E3 ubiquitin ligase locus resulting in unaffected protein expression but defective ubiquitin ligase function. This could lead to a different sub-grouping of my samples and, therefore, a better and more evidence based analysis. Furthermore, no correlation between Parkin and CKS2 was observed. This, again, might be restricted due to the sole examination of the protein expression. I argue, that Parkin degrades CKS2 via its E3 ubiquitin ligase. However, loss or a defect of the E3 ubiquitin ligase does not cause loss of protein expression per se suggesting that a more differentiated approach would be more suitable to examine the relationship between Parkin and CKS2. Nevertheless, in order to investigate if CKS2 is a potential prognostic indicator in ccRCC this approach is suitable. I found that CKS2 is weakly positively correlated with grading, but not with pT. In contrast to that, Parkin showed no correlation with grading but a weak negative correlation with pT suggesting tumor suppressive potential for Parkin (Esser et al. 2020). These findings indicate that

CKS2 is not only a putative therapeutic target, but also a potential prognostic indicator in ccRCC.

In conclusion, Parkin itself does not serve as a suitable target due to its role as a tumor suppressor and its down-regulation in many cancers. CKS2, on the other hand, is up-regulated in several malignant tissues and it was shown that CKS2 interference promotes apoptosis and cell cycle arrest (Tanaka et al. 2011; Shen et al. 2013). In addition, by inhibiting CKS2 in wild-type cells I could reverse the phenotype in Parkin-deficient cells which resulted in less aggressive behavior indicated by decreased migration. Furthermore, I could show that migration is not decreased in cells with a defective catalytic ubiquitin ligase site, suggesting that a functional E3 ubiquitin ligase is essential for the decrease in migration in ccRCC cells.

Interestingly, CKS2 was found to be associated with resistance to chemo- and radiotherapy in cervical cancer (Jonsson et al. 2019). RCCs are highly resistant to chemotherapy and radiation, which highlights the urgency for additional therapeutic approaches and insights in the biology of this cancer entity (American Society of Clinical Oncology 2021). It would be tempting to speculate if CKS2 levels in ccRCC correlate with resistance to chemotherapy as well as other therapeutic agents, which would give additional information about the prognosis and therapy options.

Nevertheless, the exact mechanism of CKS2 in ccRCC remains mostly unknown. Therefore, further research concerning the precise functional mechanisms of CKS2 is necessary to get information about the effect of CKS2 expression on the aggressive behavior in cancer cells. In addition, the possible interaction of Parkin and CKS2 needs to be elucidated in more detail and in a context-dependent manner.

Besides the urgent need of finding novel therapies in ccRCC, a proper platform for testing potential therapies is necessary in order to identify the best therapeutic agent possible.

Therefore, in the second part of this thesis, I thoroughly characterized and validated ALI PDOs as a novel model system for personalized ccRCC therapy testing (Esser et al. 2020). While the potential of organoids in therapy development and testing is immense, lack of the microenvironment has drastically restricted their use as a suitable tool. Neal and colleagues established a cultivation protocol based on an ALI system. The established

organoids, which are called ALI-PDOs, resemble the tumor of origin and retain the tumor microenvironment (Neal et al. 2018).

Here, I generated ccRCC ALI PDOs from resected tumor tissues and cultivated them for several weeks. I could show that the cultivated ALI PDOs resemble the tumor of origin histologically and genetically. Furthermore, cytotoxic immune cells were still present making it a suitable tool for therapy testing with ICI, which are commonly used in ccRCC therapy. Lastly, when treating the ALI PDOs with the common ccRCC TKI, cabozantinib, or the immune checkpoint inhibitor, nivolumab, I was able to observe the various responds rates, which are in agreement with the situation in the clinics. In conclusion, this second part of my thesis underlines the great potential for ALI PDOs in therapy testing using standard therapies such as TT and IT (Esser et al. 2020).

5.6. Generation of ALI PDOs from resected tumor tissues

The emergence of PDOs has immensely revolutionized cancer biology research. In contrast to former 2D cultures, PDOs are directly derived from resected tumors in its native form, thus, representing the molecular profile of the tumor as closely as possible. This is especially favorable for personalized therapy development and testing. RCC exhibit substantial heterogeneity which hinders many therapies from being successful. Despite great improvements in therapy regimens for ccRCC in the previous years, the patient's responses are still hardly predictable and, in addition, drug screening models which may predict therapy responses remain scarce (Motzer et al. 2018; 2019; Rini et al. 2019; Lobo et al. 2016; Grassi et al. 2019; Fendler et al. 2020). In order to treat cancers more successfully, this major hurdle needs to be addressed by appropriate model systems, which retain the relevant characteristics of the patient's situation as closely as possible. Therefore, I explored patient-derived ALI PDOs, which were established using an air-liquid interface system as previously described (Neal et al. 2018). In contrast to former organoid protocols which dissociate the tissue physically and enzymatically, the newly established protocol dissociates the tissues only physically into small fragments. The lack of enzymatic digestion ensures that the tissue is cultivated in its original complex form with different

cell subtypes. Especially the preservation of the tumor microenvironment including stromal and immune cells holds great promise for personalized therapies. My results show that the cultivation success rate is rather high with 72% (31/43) overall and 77% (20/26) for ccRCC, specifically. Different aspects might be the cause for failed ALI PDO establishment. One reason might be the handling time. Since it can never be guaranteed that the tissue is received and handled within a certain amount of time, the tissue may have undergone necrotic processes before cultivation. Furthermore, the tumor per se may have necrotic parts which hinder ALI PDO establishment *in vitro*. However, further intratumoral effects may influence successful cultivation. It was described that although the amount of necrotic tissue varies in freshly cultivated tissue, the necrotic parts are eventually removed by continuous passaging, which then results in the successful establishment of ALI PDOs (Neal et al. 2018). Moreover, it was reported that ALI PDO establishment was more successful in rapidly growing high-grade tumors (Neal et al. 2018). This shows that many aspects can affect the cultivation of tumor samples. Nevertheless, the high success rate in ALI PDO' establishment qualifies it as a proper tool for tumor biology research.

5.7. Histological and molecular verification of the established ALI PDOs

The trend towards more personalized therapies in the field of cancer has called for novel platforms that enable thorough investigation. ALI PDOs were described to highly resemble the tumors of origin (Neal et al. 2018). I could verify by IHC staining and 3'mRNA sequencing that the established ALI PDOs from this study show a close relationship to the tumor tissue of origin. The genetic profiles of the ALI PDOs and their matched tumor tissues show only a modest number of differently expressed genes. Among the most down regulated genes were genes highly expressed in whole blood including hemoglobin genes (HBB and HBA1), which is expected and can be explained by the lack of vascularization and blood circulation in ALI PDOs (Esser et al. 2020). GSEA revealed that gene sets associated with inflammatory responses such as IL-2 STAT 5 signaling are moderately enriched in ALI PDOs. This is likely explained by the supplementation of IL-2 in the culture medium in order to maintain infiltrating lymphocytes (Neal et al. 2018). The

addition of IL-2 may cause the release of pro-inflammatory cytokines leading to a higher inflammatory response. Thus, the right amount of IL-2 supplementation needs to be carefully determined. In order to provide an appropriate setting which is closest to the native situation, intrinsic and artificial immune responses need to balanced. In particular when optimizing this platform towards prediction of ICI responses, precise addition of IL-2 needs to be considered (Esser et al. 2020).

The preservation of the histology as well as the immune and stromal cell compartments opens new doors for tumor microenvironment studies. As of now, ccRCC organoids consisted mainly of epithelial cells (Grassi et al. 2019; Fendler et al. 2020; Calandrini et al. 2020). Hence, in order to study immune checkpoint inhibitors it was inevitable to add exogenous immune cells to the organoids (Yuki et al. 2020; Courau et al. 2019). However, the co-cultured immune cells do not represent the high variety of the native immune cells. Instead, T and natural killer (NK) cells were enriched by depleting B cells and monocytes before application to the organoids. Moreover, individual immune cells such as CD4 T cells, CD8 T cells and NK cells were applied alone or in combination (Courau et al. 2019). While this is great for studying individual immune cell responses, it does not recapitulate the patient's complex situation and the interplay between the different immune cell compartments, which are essential in the application and success of IT. Therefore, ALI PDOs with their preserved microenvironment may serve as promising platform. The minor differences of the ALI PDOs and their matched tumors make it possible to address the question of intratumoral immune responses towards IT within the individual tumor. These observations in addition with the presence of resident immune cells add further value to this model system (Esser et al. 2020). In addition, the above-mentioned methods from previous studies about co-cultivation of immune cells and organoids can be also applied to the ALI PDOs, which further contributes to the promising field and enhances this platform in testing therapy options.

5.8. Suitability of ALI PDOs as a tool for therapy testing and response prediction

The close similarity of ALI PDOs, including preservation of the microenvironment, and their primary tumor holds great promise for this model systems as a tool for therapy testing.

In fact, previous models have already proven to be suitable for developing novel personalized treatments. WNT and Notch inhibition was analyzed in ccRCC stem cell based organoids and patient-derived xenograft (PDX) models. Fendler and colleagues found that WNT and Notch inhibition could be applied to ccRCC organoids and resulted in reduced growth. Furthermore, they applied the inhibitors on PDX models with similar results (Fendler et al. 2020). Even though these results show the great potential of present models, it also shows the limitations. Up to date only therapies targeting signaling pathways apart from immune signaling pathways can be applied to the organoids. However, IT has become a promising therapy option for ccRCC. Thus, models representing the complex immune compartments of the original tumor are necessary. PDX models are alternative tools for testing therapies in a more complex setting. Unfortunately, PDX establishment rates are rather low. In the aforementioned study, only 15% of all PDX were successfully established (Fendler et al. 2020). This restricts PDX in serving as a pre-clinical model for choosing appropriate therapies for patients and distinguishes it from ALI PDOs. Since it is of pivotal importance for current therapy regimens that therapeutic effects can also be addressed on the tumor microenvironment, ALI PDOs benefit from their preservation of the microenvironment including immune and stromal cells (Esser et al. 2020).

Another important aspect is that RCC is highly infiltrated by immune cells and, thus, considered an immunogenic cancer (Heidegger, Pircher, and Pichler 2019). Despite the introduction of immune checkpoint inhibitors that block PD-1/PD-L1 as the standard of care, novel therapies and combinational therapies are necessary (Motzer et al. 2018; 2019).

In contrast to organoids which consist only of epithelial cells, the presence of stromal and immune cells in ALI PDOs propose it as a great tool, not only for TT, but also for IT testing and development. One major challenge in the clinics is that responses are hardly

predictable. While some patients show a great response towards a therapy, others do not respond at all. This observation has always been challenging when considering the appropriate therapy for patients. The therapy responses of the ALI PDOs in this study are in concordance with the clinical findings, since responses of ALI PDOs towards TT and IT showed a high variety. Therefore, I was curious to find potential reasons for the varying response rates. PD-L1 expression as a marker for predicting therapy responses has been widely studied and it seemed that patients with PD-L1 positive tumors show a better response in many cancers. However, studies in RCC show that it is not as clear. While some studies found that IT response was better for patients with PD-L1 positive tumors, others showed that no difference in responses between patients with and without expression of PD-L1 on tumors was observed stating that PD-L1 is not a reliable marker for therapy response (W. Xu, Atkins, and McDermott 2020; Choueiri et al. 2018). This is in agreement with the findings in this study. PD-L1 expression in the tumor tissue of origin could not predict the therapy responses of the ALI PDOs. This may have different reasons. While the presence of PD-L1 expression in the ALI PDOs was checked, it was not compared side by side to the tumor of origin. Hence, it is not guaranteed that PD-L1 expression in the ALI PDOs accurately resembles that of the tumor of origin. Further, Noguchi and colleagues showed in *in vitro* studies that PD-L1 expression on cells in the tumor microenvironment and PD-L1 expression on tumor cells differ temporally. Moreover, while PD-L1 induction on tumor cells was interferon gamma-dependent and transient, PD-L1 induction on tumor-associated macrophages was only partly dependent on interferon gamma and much more stable (Noguchi et al. 2017). Thus, it may be beneficial, when considering PD-L1 as a predictive marker, to evaluate PD-L1 expression on all cells in the immediate tumor microenvironment and not only on the tumor cells per se.

PD-1 expression on immune cells was equally no predictor for therapy response. Most tumors from which ALI PDOs were derived from showed PD-1 expression, yet, to varying degrees. Some cases showed hardly any PD-1 expression, but still, the ALI PDOs responded well to nivolumab. One case, ALI PDO 10, did not respond to cabozantinib nor nivolumab. The original tumor tissue showed no PD-1 or PD-L1 expression, lacked Granzyme B expression and only two CD8+ cells per HPF were found (Esser et al. 2020). Interestingly, I observed that the response towards the ICI, nivolumab, depends on the

amount of CD8 positive cells, which is in accordance with recent literature (W. Xu, Atkins, and McDermott 2020; Choueiri et al. 2019). Recent literature showed that CD8 positive tumor infiltrating lymphocytes are important for therapy responses towards ICI (W. Xu, Atkins, and McDermott 2020; Choueiri et al. 2019; Kvistborg et al. 2014, 4). Further, studies showed that clinical responses were associated with CD8+ and PD-1 expressing T lymphocytes. Blocking of PD-1/PD-L1 causes expansion of CD8+ PD-1 expressing T cells, which then exert anti-tumor effects (Durgeau et al. 2018; Zuazo et al. 2020; Gros et al. 2016; 2014). Intriguingly, in this presented study tumors which express the PD-1 receptor exhibit also a higher percentage of CD8+ cells. This suggests that CD8+ T cells alone or in combination with PD-1 expression may give valuable information about the prognosis of the success of IT.

Nevertheless, future prospective studies are needed in order to characterize the ALI PDOs in more detail. The ultimate goal is to develop a pre-clinical tool which can be used to determine the best-possible therapy for each individual patient and avoid unnecessary therapy side-effects.

6. Outlook

In the first part of this thesis I could show that CKS2 is a potential prognostic indicator in ccRCC. Moreover, CKS2 seems to be regulated by Parkin via its E3 ubiquitin ligase. Despite these findings, several questions remain open.

First off, the exact interaction of Parkin and CKS2 needs to be investigated in more detail. Therefore, it should be first checked if CKS2 is ubiquitinated by Parkin. For that, the different cells are transfected with ubiquitin and, subsequently, protein is extracted. Next, co-immunoprecipitation of CKS2 and ubiquitin is conducted according to standard protocols with protein A- or G-agarose beads (Choo and Zhang 2009). In short, the extracted protein is incubated with the antibody against the target of interest and the protein A- or G-agarose beads at 4°C ON. Samples are spun down, supernatant is aspirated and the pellet is washed. After washing, samples are prepared for immunoblotting and ubiquitin and target protein are detected with the respective antibodies.

Moreover, Parkin was shown to induce K63- and K48- linked polyubiquitination (Lim et al. 2005; Doss-Pepe, Chen, and Madura 2005). While K48-linked polyubiquitination induces degradation of the target protein by the proteasome enzyme complex, it was reported that polyubiquitination at lysine site 63 (K63) mediates protein-protein interactions and conformational changes influencing DNA damage repair, receptor endocytosis, kinase signaling activation and protein trafficking (Z. Liu et al. 2015; Panier and Durocher 2009; G. Wang et al. 2012). Thus, it would be interesting to investigate the specific ubiquitination which is induced by Parkin in order to determine the fate of the protein under normal and Parkin-deficient conditions. This can be achieved by altering the previously mentioned co-immunoprecipitation protocol by transfecting the cells with K63-, K47- or any other ubiquitin of interest.

Interestingly, it has been shown that proteasome inhibition can promote autophagic degradation of ubiquitinated proteins, moreover, it is even required for protein degradation (Dawei Wang et al. 2019). Thus, it would be interesting to treat cells with MG132, an proteasome inhibitor, and examine CKS2 protein levels in the different cell types. In case of elevated CKS2 decrease upon MG132 treatment, further studies about treatment efficacy with combinational therapies including a proteasome inhibitor and standard-of-

care therapies would be advisable.

In order to investigate the metastatic potential of Parkin-deficient cells in more detail, animal studies are of advantage. Cells with and without Parkin expression can be injected into the tail vein of mice to examine the colonization of the lung, a common metastatic site of ccRCC (Xue et al. 2021; Dudani et al. 2020). Moreover, intracardiac injections can be performed. For that, the cells of interest are injected into the left ventricle enabling them to enter the arterial bloodstream which can lead to the development of bone metastasis, another common metastatic site of ccRCC (Xue et al. 2021; Dudani et al. 2020). These experiments would identify the effect of Parkin expression on the metastatic potential *in vivo*. Furthermore, CKS2 knockout cells could be generated and investigated as well.

Lastly, it would be interesting to examine the involvement of CKS2 expression on therapy resistance. Jonnson and colleagues found that CKS2 levels are associated with radio- and chemotherapy resistance (Jonsson et al. 2019). Renal cancers are commonly resistant to conventional systemic therapies (Rini, Campbell, and Escudier 2009). Nevertheless, it is tempting to ask if CKS2 levels are also involved in resistance to targeted therapy agents. For that, cells with wild-type and depleted CKS2 levels can be analyzed by applying different therapeutic agents and combinations. The results can be read-out by a viability assay such as CellTiter-Glo®.

In the second part of this thesis I showed that the generated ALI PDOs resemble the tumor of origin in histological and molecular aspects. Thus, they serve as suitable tool to develop novel therapies as well as test therapy combinations to find the best possible treatment for each patient. Despite these findings, several aspects need to be researched further.

First off, the exact correlation of therapy response in the ALI PDOs and patients needs to be investigated further. For that, the established ALI PDOs and the patient from which the tissue was obtained need to be treated and observed side by side. Another option to observe the responses would be to treat ALI PDOs retrospectively and compare their response to the already documented patient's response.

Second, the exact immune compartments of the ccRCC ALI PDOs need to be researched in detail. Especially for the application of IT it would be of advantage if the immune cell compartment resembles the patient's as closely as possible. Furthermore, the IL-2

supplementation needs to be observed carefully to determine the appropriate concentration which stimulates T-cells but maintains the *in vivo* situation.

Lastly, the exact time point for beginning of the therapy needs to be determined precisely. The earlier the therapy is started, the less genetic differences have occurred. Hence, the cultured ALI PDOs are closest to the patients' situation. In addition, cytotoxic T cells are stimulated by IL-2, yet, they vanish over time which restricts the use of IT at later time points. Therefore, it is necessary to determine the best time point when cultivating the ALI PDOs. The accumulation of genetic differences upon cultivation and the loss of cytotoxic T cells over time needs to be always taken into account.

7. Bibliography

Aichem, Annette, Christiane Pelzer, Sebastian Lukasiak, Birte Kalveram, Paul W. Sheppard, Neha Rani, Gunter Schmidtke, and Marcus Groettrup. 2010. "USE1 Is a Bispecific Conjugating Enzyme for Ubiquitin and FAT10, Which FAT10ylates Itself in Cis." *Nature Communications* 1 (May): 13. https://doi.org/10.1038/ncomms1012.

American Society of Clinical Oncology. 2021. "Kidney Cancer." Cancer.Net. 2021. https://www.cancer.net/cancer-types/kidney-cancer/.

Bedke, Jens, Laurence Albiges, Umberto Capitanio, Rachel H. Giles, Milan Hora, Thomas B. Lam, Börje Ljungberg, et al. 2021. "Updated European Association of Urology Guidelines on Renal Cell Carcinoma: Nivolumab plus Cabozantinib Joins Immune Checkpoint Inhibition Combination Therapies for Treatment-Naïve Metastatic Clear-Cell Renal Cell Carcinoma." *European Urology* 79 (3): 339–42. https://doi.org/10.1016/j.eururo.2020.12.005.

Bernardini, J. P., M. Lazarou, and G. Dewson. 2017. "Parkin and Mitophagy in Cancer." *Oncogene* 36 (10): 1315–27. https://doi.org/10.1038/onc.2016.302.

Blighe, Kevin. 2018. *EnhancedVolcano*. Bioconductor. https://doi.org/10.18129/B9.BIOC.ENHANCEDVOLCANO.

Brodaczewska, Klaudia K., Cezary Szczylik, Michal Fiedorowicz, Camillo Porta, and Anna M. Czarnecka. 2016. "Choosing the Right Cell Line for Renal Cell Cancer Research." *Molecular Cancer* 15 (1): 83. https://doi.org/10.1186/s12943-016-0565-8.

Brownlee, Peter M., Anna L. Chambers, Ross Cloney, Alessandro Bianchi, and Jessica A. Downs. 2014. "BAF180 Promotes Cohesion and Prevents Genome Instability and Aneuploidy." *Cell Reports* 6 (6): 973–81. https://doi.org/10.1016/j.celrep.2014.02.012.

Calandrini, Camilla, Frans Schutgens, Rurika Oka, Thanasis Margaritis, Tito Candelli, Luka Mathijsen, Carola Ammerlaan, et al. 2020. "An Organoid Biobank for Childhood Kidney Cancers That Captures Disease and Tissue Heterogeneity." *Nature Communications* 11 (1): 1310. https://doi.org/10.1038/s41467-020-15155-6.

Carbone, Michele, J. William Harbour, James Brugarolas, Angela Bononi, Ian Pagano, Anwesha Dey, Thomas Krausz, Harvey I. Pass, Haining Yang, and Giovanni Gaudino. 2020. "Biological Mechanisms and Clinical Significance of *BAP1* Mutations in Human

Cancer." *Cancer Discovery* 10 (8): 1103–20. https://doi.org/10.1158/2159-8290.CD-19-1220.

Carroll, Richard G., Emilie Hollville, and Seamus J. Martin. 2014. "Parkin Sensitizes toward Apoptosis Induced by Mitochondrial Depolarization through Promoting Degradation of Mcl-1." *Cell Reports* 9 (4): 1538–53. https://doi.org/10.1016/j.celrep.2014.10.046.

Chai, Zhengbin, Li Wang, Yabing Zheng, Na Liang, Xiwei Wang, Yingying Zheng, Zhiwei Zhang, Chuanxi Zhao, Tingting Zhu, and Chunyan Liu. 2019. "PADI3 Plays an Antitumor Role via the Hsp90/CKS1 Pathway in Colon Cancer." *Cancer Cell International* 19: 277. https://doi.org/10.1186/s12935-019-0999-3.

Chen, Hui, Kristin Gotimer, Cristabelle De Souza, Clifford G. Tepper, Anthony N. Karnezis, Gary S. Leiserowitz, Jeremy Chien, and Lloyd H. Smith. 2020. "Short-Term Organoid Culture for Drug Sensitivity Testing of High-Grade Serous Carcinoma." *Gynecologic Oncology*, April, S0090825820302511. https://doi.org/10.1016/j.ygyno.2020.03.026.

Chen, R., C. Feng, and Y. Xu. 2011. "Cyclin-Dependent Kinase-Associated Protein Cks2 Is Associated with Bladder Cancer Progression." *The Journal of International Medical Research* 39 (2): 533–40. https://doi.org/10.1177/147323001103900222.

Chen, Rui, Wei-Qing Zhao, Cheng Fang, Xin Yang, and Mei Ji. 2020. "Histone Methyltransferase SETD2: A Potential Tumor Suppressor in Solid Cancers." *Journal of Cancer* 11 (11): 3349–56. https://doi.org/10.7150/jca.38391.

Choo, Yeun Su, and Zhuohua Zhang. 2009. "Detection of Protein Ubiquitination." *Journal of Visualized Experiments: JoVE*, no. 30 (August): 1293. https://doi.org/10.3791/1293.

Choueiri, Toni K., Laurence Albiges, John B. A. G. Haanen, James M.G. Larkin, Motohide Uemura, Sumanta K. Pal, Gwenaelle Gravis, et al. 2019. "Biomarker Analyses from JAVELIN Renal 101: Avelumab + Axitinib (A+Ax) versus Sunitinib (S) in Advanced Renal Cell Carcinoma (ARCC)." *Journal of Clinical Oncology* 37 (15_suppl): 101–101. https://doi.org/10.1200/JCO.2019.37.15_suppl.101.

Choueiri, Toni K, James Larkin, Mototsugu Oya, Fiona Thistlethwaite, Marcella Martignoni, Paul Nathan, Thomas Powles, et al. 2018. "Preliminary Results for Avelumab plus Axitinib as First-Line Therapy in Patients with Advanced Clear-Cell Renal-Cell

Carcinoma (JAVELIN Renal 100): An Open-Label, Dose-Finding and Dose-Expansion, Phase 1b Trial." *The Lancet Oncology* 19 (4): 451–60. https://doi.org/10.1016/S1470-2045(18)30107-4.

Courau, Tristan, Julie Bonnereau, Justine Chicoteau, Hugo Bottois, Romain Remark, Laura Assante Miranda, Antoine Toubert, et al. 2019. "Cocultures of Human Colorectal Tumor Spheroids with Immune Cells Reveal the Therapeutic Potential of MICA/B and NKG2A Targeting for Cancer Treatment." *Journal for Immunotherapy of Cancer* 7 (1): 74. https://doi.org/10.1186/s40425-019-0553-9.

Dalgliesh, Gillian L., Kyle Furge, Chris Greenman, Lina Chen, Graham Bignell, Adam Butler, Helen Davies, et al. 2010. "Systematic Sequencing of Renal Carcinoma Reveals Inactivation of Histone Modifying Genes." *Nature* 463 (7279): 360–63. https://doi.org/10.1038/nature08672.

Deng, Lu, Tong Meng, Lei Chen, Wenyi Wei, and Ping Wang. 2020. "The Role of Ubiquitination in Tumorigenesis and Targeted Drug Discovery." *Signal Transduction and Targeted Therapy* 5 (1): 11. https://doi.org/10.1038/s41392-020-0107-0.

Dickerson, Tyler, Catherine E. Jauregui, and Yong Teng. 2017. "Friend or Foe? Mitochondria as a Pharmacological Target in Cancer Treatment." *Future Medicinal Chemistry* 9 (18): 2197–2210. https://doi.org/10.4155/fmc-2017-0110.

Doss-Pepe, Ellen W., Li Chen, and Kiran Madura. 2005. "α-Synuclein and Parkin Contribute to the Assembly of Ubiquitin Lysine 63-Linked Multiubiquitin Chains." *Journal of Biological Chemistry* 280 (17): 16619–24. https://doi.org/10.1074/jbc.M413591200.

Dove, Katja K, Benjamin Stieglitz, Emily D Duncan, Katrin Rittinger, and Rachel E Klevit. 2016. "Molecular Insights into RBR E3 Ligase Ubiquitin Transfer Mechanisms." *EMBO Reports* 17 (8): 1221–35. https://doi.org/10.15252/embr.201642641.

Drost, Jarno, and Hans Clevers. 2018. "Organoids in Cancer Research." *Nature Reviews Cancer* 18 (7): 407–18. https://doi.org/10.1038/s41568-018-0007-6.

Duan, Huijie, Zhong Lei, Fei Xu, Tao Pan, Demin Lu, Peili Ding, Chunpeng Zhu, Chi Pan, and Suzhan Zhang. 2019. "PARK2 Suppresses Proliferation and Tumorigenicity in Non-Small Cell Lung Cancer." *Frontiers in Oncology* 9 (August): 790. https://doi.org/10.3389/fonc.2019.00790.

Dudani, Shaan, Guillermo de Velasco, Connor Wells, Chun Loo Gan, Frede Donskov, Camillo Porta, Anna Fraccon, et al. 2020. “Characterizing Sites of Metastatic Involvement in Metastatic Clear-Cell, Papillary, and Chromophobe Renal Cell Carcinoma.” *Journal of Clinical Oncology* 38 (15_suppl): 5071–5071. https://doi.org/10.1200/JCO.2020.38.15_suppl.5071.

Duns, Gerben, Robert M.W. Hofstra, Jantine G. Sietzema, Harry Hollema, Inge van Duivenbode, Angela Kuik, Cor Giezen, et al. 2012. “Targeted Exome Sequencing in Clear Cell Renal Cell Carcinoma Tumors Suggests Aberrant Chromatin Regulation as a Crucial Step in CcRCC Development.” *Human Mutation* 33 (7): 1059–62. https://doi.org/10.1002/humu.22090.

Durcan, Thomas M., and Edward A. Fon. 2015. “The Three ’P’s of Mitophagy: PARKIN, PINK1, and Post-Translational Modifications.” *Genes & Development* 29 (10): 989–99. https://doi.org/10.1101/gad.262758.115.

Durgeau, Aurélie, Yasemin Virk, Stéphanie Corgnac, and Fathia Mami-Chouaib. 2018. “Recent Advances in Targeting CD8 T-Cell Immunity for More Effective Cancer Immunotherapy.” *Frontiers in Immunology* 9 (January): 14. https://doi.org/10.3389/fimmu.2018.00014.

Edfors, Fredrik, Frida Danielsson, Björn M Hallström, Lukas Käll, Emma Lundberg, Fredrik Pontén, Björn Forsström, and Mathias Uhlén. 2016. “Gene−specific Correlation of RNA and Protein Levels in Human Cells and Tissues.” *Molecular Systems Biology* 12 (10): 883. https://doi.org/10.15252/msb.20167144.

Esser, Laura K., Vittorio Branchi, Sonia Leonardelli, Natalie Pelusi, Adrian G. Simon, Niklas Klümper, Jörg Ellinger, et al. 2020. “Cultivation of Clear Cell Renal Cell Carcinoma Patient-Derived Organoids in an Air-Liquid Interface System as a Tool for Studying Individualized Therapy.” *Frontiers in Oncology* 10: 1775. https://doi.org/10.3389/fonc.2020.01775.

Esser, Laura K., Vittorio Branchi, Farhad Shakeri, Adrian G. Simon, Glen Kristiansen, Andreas Buness, Hubert Schorle, and Marieta I. Toma. in press. “Overexpression of Parkin in Clear Cell Renal Cell Carcinoma Decreases Tumor Aggressiveness by Regulating CKS2 Levels.” *International Journal of Oncology*.

Favazza, Laura, Dhananjay A Chitale, Ravi Barod, Craig G Rogers, Shanker Kalyana-Sundaram, Nallasivam Palanisamy, Nilesh S Gupta, and Sean R Williamson. 2017. “Renal

Cell Tumors with Clear Cell Histology and Intact VHL and Chromosome 3p: A Histological Review of Tumors from the Cancer Genome Atlas Database." *Modern Pathology* 30 (11): 1603–12. https://doi.org/10.1038/modpathol.2017.72.

Fendler, Annika, Daniel Bauer, Jonas Busch, Klaus Jung, Annika Wulf-Goldenberg, Severine Kunz, Kun Song, et al. 2020. "Inhibiting WNT and NOTCH in Renal Cancer Stem Cells and the Implications for Human Patients." *Nature Communications* 11 (1): 929. https://doi.org/10.1038/s41467-020-14700-7.

Ferlay, J, M Ervik, F Lam, M Colombet, L Mery, M Piñeros, A Znaor, I Soerjomataram, and F Bray. 2020. "Global Cancer Observatory: Cancer Today." Lyon, France: International Agency for Research on Cancer. 2020. https://gco.iarc.fr/today.

Frappart, Pierre-Olivier, Karolin Walter, Johann Gout, Alica K Beutel, Mareen Morawe, Frank Arnold, Markus Breunig, et al. 2020. "Pancreatic Cancer-Derived Organoids – a Disease Modeling Tool to Predict Drug Response." *United European Gastroenterology Journal*, February, 205064062090518. https://doi.org/10.1177/2050640620905183.

Gao, Fei, Chong Li, Xiqun Zhao, Jianli Xie, Guiqing Fang, and Ying Li. 2021. "CKS2 Modulates Cell−cycle Progression of Tongue Squamous Cell Carcinoma Cells Partly via Modulating the Cellular Distribution of DUTPase." *Journal of Oral Pathology & Medicine* 50 (2): 175–82. https://doi.org/10.1111/jop.13116.

George, Arlene J., Yarely C. Hoffiz, Antoinette J. Charles, Ying Zhu, and Angela M. Mabb. 2018. "A Comprehensive Atlas of E3 Ubiquitin Ligase Mutations in Neurological Disorders." *Frontiers in Genetics* 9 (February): 29. https://doi.org/10.3389/fgene.2018.00029.

Gerlinger, Marco, Stuart Horswell, James Larkin, Andrew J. Rowan, Max P. Salm, Ignacio Varela, Rosalie Fisher, et al. 2014. "Genomic Architecture and Evolution of Clear Cell Renal Cell Carcinomas Defined by Multiregion Sequencing." *Nature Genetics* 46 (3): 225–33. https://doi.org/10.1038/ng.2891.

Ghosh, Soma, and Tapas Saha. 2012. "Central Role of Ubiquitination in Genome Maintenance: DNA Replication and Damage Repair." *ISRN Molecular Biology* 2012 (February): 1–9. https://doi.org/10.5402/2012/146748.

González-Rodríguez, Patricia, Pinelopi Engskog-Vlachos, Hanzhao Zhang, Adriana-Natalia Murgoci, Ioannis Zerdes, and Bertrand Joseph. 2020. "SETD2 Mutation in Renal

Clear Cell Carcinoma Suppress Autophagy via Regulation of ATG12." *Cell Death & Disease* 11 (1): 69. https://doi.org/10.1038/s41419-020-2266-x.

Gossage, Lucy, Tim Eisen, and Eamonn R. Maher. 2015. "VHL, the Story of a Tumour Suppressor Gene." *Nature Reviews Cancer* 15 (1): 55–64. https://doi.org/10.1038/nrc3844.

Grassi, Ludovica, Romina Alfonsi, Federica Francescangeli, Michele Signore, Maria Laura De Angelis, Antonio Addario, Manuela Costantini, et al. 2019. "Organoids as a New Model for Improving Regenerative Medicine and Cancer Personalized Therapy in Renal Diseases." *Cell Death & Disease* 10 (3): 201. https://doi.org/10.1038/s41419-019-1453-0.

Gros, Alena, Maria R. Parkhurst, Eric Tran, Anna Pasetto, Paul F. Robbins, Sadia Ilyas, Todd D. Prickett, et al. 2016. "Prospective Identification of Neoantigen-Specific Lymphocytes in the Peripheral Blood of Melanoma Patients." *Nature Medicine* 22 (4): 433–38. https://doi.org/10.1038/nm.4051.

Gros, Alena, Paul F. Robbins, Xin Yao, Yong F. Li, Simon Turcotte, Eric Tran, John R. Wunderlich, et al. 2014. "PD-1 Identifies the Patient-Specific $CD8^+$ Tumor-Reactive Repertoire Infiltrating Human Tumors." *The Journal of Clinical Investigation* 124 (5): 2246–59. https://doi.org/10.1172/JCI73639.

Gu, Xing, Feng Zhao, Mei Zheng, Xiangwei Fei, Xudong Chen, Shengdong Huang, Yi Xie, and Yumin Mao. 2007. "Cloning and Characterization of a Gene Encoding the Human Putative Ubiquitin Conjugating Enzyme E2Z (UBE2Z)." *Molecular Biology Reports* 34 (3): 183–88. https://doi.org/10.1007/s11033-006-9033-7.

Guan, Xiangming. 2015. "Cancer Metastases: Challenges and Opportunities." *Acta Pharmaceutica Sinica B* 5 (5): 402–18. https://doi.org/10.1016/j.apsb.2015.07.005.

Guo, Guangwu, Yaoting Gui, Shengjie Gao, Aifa Tang, Xueda Hu, Yi Huang, Wenlong Jia, et al. 2012. "Frequent Mutations of Genes Encoding Ubiquitin-Mediated Proteolysis Pathway Components in Clear Cell Renal Cell Carcinoma." *Nature Genetics* 44 (1): 17–19. https://doi.org/10.1038/ng.1014.

Haas, A L, J V Warms, A Hershko, and I A Rose. 1982. "Ubiquitin-Activating Enzyme. Mechanism and Role in Protein-Ubiquitin Conjugation." *Journal of Biological Chemistry* 257 (5): 2543–48. https://doi.org/10.1016/S0021-9258(18)34958-5.

Hanahan, Douglas, and Robert A Weinberg. 2000. "The Hallmarks of Cancer." *Cell* 100

(1): 57–70. https://doi.org/10.1016/S0092-8674(00)81683-9.

Hanahan, Douglas, and Robert A. Weinberg. 2011. “Hallmarks of Cancer: The Next Generation.” *Cell* 144 (5): 646–74. https://doi.org/10.1016/j.cell.2011.02.013.

Heidegger, Isabel, Andreas Pircher, and Renate Pichler. 2019. “Targeting the Tumor Microenvironment in Renal Cell Cancer Biology and Therapy.” *Frontiers in Oncology* 9 (June): 490. https://doi.org/10.3389/fonc.2019.00490.

Hershko, Avram, and Aaron Ciechanover. 1998. “THE UBIQUITIN SYSTEM.” *Annual Review of Biochemistry* 67 (1): 425–79. https://doi.org/10.1146/annurev.biochem.67.1.425.

Ho, Thai H., Payal Kapur, Richard W. Joseph, Daniel J. Serie, Jeanette E. Eckel-Passow, Pan Tong, Jing Wang, et al. 2016. “Loss of Histone H3 Lysine 36 Trimethylation Is Associated with an Increased Risk of Renal Cell Carcinoma-Specific Death.” *Modern Pathology: An Official Journal of the United States and Canadian Academy of Pathology, Inc* 29 (1): 34–42. https://doi.org/10.1038/modpathol.2015.123.

Hopson, Sarah, and Martin J. Thompson. 2017. “BAF180: Its Roles in DNA Repair and Consequences in Cancer.” *ACS Chemical Biology* 12 (10): 2482–90. https://doi.org/10.1021/acschembio.7b00541.

Hsieh, James J., David Chen, Patricia I. Wang, Mahtab Marker, Almedina Redzematovic, Ying-Bei Chen, S. Duygu Selcuklu, et al. 2017. “Genomic Biomarkers of a Randomized Trial Comparing First-Line Everolimus and Sunitinib in Patients with Metastatic Renal Cell Carcinoma.” *European Urology* 71 (3): 405–14. https://doi.org/10.1016/j.eururo.2016.10.007.

Hsieh, James J., Mark P. Purdue, Sabina Signoretti, Charles Swanton, Laurence Albiges, Manuela Schmidinger, Daniel Y. Heng, James Larkin, and Vincenzo Ficarra. 2017. “Renal Cell Carcinoma.” *Nature Reviews. Disease Primers* 3 (March): 17009. https://doi.org/10.1038/nrdp.2017.9.

Hu, Cheng-Jun, Li-Yi Wang, Lewis A. Chodosh, Brian Keith, and M. Celeste Simon. 2003. “Differential Roles of Hypoxia-Inducible Factor 1alpha (HIF-1alpha) and HIF-2alpha in Hypoxic Gene Regulation.” *Molecular and Cellular Biology* 23 (24): 9361–74. https://doi.org/10.1128/mcb.23.24.9361-9374.2003.

Hu, Hongbo, and Shao-Cong Sun. 2016. “Ubiquitin Signaling in Immune Responses.” *Cell*

Research 26 (4): 457–83. https://doi.org/10.1038/cr.2016.40.

Hua, Kaiyao, Jiali Jin, Huiwen Zhang, Bingkun Zhao, Chenyang Wu, Hui Xu, and Lin Fang. 2016. "MicroRNA-7 Inhibits Proliferation, Migration and Invasion of Thyroid Papillary Cancer Cells via Targeting CKS2." *International Journal of Oncology* 49 (4): 1531–40. https://doi.org/10.3892/ijo.2016.3660.

Huang, L. E., Z. Arany, D. M. Livingston, and H. F. Bunn. 1996. "Activation of Hypoxia-Inducible Transcription Factor Depends Primarily upon Redox-Sensitive Stabilization of Its Alpha Subunit." *The Journal of Biological Chemistry* 271 (50): 32253–59. https://doi.org/10.1074/jbc.271.50.32253.

Huang, Naiqi, Zuli Wu, Hong Hong, Xiangming Wang, Fengqiang Yang, and Hengguo Li. 2019. "Overexpression of CKS2 Is Associated with a Poor Prognosis and Promotes Cell Proliferation and Invasion in Breast Cancer." *Molecular Medicine Reports* 19 (6): 4761–69. https://doi.org/10.3892/mmr.2019.10134.

Huber, W, A von Heydebreck, H Sueltmann, A Poustka, and M Vingron. 2002. *Variance Stabilization Applied to Microarray Data Calibration and to the Quantification of Differential Expression*. Vol. 18. Suppl. 1: Bioinformatics.

Ikeuchi, Kyoko, Hiroyuki Marusawa, Mikio Fujiwara, Yuko Matsumoto, Yoko Endo, Tomohiro Watanabe, Akio Iwai, Yoshiharu Sakai, Ryosuke Takahashi, and Tsutomu Chiba. 2009. "Attenuation of Proteolysis-Mediated Cyclin E Regulation by Alternatively Spliced Parkin in Human Colorectal Cancers." *International Journal of Cancer* 125 (9): 2029–35. https://doi.org/10.1002/ijc.24565.

Jonsson, Marte, Christina Sæten Fjeldbo, Ruth Holm, Trond Stokke, Gunnar Balle Kristensen, and Heidi Lyng. 2019. "Mitochondrial Function of CKS2 Oncoprotein Links Oxidative Phosphorylation with Cell Division in Chemoradioresistant Cervical Cancer." *Neoplasia (New York, N.Y.)* 21 (4): 353–62. https://doi.org/10.1016/j.neo.2019.01.002.

Jun, Jonathan C., Aman Rathore, Haris Younas, Daniele Gilkes, and Vsevolod Y. Polotsky. 2017. "Hypoxia-Inducible Factors and Cancer." *Current Sleep Medicine Reports* 3 (1): 1–10. https://doi.org/10.1007/s40675-017-0062-7.

Justus, Calvin R., Nancy Leffler, Maria Ruiz-Echevarria, and Li V. Yang. 2014. "In Vitro Cell Migration and Invasion Assays." *Journal of Visualized Experiments: JoVE*, no. 88 (June). https://doi.org/10.3791/51046.

Kakarougkas, Andreas, Amani Ismail, Anna L. Chambers, Enriqueta Riballo, Alex D. Herbert, Julia Künzel, Markus Löbrich, Penny A. Jeggo, and Jessica A. Downs. 2014. "Requirement for PBAF in Transcriptional Repression and Repair at DNA Breaks in Actively Transcribed Regions of Chromatin." *Molecular Cell* 55 (5): 723–32. https://doi.org/10.1016/j.molcel.2014.06.028.

Kang, Yu-Seon, Eun-Jeong Jeong, Hyun-Jeong Seok, Seon-Kyu Kim, Jin-Seong Hwang, Mu Lim Choi, Dong-Gyu Jo, et al. 2019. "Cks1 Regulates Human Hepatocellular Carcinoma Cell Progression through Osteopontin Expression." *Biochemical and Biophysical Research Communications* 508 (1): 275–81. https://doi.org/10.1016/j.bbrc.2018.11.070.

Kapałczyńska, Marta, Tomasz Kolenda, Weronika Przybyła, Maria Zajączkowska, Anna Teresiak, Violetta Filas, Matthew Ibbs, Renata Bliźniak, Łukasz Łuczewski, and Katarzyna Lamperska. 2018. "2D and 3D Cell Cultures - a Comparison of Different Types of Cancer Cell Cultures." *Archives of Medical Science: AMS* 14 (4): 910–19. https://doi.org/10.5114/aoms.2016.63743.

Kassambara, Alboukadel, Marcin Kosinski, and Przemyslaw Biecek. 2021. "Survminer: Drawing Survival Curves Using 'Ggplot2.'" https://CRAN.R-project.org/package=survminer.

Kim, Daehwan, Joseph M. Paggi, Chanhee Park, Christopher Bennett, and Steven L. Salzberg. 2019. "Graph-Based Genome Alignment and Genotyping with HISAT2 and HISAT-Genotype." *Nature Biotechnology* 37 (8): 907–15. https://doi.org/10.1038/s41587-019-0201-4.

Kitada, T., S. Asakawa, N. Hattori, H. Matsumine, Y. Yamamura, S. Minoshima, M. Yokochi, Y. Mizuno, and N. Shimizu. 1998. "Mutations in the Parkin Gene Cause Autosomal Recessive Juvenile Parkinsonism." *Nature* 392 (6676): 605–8. https://doi.org/10.1038/33416.

Kvistborg, Pia, Daisy Philips, Sander Kelderman, Lois Hageman, Christian Ottensmeier, Deborah Joseph-Pietras, Marij J. P. Welters, et al. 2014. "Anti-CTLA-4 Therapy Broadens the Melanoma-Reactive CD8+ T Cell Response." *Science Translational Medicine* 6 (254): 254ra128. https://doi.org/10.1126/scitranslmed.3008918.

Latif, F, K Tory, J Gnarra, M Yao, F. Duh, M. Orcutt, T Stackhouse, et al. 1993. "Identification of the von Hippel-Lindau Disease Tumor Suppressor Gene." *Science* 260

(5112): 1317–20. https://doi.org/10.1126/science.8493574.

Lee, Yong Sun, Yu Yeon Jung, Mi Hee Park, In Jun Yeo, Hyung Sik Im, Kyung Tak Nam, Hae Deun Kim, et al. 2018. “Deficiency of Parkin Suppresses Melanoma Tumor Development and Metastasis through Inhibition of MFN2 Ubiquitination.” *Cancer Letters* 433 (October): 156–64. https://doi.org/10.1016/j.canlet.2018.07.007.

León, Ileana R., Veit Schwämmle, Ole N. Jensen, and Richard R. Sprenger. 2013. “Quantitative Assessment of In-Solution Digestion Efficiency Identifies Optimal Protocols for Unbiased Protein Analysis.” *Molecular & Cellular Proteomics* 12 (10): 2992–3005. https://doi.org/10.1074/mcp.M112.025585.

Letessier, A, S Garrido-Urbani, C Ginestier, G Fournier, B Esterni, F Monville, J Adélaïde, et al. 2007. “Correlated Break at PARK2/FRA6E and Loss of AF-6/Afadin Protein Expression Are Associated with Poor Outcome in Breast Cancer.” *Oncogene* 26 (2): 298–307. https://doi.org/10.1038/sj.onc.1209772.

Li, H., B. Handsaker, A. Wysoker, T. Fennell, J. Ruan, N. Homer, G. Marth, G. Abecasis, R. Durbin, and 1000 Genome Project Data Processing Subgroup. 2009. “The Sequence Alignment/Map Format and SAMtools.” *Bioinformatics* 25 (16): 2078–79. https://doi.org/10.1093/bioinformatics/btp352.

Liao, Y., G. K. Smyth, and W. Shi. 2014. “FeatureCounts: An Efficient General Purpose Program for Assigning Sequence Reads to Genomic Features.” *Bioinformatics* 30 (7): 923–30. https://doi.org/10.1093/bioinformatics/btt656.

Liberal, Vasco, Hanna-Stina Martinsson-Ahlzén, Jennifer Liberal, Charles H. Spruck, Martin Widschwendter, Clare H. McGowan, and Steven I. Reed. 2012. “Cyclin-Dependent Kinase Subunit (Cks) 1 or Cks2 Overexpression Overrides the DNA Damage Response Barrier Triggered by Activated Oncoproteins.” *Proceedings of the National Academy of Sciences of the United States of America* 109 (8): 2754–59. https://doi.org/10.1073/pnas.1102434108.

Lim, Kah Leong, Katherine C. M. Chew, Jeanne M. M. Tan, Cheng Wang, Kenny K. K. Chung, Yi Zhang, Yuji Tanaka, et al. 2005. “Parkin Mediates Nonclassical, Proteasomal-Independent Ubiquitination of Synphilin-1: Implications for Lewy Body Formation.” *The Journal of Neuroscience: The Official Journal of the Society for Neuroscience* 25 (8): 2002–9. https://doi.org/10.1523/JNEUROSCI.4474-04.2005.

Linehan, W. Marston, McClellan M. Walther, and Berton Zbar. 2003. “The Genetic Basis of Cancer of the Kidney.” *The Journal of Urology* 170 (6 Pt 1): 2163–72. https://doi.org/10.1097/01.ju.0000096060.92397.ed.

Liu, Juan, Cen Zhang, Wenwei Hu, and Zhaohui Feng. 2018. “Parkinson’s Disease-Associated Protein Parkin: An Unusual Player in Cancer.” *Cancer Communications* 38 (1): 40. https://doi.org/10.1186/s40880-018-0314-z.

Liu, Juan, Cen Zhang, Yuhan Zhao, Xuetian Yue, Hao Wu, Shan Huang, James Chen, et al. 2017. “Parkin Targets HIF-1α for Ubiquitination and Degradation to Inhibit Breast Tumor Progression.” *Nature Communications* 8 (1): 1823. https://doi.org/10.1038/s41467-017-01947-w.

Liu, Kun, Fanzhou Li, Haichao Han, Yue Chen, Zebin Mao, Jianyuan Luo, Yingming Zhao, Bin Zheng, Wei Gu, and Wenhui Zhao. 2016. “Parkin Regulates the Activity of Pyruvate Kinase M2.” *The Journal of Biological Chemistry* 291 (19): 10307–17. https://doi.org/10.1074/jbc.M115.703066.

Liu, Lei, Renbo Guo, Xiang Zhang, Yiran Liang, Feng Kong, Jue Wang, and Zhonghua Xu. 2017. “Loss of SETD2, but Not H3K36me3, Correlates with Aggressive Clinicopathological Features of Clear Cell Renal Cell Carcinoma Patients.” *Bioscience Trends* 11 (2): 214–20. https://doi.org/10.5582/bst.2016.01228.

Liu, Weisi, Qiang Fu, Huimin An, Yuan Chang, Weijuan Zhang, Yu Zhu, Le Xu, and Jiejie Xu. 2015. “Decreased Expression of SETD2 Predicts Unfavorable Prognosis in Patients With Nonmetastatic Clear-Cell Renal Cell Carcinoma.” *Medicine* 94 (45): e2004. https://doi.org/10.1097/MD.0000000000002004.

Liu, Zhu, Zhou Gong, Wen-Xue Jiang, Ju Yang, Wen-Kai Zhu, Da-Chuan Guo, Wei-Ping Zhang, Mai-Li Liu, and Chun Tang. 2015. “Lys63-Linked Ubiquitin Chain Adopts Multiple Conformational States for Specific Target Recognition.” *ELife* 4 (June): e05767. https://doi.org/10.7554/eLife.05767.

Livak, Kenneth J., and Thomas D. Schmittgen. 2001. “Analysis of Relative Gene Expression Data Using Real-Time Quantitative PCR and the 2−ΔΔCT Method.” *Methods* 25 (4): 402–8. https://doi.org/10.1006/meth.2001.1262.

Lobo, Nazleen C., Craig Gedye, Anthony J. Apostoli, Kevin R. Brown, Joshua Paterson, Natalie Stickle, Michael Robinette, et al. 2016. “Efficient Generation of Patient-Matched

Malignant and Normal Primary Cell Cultures from Clear Cell Renal Cell Carcinoma Patients: Clinically Relevant Models for Research and Personalized Medicine." *BMC Cancer* 16: 485. https://doi.org/10.1186/s12885-016-2539-z.

Manley, Brandon J., and Abraham Ari Hakimi. 2016. "Molecular Profiling of Renal Cell Carcinoma: Building a Bridge toward Clinical Impact." *Current Opinion in Urology* 26 (5): 383–87. https://doi.org/10.1097/MOU.0000000000000307.

Manza, Linda L., Sheryl L. Stamer, Amy-Joan L. Ham, Simona G. Codreanu, and Daniel C. Liebler. 2005. "Sample Preparation and Digestion for Proteomic Analyses Using Spin Filters." *PROTEOMICS* 5 (7): 1742–45. https://doi.org/10.1002/pmic.200401063.

Mark, Kevin G, and Michael Rape. 2021. "Ubiquitin−dependent Regulation of Transcription in Development and Disease." *EMBO Reports* 22 (4). https://doi.org/10.15252/embr.202051078.

Massagué, Joan, and Anna C. Obenauf. 2016. "Metastatic Colonization by Circulating Tumour Cells." *Nature* 529 (7586): 298–306. https://doi.org/10.1038/nature17038.

Masuda, Takeshi, Masaru Tomita, and Yasushi Ishihama. 2008. "Phase Transfer Surfactant-Aided Trypsin Digestion for Membrane Proteome Analysis." *Journal of Proteome Research* 7 (2): 731–40. https://doi.org/10.1021/pr700658q.

Medvar, Barbara, Viswanathan Raghuram, Trairak Pisitkun, Abhijit Sarkar, and Mark A. Knepper. 2016. "Comprehensive Database of Human E3 Ubiquitin Ligases: Application to Aquaporin-2 Regulation." *Physiological Genomics* 48 (7): 502–12. https://doi.org/10.1152/physiolgenomics.00031.2016.

Michael Love, Simon Anders. 2017. *DESeq2*. Bioconductor. https://doi.org/10.18129/B9.BIOC.DESEQ2.

Motzer, Robert J., Konstantin Penkov, John Haanen, Brian Rini, Laurence Albiges, Matthew T. Campbell, Balaji Venugopal, et al. 2019. "Avelumab plus Axitinib versus Sunitinib for Advanced Renal-Cell Carcinoma." *New England Journal of Medicine* 380 (12): 1103–15. https://doi.org/10.1056/NEJMoa1816047.

Motzer, Robert J., Paul Russo, Naomi Haas, Christian Doehn, Frede Donskov, Marine Gross-Goupil, Sergei Varlamov, et al. 2021. "Adjuvant Pazopanib Versus Placebo After Nephrectomy in Patients With Localized or Locally Advanced Renal Cell Carcinoma:

Final Overall Survival Analysis of the Phase 3 PROTECT Trial." *European Urology* 79 (3): 334–38. https://doi.org/10.1016/j.eururo.2020.12.029.

Motzer, Robert J., Nizar M. Tannir, David F. McDermott, Osvaldo Arén Frontera, Bohuslav Melichar, Toni K. Choueiri, Elizabeth R. Plimack, et al. 2018. "Nivolumab plus Ipilimumab versus Sunitinib in Advanced Renal-Cell Carcinoma." *New England Journal of Medicine* 378 (14): 1277–90. https://doi.org/10.1056/NEJMoa1712126.

Murakami, A, L Wang, S Kalhorn, P Schraml, W K Rathmell, A C Tan, R Nemenoff, et al. 2017. "Context-Dependent Role for Chromatin Remodeling Component PBRM1/BAF180 in Clear Cell Renal Cell Carcinoma." *Oncogenesis* 6 (1): e287–e287. https://doi.org/10.1038/oncsis.2016.89.

Nakayama, Keiichi I., and Keiko Nakayama. 2006. "Ubiquitin Ligases: Cell-Cycle Control and Cancer." *Nature Reviews Cancer* 6 (5): 369–81. https://doi.org/10.1038/nrc1881.

NCBI Resource Coordinators. 2018. "Database Resources of the National Center for Biotechnology Information." *Nucleic Acids Research* 46 (D1): D8–13. https://doi.org/10.1093/nar/gkx1095.

Neal, James T., Xingnan Li, Junjie Zhu, Valeria Giangarra, Caitlin L. Grzeskowiak, Jihang Ju, Iris H. Liu, et al. 2018. "Organoid Modeling of the Tumor Immune Microenvironment." *Cell* 175 (7): 1972-1988.e16. https://doi.org/10.1016/j.cell.2018.11.021.

Ni, Haifeng, Zhen Zhou, Bo Jiang, Xiaoyang Yuan, Xiaolin Cao, Guangwu Huang, and Yong Li. 2017. "Inactivation of *Parkin* by Promoter Methylation Correlated with Lymph Node Metastasis and Genomic Instability in Nasopharyngeal Carcinoma." *Tumor Biology* 39 (3): 101042831769502. https://doi.org/10.1177/1010428317695025.

Noguchi, Takuro, Jeffrey P. Ward, Matthew M. Gubin, Cora D. Arthur, Sang Hun Lee, Jasreet Hundal, Mark J. Selby, et al. 2017. "Temporally Distinct PD-L1 Expression by Tumor and Host Cells Contributes to Immune Escape." *Cancer Immunology Research* 5 (2): 106–17. https://doi.org/10.1158/2326-6066.CIR-16-0391.

Padala, Sandeep Anand, Adam Barsouk, Krishna Chaitanya Thandra, Kalyan Saginala, Azeem Mohammed, Anusha Vakiti, Prashanth Rawla, and Alexander Barsouk. 2020. "Epidemiology of Renal Cell Carcinoma." *World Journal of Oncology* 11 (3): 79–87. https://doi.org/10.14740/wjon1279.

Panier, Stephanie, and Daniel Durocher. 2009. “Regulatory Ubiquitylation in Response to DNA Double-Strand Breaks.” *DNA Repair* 8 (4): 436–43. https://doi.org/10.1016/j.dnarep.2009.01.013.

Pelzer, Christiane, Ingrid Kassner, Konstantin Matentzoglu, Rajesh K. Singh, Hans-Peter Wollscheid, Martin Scheffner, Gunter Schmidtke, and Marcus Groettrup. 2007. “UBE1L2, a Novel E1 Enzyme Specific for Ubiquitin.” *The Journal of Biological Chemistry* 282 (32): 23010–14. https://doi.org/10.1074/jbc.C700111200.

Peña-Llopis, Samuel, Alana Christie, Xian-Jin Xie, and James Brugarolas. 2013. “Cooperation and Antagonism among Cancer Genes: The Renal Cancer Paradigm.” *Cancer Research* 73 (14): 4173–79. https://doi.org/10.1158/0008-5472.CAN-13-0360.

Peña-Llopis, Samuel, Silvia Vega-Rubín-de-Celis, Arnold Liao, Nan Leng, Andrea Pavía-Jiménez, Shanshan Wang, Toshinari Yamasaki, et al. 2012. “BAP1 Loss Defines a New Class of Renal Cell Carcinoma.” *Nature Genetics* 44 (7): 751–59. https://doi.org/10.1038/ng.2323.

Pickart, Cecile M. 2001. “Mechanisms Underlying Ubiquitination.” *Annual Review of Biochemistry* 70 (1): 503–33. https://doi.org/10.1146/annurev.biochem.70.1.503.

Poulogiannis, G., R. E. McIntyre, M. Dimitriadi, J. R. Apps, C. H. Wilson, K. Ichimura, F. Luo, et al. 2010. “PARK2 Deletions Occur Frequently in Sporadic Colorectal Cancer and Accelerate Adenoma Development in Apc Mutant Mice.” *Proceedings of the National Academy of Sciences* 107 (34): 15145–50. https://doi.org/10.1073/pnas.1009941107.

R Development Core Team. 2021. “R: A Language and Environment for Statistical Computing.” R Foundation for Statistical Computing, Vienna, Austria. http://www.r-project.org/.

Riley, B.E., J.C. Lougheed, K. Callaway, M. Velasquez, E. Brecht, L. Nguyen, T. Shaler, et al. 2013. “Structure and Function of Parkin E3 Ubiquitin Ligase Reveals Aspects of RING and HECT Ligases.” *Nature Communications* 4 (1): 1982. https://doi.org/10.1038/ncomms2982.

Rini, Brian I, Steven C Campbell, and Bernard Escudier. 2009. “Renal Cell Carcinoma.” *The Lancet* 373 (9669): 1119–32. https://doi.org/10.1016/S0140-6736(09)60229-4.

Rini, Brian I., Elizabeth R. Plimack, Viktor Stus, Rustem Gafanov, Robert Hawkins,

Dmitry Nosov, Frédéric Pouliot, et al. 2019. “Pembrolizumab plus Axitinib versus Sunitinib for Advanced Renal-Cell Carcinoma.” *New England Journal of Medicine* 380 (12): 1116–27. https://doi.org/10.1056/NEJMoa1816714.

Ritchie, M. E., B Phipson, D Wu, C.W. Law, W Shi, and G. K. Smyth. 2015. “Limma Powers Differential Expression Analyses for RNA-Sequencing and Microarray Studies.” *Nucleic Acids Research* 43 (7): e47.

Roverato, Nicola D., Carolin Sailer, Nicola Catone, Annette Aichem, Florian Stengel, and Marcus Groettrup. 2021. “Parkin Is an E3 Ligase for the Ubiquitin-like Modifier FAT10, Which Inhibits Parkin Activation and Mitophagy.” *Cell Reports* 34 (11): 108857. https://doi.org/10.1016/j.celrep.2021.108857.

Sachs, Norman, Joep de Ligt, Oded Kopper, Ewa Gogola, Gergana Bounova, Fleur Weeber, Anjali Vanita Balgobind, et al. 2018. “A Living Biobank of Breast Cancer Organoids Captures Disease Heterogeneity.” *Cell* 172 (1–2): 373-386.e10. https://doi.org/10.1016/j.cell.2017.11.010.

Sanchez, Danielle J., and M. Celeste Simon. 2018. “Genetic and Metabolic Hallmarks of Clear Cell Renal Cell Carcinoma.” *Biochimica et Biophysica Acta (BBA) - Reviews on Cancer* 1870 (1): 23–31. https://doi.org/10.1016/j.bbcan.2018.06.003.

Sarraf, Shireen A., Malavika Raman, Virginia Guarani-Pereira, Mathew E. Sowa, Edward L. Huttlin, Steven P. Gygi, and J. Wade Harper. 2013. “Landscape of the PARKIN-Dependent Ubiquitylome in Response to Mitochondrial Depolarization.” *Nature* 496 (7445): 372–76. https://doi.org/10.1038/nature12043.

Sato, Toshiro, Robert G. Vries, Hugo J. Snippert, Marc van de Wetering, Nick Barker, Daniel E. Stange, Johan H. van Es, et al. 2009. “Single Lgr5 Stem Cells Build Crypt-Villus Structures in Vitro without a Mesenchymal Niche.” *Nature* 459 (7244): 262–65. https://doi.org/10.1038/nature07935.

Sato, Yusuke, Tetsuichi Yoshizato, Yuichi Shiraishi, Shigekatsu Maekawa, Yusuke Okuno, Takumi Kamura, Teppei Shimamura, et al. 2013. “Integrated Molecular Analysis of Clear-Cell Renal Cell Carcinoma.” *Nature Genetics* 45 (8): 860–67. https://doi.org/10.1038/ng.2699.

Schindelin, Johannes, Ignacio Arganda-Carreras, Erwin Frise, Verena Kaynig, Mark Longair, Tobias Pietzsch, Stephan Preibisch, et al. 2012. “Fiji: An Open-Source Platform

for Biological-Image Analysis." *Nature Methods* 9 (7): 676–82. https://doi.org/10.1038/nmeth.2019.

Schmidtke, Gunter, Annette Aichem, and Marcus Groettrup. 2014. "FAT10ylation as a Signal for Proteasomal Degradation." *Biochimica et Biophysica Acta (BBA) - Molecular Cell Research* 1843 (1): 97–102. https://doi.org/10.1016/j.bbamcr.2013.01.009.

SEER*Explorer. 2021. "An Interactive Website for SEER Cancer Statistics [Internet]." Surveillance Research Program, National Cancer Institute. 2021. https://seer.cancer.gov/explorer/.

Shen, Dong-Yan, Yi-Hong Zhan, Qian-Ming Wang, Gang Rui, and Zhi-Ming Zhang. 2013. "Oncogenic Potential of Cyclin Kinase Subunit-2 in Cholangiocarcinoma." *Liver International: Official Journal of the International Association for the Study of the Liver* 33 (1): 137–48. https://doi.org/10.1111/liv.12014.

Shi, Xiaokang, Bin Wang, Xiaoyan Chen, Yuyang Zheng, Youming Ding, and Changhua Wang. 2020. "Upregulation of Ubiquitin-Conjugating Enzyme E2Z Is Associated with Human Hepatocellular Carcinoma." *Biochemical and Biophysical Research Communications* 523 (1): 25–32. https://doi.org/10.1016/j.bbrc.2019.11.170.

Shimura, H., N. Hattori, S. i Kubo, Y. Mizuno, S. Asakawa, S. Minoshima, N. Shimizu, et al. 2000. "Familial Parkinson Disease Gene Product, Parkin, Is a Ubiquitin-Protein Ligase." *Nature Genetics* 25 (3): 302–5. https://doi.org/10.1038/77060.

Simon, Adrian G., Yuri Tolkach, Laura K. Esser, Jörg Ellinger, Christine Stöhr, Manuel Ritter, Sven Wach, et al. 2020. "Mitophagy-Associated Genes PINK1 and PARK2 Are Independent Prognostic Markers of Survival in Papillary Renal Cell Carcinoma and Associated with Aggressive Tumor Behavior." *Scientific Reports* 10 (1): 18857. https://doi.org/10.1038/s41598-020-75258-4.

Simon, Adrian Georg, Laura K. Esser, Jörg Ellinger, Vittorio Branchi, Yuri Tolkach, Stefan Müller, Manuel Ritter, et al. 2020. "Targeting Glycolysis with 2-Deoxy-D-Glucose Sensitizes Primary Cell Cultures of Renal Cell Carcinoma to Tyrosine Kinase Inhibitors." *Journal of Cancer Research and Clinical Oncology* 146 (9): 2255–65. https://doi.org/10.1007/s00432-020-03278-8.

Simon, Jeremy M., Kathryn E. Hacker, Darshan Singh, A. Rose Brannon, Joel S. Parker, Matthew Weiser, Thai H. Ho, et al. 2014. "Variation in Chromatin Accessibility in Human

Kidney Cancer Links H3K36 Methyltransferase Loss with Widespread RNA Processing Defects." *Genome Research* 24 (2): 241–50. https://doi.org/10.1101/gr.158253.113.

Singh, Komudi, Kim Han, Sharada Tilve, Kaiyuan Wu, Herbert M. Geller, and Michael N. Sack. 2018. "Parkin Targets NOD2 to Regulate Astrocyte Endoplasmic Reticulum Stress and Inflammation." *Glia* 66 (11): 2427–37. https://doi.org/10.1002/glia.23482.

Sirohi, Deepika, Steven C. Smith, Neeraj Agarwal, and Benjamin L. Maughan. 2018. "Unclassified Renal Cell Carcinoma: Diagnostic Difficulties and Treatment Modalities." *Research and Reports in Urology* Volume 10 (November): 205–17. https://doi.org/10.2147/RRU.S154932.

Spruck, Charles H., Maria P. de Miguel, Adrian P. L. Smith, Aimee Ryan, Paula Stein, Richard M. Schultz, A. Jeannine Lincoln, Peter J. Donovan, and Steven I. Reed. 2003. "Requirement of Cks2 for the First Metaphase/Anaphase Transition of Mammalian Meiosis." *Science (New York, N.Y.)* 300 (5619): 647–50. https://doi.org/10.1126/science.1084149.

Stewart, Mikaela D, Tobias Ritterhoff, Rachel E Klevit, and Peter S Brzovic. 2016. "E2 Enzymes: More than Just Middle Men." *Cell Research* 26 (4): 423–40. https://doi.org/10.1038/cr.2016.35.

Subramanian, A., P. Tamayo, V. K. Mootha, S. Mukherjee, B. L. Ebert, M. A. Gillette, A. Paulovich, et al. 2005. "Gene Set Enrichment Analysis: A Knowledge-Based Approach for Interpreting Genome-Wide Expression Profiles." *Proceedings of the National Academy of Sciences* 102 (43): 15545–50. https://doi.org/10.1073/pnas.0506580102.

Tanaka, Fumiaki, Shinji Matsuzaki, Koshi Mimori, Yoshiaki Kita, Hiroshi Inoue, and Masaki Mori. 2011. "Clinicopathological and Biological Significance of CDC28 Protein Kinase Regulatory Subunit 2 Overexpression in Human Gastric Cancer." *International Journal of Oncology* 39 (2): 361–72. https://doi.org/10.3892/ijo.2011.1056.

The Cancer Genome Atlas Research Network. 2013. "Comprehensive Molecular Characterization of Clear Cell Renal Cell Carcinoma." *Nature* 499 (7456): 43–49. https://doi.org/10.1038/nature12222.

Therneau, Terry. 2020. "A Package for Survival Analysis in R." https://CRAN.R-project.org/package=survival.

Toma, Marieta I., Daniela Wuttig, Sandy Kaiser, Alexander Herr, Thomas Weber, Stefan Zastrow, Rainer Koch, et al. 2013. “PARK2 and PACRG Are Commonly Downregulated in Clear-Cell Renal Cell Carcinoma and Are Associated with Aggressive Disease and Poor Clinical Outcome.” *Genes, Chromosomes & Cancer* 52 (3): 265–73. https://doi.org/10.1002/gcc.22026.

Trempe, Jean-François, Véronique Sauvé, Karl Grenier, Marjan Seirafi, Matthew Y. Tang, Marie Ménade, Sameer Al-Abdul-Wahid, et al. 2013. “Structure of Parkin Reveals Mechanisms for Ubiquitin Ligase Activation.” *Science (New York, N.Y.)* 340 (6139): 1451–55. https://doi.org/10.1126/science.1237908.

Tsai, Yi-Shan, Hui-Chiu Chang, Lea-Yea Chuang, and Wen-Chun Hung. 2005. “RNA Silencing of Cks1 Induced G2/M Arrest and Apoptosis in Human Lung Cancer Cells.” *IUBMB Life* 57 (8): 583–89. https://doi.org/10.1080/15216540500215531.

Uhlen, Mathias, Cheng Zhang, Sunjae Lee, Evelina Sjöstedt, Linn Fagerberg, Gholamreza Bidkhori, Rui Benfeitas, et al. 2017. “A Pathology Atlas of the Human Cancer Transcriptome.” *Science (New York, N.Y.)* 357 (6352): eaan2507. https://doi.org/10.1126/science.aan2507.

Varela, Ignacio, Patrick Tarpey, Keiran Raine, Dachuan Huang, Choon Kiat Ong, Philip Stephens, Helen Davies, et al. 2011. “Exome Sequencing Identifies Frequent Mutation of the SWI/SNF Complex Gene PBRM1 in Renal Carcinoma.” *Nature* 469 (7331): 539–42. https://doi.org/10.1038/nature09639.

Veeriah, Selvaraju, Barry S Taylor, Shasha Meng, Fang Fang, Emrullah Yilmaz, Igor Vivanco, Manickam Janakiraman, et al. 2010. “Somatic Mutations of the Parkinson’s Disease–Associated Gene PARK2 in Glioblastoma and Other Human Malignancies.” *Nature Genetics* 42 (1): 77–82. https://doi.org/10.1038/ng.491.

Wang, Dawei, Qingqing Xu, Quan Yuan, Mengqi Jia, Huanmin Niu, Xiaofei Liu, Jinsan Zhang, Charles Yf Young, and Huiqing Yuan. 2019. “Proteasome Inhibition Boosts Autophagic Degradation of Ubiquitinated-AGR2 and Enhances the Antitumor Efficiency of Bevacizumab.” *Oncogene* 38 (18): 3458–74. https://doi.org/10.1038/s41388-019-0675-z.

Wang, Dong, Leina Ma, Bin Wang, Jia Liu, and Wenyi Wei. 2017. “E3 Ubiquitin Ligases in Cancer and Implications for Therapies.” *Cancer Metastasis Reviews* 36 (4): 683–702. https://doi.org/10.1007/s10555-017-9703-z.

Wang, Guocan, Yuan Gao, Liren Li, Guoxiang Jin, Zhen Cai, Jui-I Chao, and Hui-Kuan Lin. 2012. “K63-Linked Ubiquitination in Kinase Activation and Cancer.” *Frontiers in Oncology* 2. https://doi.org/10.3389/fonc.2012.00005.

Wang, HongKai, YuanYuan Qu, Bo Dai, Yao Zhu, GuoHai Shi, YiPing Zhu, YiJun Shen, HaiLiang Zhang, and DingWei Ye. 2017. “PBRM1 Regulates Proliferation and the Cell Cycle in Renal Cell Carcinoma through a Chemokine/Chemokine Receptor Interaction Pathway.” Edited by Aamir Ahmad. *PLOS ONE* 12 (8): e0180862. https://doi.org/10.1371/journal.pone.0180862.

Wang, Hongxia, Bingbing Liu, Chao Zhang, Guoyuan Peng, Min Liu, Dengwen Li, Feng Gu, et al. 2009. “Parkin Regulates Paclitaxel Sensitivity in Breast Cancer via a Microtubule-Dependent Mechanism.” *The Journal of Pathology* 218 (1): 76–85. https://doi.org/10.1002/path.2512.

Wang, Jiani, Lihua Xu, Yu Liu, Jianning Chen, Hua Jiang, Shaojiang Yang, and Huo Tan. 2014. “Expression of Cyclin Kinase Subunit 2 in Human Breast Cancer and Its Prognostic Significance.” *International Journal of Clinical and Experimental Pathology* 7 (12): 8593–8601.

Wang, Sen, Xing Zhang, Zheng Li, Weizhi Wang, Bowen Li, Xiaoxu Huang, Guangli Sun, et al. 2019. “Circular RNA Profile Identifies CircOSBPL10 as an Oncogenic Factor and Prognostic Marker in Gastric Cancer.” *Oncogene* 38 (44): 6985–7001. https://doi.org/10.1038/s41388-019-0933-0.

Wenzel, Dawn M., Alexei Lissounov, Peter S. Brzovic, and Rachel E. Klevit. 2011. “UBCH7 Reactivity Profile Reveals Parkin and HHARI to Be RING/HECT Hybrids.” *Nature* 474 (7349): 105–8. https://doi.org/10.1038/nature09966.

Westbrook, Louise, Marina Manuvakhova, Francis G. Kern, Norman R. Estes, Harish N. Ramanathan, and Jaideep V. Thottassery. 2007. “Cks1 Regulates Cdk1 Expression: A Novel Role during Mitotic Entry in Breast Cancer Cells.” *Cancer Research* 67 (23): 11393–401. https://doi.org/10.1158/0008-5472.CAN-06-4173.

Wickham, Hadley. 2016. *Ggplot2: Elegant Graphics for Data Analysis*. Second edition. Use R! Cham: Springer.

Wiśniewski, Jacek R, Alexandre Zougman, Nagarjuna Nagaraj, and Matthias Mann. 2009. “Universal Sample Preparation Method for Proteome Analysis.” *Nature Methods* 6 (5):

359–62. https://doi.org/10.1038/nmeth.1322.

Xiao, Dayong, Siyuan Dong, Shize Yang, and Zhenghua Liu. 2020. “CKS2 and RMI2 Are Two Prognostic Biomarkers of Lung Adenocarcinoma.” *PeerJ* 8: e10126. https://doi.org/10.7717/peerj.10126.

Xu, J.-H., Y. Wang, and D. Xu. 2019. “CKS2 Promotes Tumor Progression and Metastasis and Is an Independent Predictor of Poor Prognosis in Epithelial Ovarian Cancer.” *European Review for Medical and Pharmacological Sciences* 23 (8): 3225–34. https://doi.org/10.26355/eurrev_201904_17681.

Xu, Liang, De-chen Lin, Dong Yin, and H. Phillip Koeffler. 2014. “An Emerging Role of PARK2 in Cancer.” *Journal of Molecular Medicine* 92 (1): 31–42. https://doi.org/10.1007/s00109-013-1107-0.

Xu, Wenxin, Michael B. Atkins, and David F. McDermott. 2020. “Checkpoint Inhibitor Immunotherapy in Kidney Cancer.” *Nature Reviews Urology* 17 (3): 137–50. https://doi.org/10.1038/s41585-020-0282-3.

Xue, Jianxin, Wensun Chen, Wenbo Xu, Zicheng Xu, Xiao Li, Feng Qi, and Zengjun Wang. 2021. “Patterns of Distant Metastases in Patients with Clear Cell Renal Cell Carcinoma--A Population-Based Analysis.” *Cancer Medicine* 10 (1): 173–87. https://doi.org/10.1002/cam4.3596.

Yan, Fangrong, Yue Wang, Chunhui Liu, Huiling Zhao, Liya Zhang, Xiaofan Lu, Chen Chen, Yaoyan Wang, Tao Lu, and Fei Wang. 2017. “Identify Clear Cell Renal Cell Carcinoma Related Genes by Gene Network.” *Oncotarget* 8 (66): 110358–66. https://doi.org/10.18632/oncotarget.22769.

Yang, Shanshan, Yiwen Jiang, Xiaoli Ren, Dan Feng, Liaoyun Zhang, Deying He, Shiyao Hong, Li Jin, Fang Zhang, and Shun Lu. 2020. “FOXA1-Induced CircOSBPL10 Potentiates Cervical Cancer Cell Proliferation and Migration through MiR-1179/UBE2Q1 Axis.” *Cancer Cell International* 20: 389. https://doi.org/10.1186/s12935-020-01360-2.

Yeo, Calvin W.S., Felicia S.L. Ng, Chou Chai, Jeanne M.M. Tan, Geraldene R.H. Koh, Yuk Kien Chong, Lynnette W.H. Koh, et al. 2012. “Parkin Pathway Activation Mitigates Glioma Cell Proliferation and Predicts Patient Survival.” *Cancer Research* 72 (10): 2543–53. https://doi.org/10.1158/0008-5472.CAN-11-3060.

You, Hanyu, Huayue Lin, and Zhongying Zhang. 2015. “CKS2 in Human Cancers: Clinical Roles and Current Perspectives (Review).” *Molecular and Clinical Oncology* 3 (3): 459–63. https://doi.org/10.3892/mco.2015.501.

Yu, Min-Hao, Yang Luo, Shao-Lan Qin, Zheng-Shi Wang, Yi-Fei Mu, and Ming Zhong. 2015. “Up-Regulated CKS2 Promotes Tumor Progression and Predicts a Poor Prognosis in Human Colorectal Cancer.” *American Journal of Cancer Research* 5 (9): 2708–18.

Yuki, Kanako, Ning Cheng, Michitaka Nakano, and Calvin J. Kuo. 2020. “Organoid Models of Tumor Immunology.” *Trends in Immunology* 41 (8): 652–64. https://doi.org/10.1016/j.it.2020.06.010.

Zbar, B., H. Brauch, C. Talmadge, and M. Linehan. 1987. “Loss of Alleles of Loci on the Short Arm of Chromosome 3 in Renal Cell Carcinoma.” *Nature* 327 (6124): 721–24. https://doi.org/10.1038/327721a0.

Zheng, Weifeng, Chaoying Chen, Jianghao Yu, Chengfeng Jin, and Tiemei Han. 2021. “An Energy Metabolism-Based Eight-Gene Signature Correlates with the Clinical Outcome of Esophagus Carcinoma.” *BMC Cancer* 21 (1): 345. https://doi.org/10.1186/s12885-021-08030-0.

Zheng, Xinde, and Tony Hunter. 2013. “Parkin Mitochondrial Translocation Is Achieved through a Novel Catalytic Activity Coupled Mechanism.” *Cell Research* 23 (7): 886–97. https://doi.org/10.1038/cr.2013.66.

Zhu, Anqi, Joseph G Ibrahim, and Michael I Love. 2019. “Heavy-Tailed Prior Distributions for Sequence Count Data: Removing the Noise and Preserving Large Differences.” Edited by Oliver Stegle. *Bioinformatics* 35 (12): 2084–92. https://doi.org/10.1093/bioinformatics/bty895.

Zuazo, Miren, Hugo Arasanz, Ana Bocanegra, Gonzalo Fernandez, Luisa Chocarro, Ruth Vera, Grazyna Kochan, and David Escors. 2020. “Systemic CD4 Immunity as a Key Contributor to PD-L1/PD-1 Blockade Immunotherapy Efficacy.” *Frontiers in Immunology* 11 (November): 586907. https://doi.org/10.3389/fimmu.2020.586907.

8. Supplementary data

8.1. Supplementary figures

Supplementary figure 8.1| Sequence of PARK2 cloned into pLVX-EF1α-IRES-mCherry. **(a)** pLVX-EF1α-IRES-PARK2-mCherry plasmid (clone number 4) sequenced with EF1α forward primer. Highlighted area represents the PARK2 gene. **(b)** pLVX-EF1α-IRES-PARK2-mCherry plasmid (clone number 4) sequenced with IRES reverse primer. Highlighted area represents the PARK2 gene. **(c, d)** PARK2 sequence of clone number 4 aligned to the wild-type PARK2 sequence retrieved from NCBI (NCBI Resource Coordinators 2018). Red areas indicate mismatches.

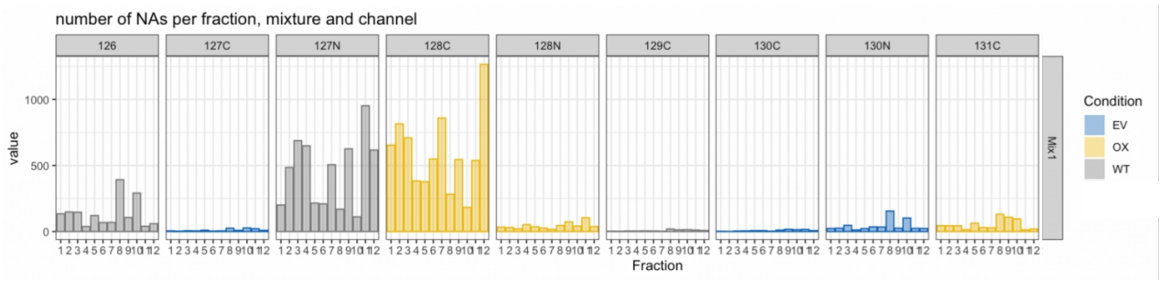

Supplementary figure 8.2| Number of missing values per fraction, mixture and channel. Extreme amount of missing values in one sample of WT (channel 127N) and OX (channel 128C). Figure re-used from (Esser et al. in press).

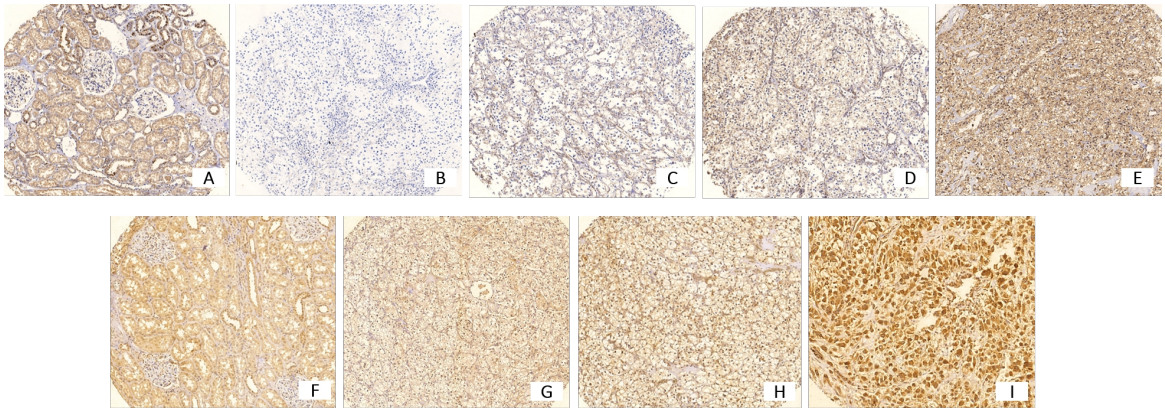

Supplementary figure 8.3| Representative images of the grading system used in the tissue microarray analysis. (A-E) Different staining intensities of Parkin in **(A)** non-malignant and **(B-E)** ccRCC tissue are shown; **(B)** negative, **(C)** weakly positive, **(D)** moderately positive, **(E)** strongly positive. **(F-I)** Different staining intensities of CKS2 in **(F)** non-malignant **(G-I)** and ccRCC tissue **(G)** weakly positive, **(H)** moderately positive, **(I)** strongly positive. Figure re-used from (Esser et al. in press).

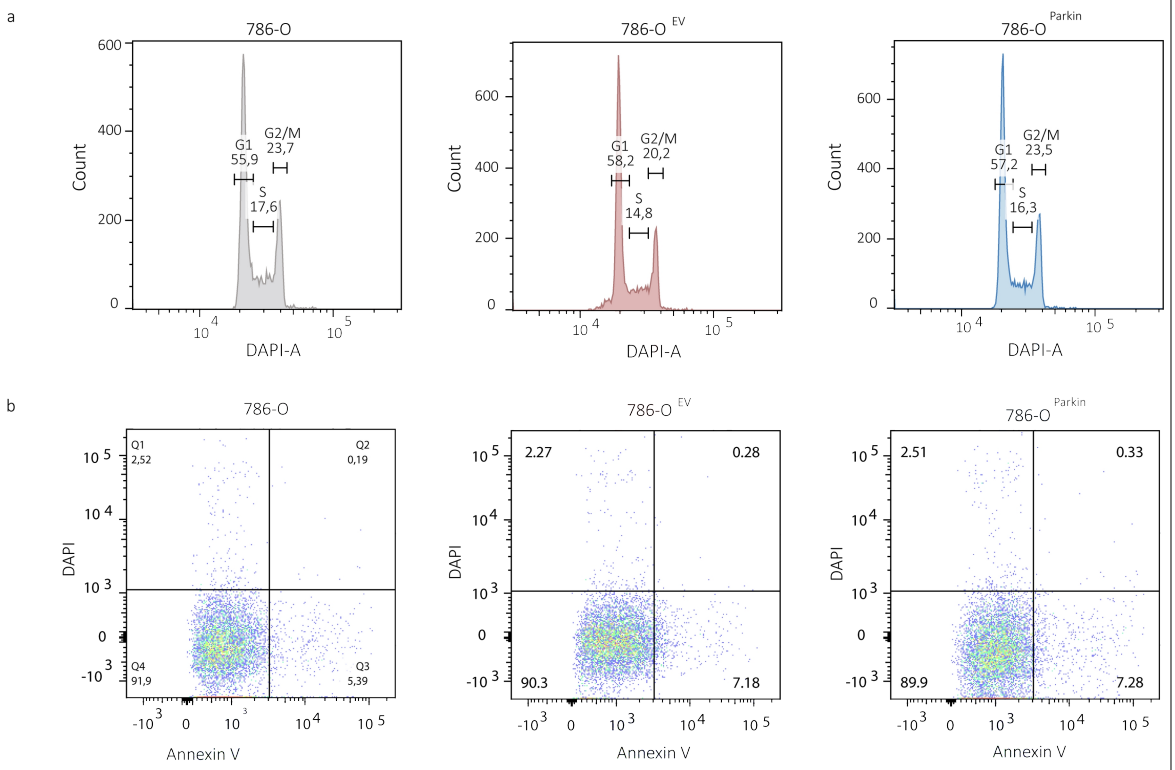

Supplementary figure 8.4| Cell cycle and apoptosis analysis in cells with different Parkin expression. (a) Cell cycle was analyzed by flow-cytometry and PARK2 overexpression showed no difference in G1, S or G2/M phase. **(b)** Apoptosis was analyzed by Annexin V staining. No effect on apoptosis compared to control or wild-type cells was observed when overexpressing PARK2. Figure re-used from (Esser et al. in press).

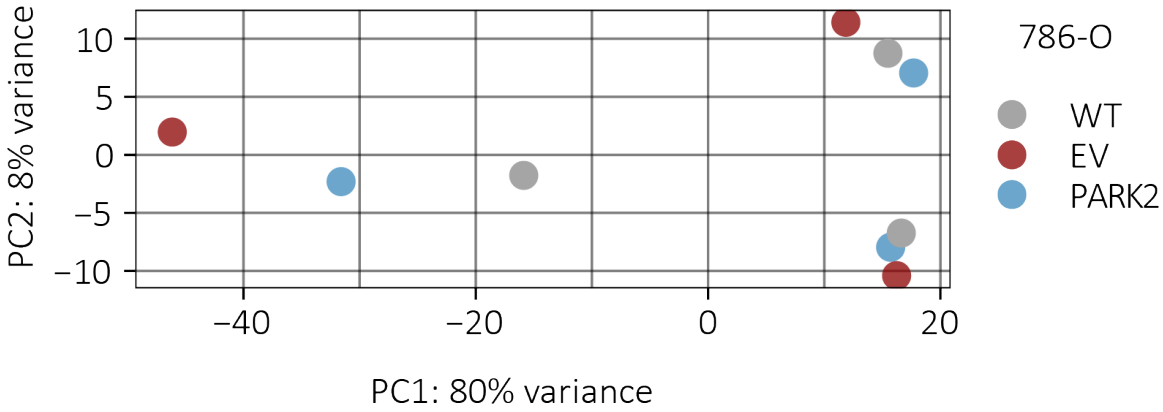

Supplementary figure 8.5| RNA sequencing of 786-O cells with and without Parkin expression. 3'mRNA Seq analysis reveals no difference in the gene expression profile. The samples' gene expression profile was projected onto the first two principal components in a PCA plot. Figure re-used from (Esser et al. in press).

8.2. Supplementary tables

Supplementary table 8.1| RNA sequencing analysis of 786-O vs 786-O^{PARK2} revealed no difference in the molecular gene profile except for PARK2. Top 10 genes are sorted according to adjusted p-value are displayed in the table, including gene name, baseMean, log2 fold change, lfcSE, p-value and adjusted p-value. Table re-used from (Esser et al. in press).

Gene name	BaseMean	Log2 fold change	LfcSE	P-value	Adjusted p-value
PARK2	33.9896130214	-4.884021	0.716252533897868	1.11×10^{-12}	3.25×10^{-8}
DDX11L1	2.27210591102	-1.32×10^{-7}	0.001442694731191	0.77050596251957	0.999945
WASH7P	69.9607934022	3.55×10^{-7}	0.001442690950203	0.83914998092367	0.999945
MIR1302-2HG	0.36755013877	-1.57×10^{-7}	0.001442695007989	0.71903402031267	0.999945
FAM138A	0.69052652291	-2.05×10^{-7}	0.001442695027136	0.39418554853961	0.999945
OR4G4P	1.75735514053	-2.08×10^{-7}	0.001442694828330	0.59224826706012	0.999945
OR4F5	0.36015966695	-9.74×10^{-8}	0.001442695012797	0.60158002213490	0.999945
AL627309.1	4.55983006206	3.75×10^{-7}	0.001442694440266	0.57489684717028	0.999945
CICP27	8.70933284448	3.01×10^{-6}	0.001442694779313	0.36275493691473	0.999945
AL627309.6	2.79536944560	-5.42×10^{-7}	0.001442694535360	0.40018298042801	0.999945

Supplementary table 8.2| RNA sequencing analysis of 786-O^{EV} vs 786-O^{PARK2} revealed no difference in the molecular gene profile except for PARK2. Top 10 genes are sorted according to adjusted p-value are displayed in the table, including gene name, baseMean, log2 fold change, lfcSE, p-value and adjusted p-value. Table re-used from (Esser et al. in press).

Gene name	BaseMean	Log2 fold change	LfcSE	P-value	Adjusted p-value
PARK2	33.9896130214	-5.001062	0.763408500543180	6.98×10^{-12}	2.04×10^{-7}
DDX11L1	2.27210591102	-5.82×10^{-7}	0.001442695016244	0.07978226011397	0.9994839
WASH7P	69.9607934022	4.80×10^{-7}	0.001442690991013	0.78385610682403	0.999484
MIR1302-	0.36755013877	2.78×10^{-8}	0.001442694944129	0.90240206984844	0.999484

2HG					
FAM138A	0.69052652291	-1.42×10^{-7}	0.001442694979057	0.59401627218400	0.999484
OR4G4P	1.75735514053	1.33×10^{-7}	0.001442694772487	0.79312306461345	0.999484
OR4F5	0.36015966695	-7.07×10^{-8}	0.001442694958331	0.82930561150230	0.999484
AL627309.1	4.55983006206	-9.65×10^{-7}	0.001442694896470	0.06565380504873	0.999484
CICP27	8.70933284448	-4.39×10^{-7}	0.001442693325107	0.69893499564382	0.999484
AL627309.6	2.79536944560	-5.23×10^{-7}	0.001442694529232	0.42197480315186	0.999484

Supplementary table 8.3| RNA sequencing analysis of 786-O cells^{EV} vs 786-O revealed no difference in the molecular gene profile. Top 10 genes are sorted according to adjusted p-value are displayed in the table, including gene name, baseMean, log2 fold change, lfcSE, p-value and adjusted p-value. Table re-used from (Esser et al. in press).

Gene name	BaseMean	Log2 fold change	LfcSE	P-value	Adjusted p-value
DDX11L1	2.27210591102	-5.36×10^{-7}	0.001442694986034	0.14078113043779	0.994782
WASH7P	69.9607934022	1.31×10^{-7}	0.001442690950884	0.94279472138870	0.994782
MIR1302-2HG	0.36755013877	1.60×10^{-7}	0.001442695006164	0.63004196095137	0.994782
FAM138A	0.69052652291	1.29×10^{-7}	0.001442694996577	0.75813527112956	0.994782
OR4G4P	1.75735514053	3.27×10^{-7}	0.001442694856021	0.43399233590498	0.994782
OR4F5	0.36015966695	1.25×10^{-7}	0.001442694999091	0.76408172691236	0.994782
AL627309.1	4.55983006206	-1.13×10^{-6}	0.001442695027627	0.02156102747565	0.994782
CICP27	8.70933284448	-1.42×10^{-6}	0.001442693721344	0.20723843831629	0.994782
AL627309.5	14.7681641547	8.05×10^{-6}	0.001442704340417	0.36016995875516	0.994782
RNU6-1100P	0.49696367994	2.06×10^{-7}	0.001442695021516	0.44276317785818	0.994782

Supplementary table 8.4| 786-O and 786-O^{EV} protein levels were compared in LC-MS. All proteins, which have |logFC| >1 are displayed in the table, including gene name, protein name, logFC, p-value and adjusted p-value.

Genes	Protein	LogFC	P-value	Adj. p-value
HRG	P04196	1.62717408612414	0.0885426025624230	0.9998045053087
KRT16	P08779	1.14727457342407	0.0048589817100365	0.9998045053087
H/ IST2/2AC/ IST3/2A/ IST2/2AB/ 2AFX	Q16777;Q7L7L0; Q8IUE6;P16104	0.83645709699949	0.0547372900610951	0.9998045053087
HIST2H2AC	Q16777	-0.69116610408392	0.2079549990081480	0.9998045053087

Supplementary table 8.5| 786-O and 786-O^{PARK2} protein levels were compared in LC-MS. All proteins, which have |logFC| >1 are displayed in the table, including gene name, protein name, logFC, p-value and adjusted p-value. Table re-used from (Esser et al. in press).

Genes	Protein	LogFC	P-value	Adj. p-value
CASC4	Q6P4E1	1.90649775822507	0.000767193581727	0.1631371122464
COX4I1	P13073	1.63621566972616	0.013289729393406	0.2972901705722
LUC7L;LU C7L2	Q9NQ29;Q9Y38 3	1.61914327763991	0.004491512178460	0.2557576917032
CAVIN3	Q969G5	1.60114434369439	0.000380752794873	0.1628775844733
CEP131	Q9UPN4	1.57489787224771	0.001206068105893	0.1926164869879
S100A6	P06703	1.57299616517471	$7.47859175432\times10^{-5}$	0.0922191381575
SNRPD1	P62314	1.42199714828708	0.002503185089742	0.2443469019046
HMGB2	P26583	1.40368105849396	0.005794990835673	0.2594269153179
TRAM1	Q15629	1.37974874055990	0.000143718137388	0.0922191381575
UBE2Z	Q9H832	1.32908211730412	$6.27013490360\times10^{-6}$	0.0146817606842
P/SMD4/I/ SL	P55036;A2A3N6	1.31449978729681	0.000186210664605	0.1024158655326
FAM98B	Q52LJ0	1.30826765283546	0.00084583954068	0.1631371122464
RPL36A/L/	Q969Q0;P83881	1.30504608267273	0.01491831708250	0.3035864817869
IFI35	P80217	1.29598518066094	0.02286751467670	0.3386151211743

COMMD6	Q7Z4G1	1.27380433552746	0.007429469901025	0.2814429315991
OSBPL10	Q9BXB5	1.24822216953448	$7.62688866717\times10^{-6}$	0.0146817606843
USE1	Q9NZ43	1.19264742511238	0.017876047768052	0.3171556862074
GPT2	Q8TD30	1.18249221612968	0.001652221394229	0.2120350789261
EXOSC7	Q15024	1.16774941785418	0.000121210774835	0.0922191381575
PEA15	Q15121	1.10711225556391	0.000615606981521	0.1631371122464
HDAC2	Q92769	1.10557775821597	0.001738824443442	0.2159507776533
GSPT1	P15170	1.09869202941554	0.003200093615935	0.2503188037281
KHDRBS3	O75525	1.09107821133665	0.000796613965928	0.1631371122464
TPM/4/3	P67936;P06753	1.08533303534469	0.021500161495751	0.3361219193471
SMARCC1	Q92922	1.07410499815462	0.024209642751182	0.3450252154191
APIP	Q96GX9	1.04669904659247	0.003493035033837	0.2503188037281
GPRIN1	Q7Z2K8	1.04310485702837	0.004071096485651	0.2503188037280
SLIRP	Q9GZT3	1.02807382555809	0.061178695149837	0.4378556068218
SPECC1	Q5M775	1.02390048749831	0.001300786665373	0.1926164869879
ACT/G2/B	P63267;P60709	-1.00024333725875	0.140591552866731	0.5504194067596
SNX27	Q96L92	-1.00447612293308	0.000874405996612	0.1631371122464
KLF16	Q9BXK1	-1.01538213098721	0.021636535469631	0.3361219193471
AATF	Q9NY61	-1.02012130469540	0.198695684814335	0.6316914835138
PIGG	Q5H8A4	-1.03872103061149	0.002558602402681	0.2443469019046
FAM45BP	Q6NSW5	-1.04838468817009	0.085680782056510	0.4742085434108
YBX3	P16989	-1.08539595688636	0.070489197412078	0.4561065714899
HINT1	P49773	-1.12897570624977	0.013326746740967	0.2972901705722
H/3F3A/ IST3/3	P84243;Q16695	-1.16304276872839	0.256138977134433	0.6791563787655
HMGN4	O00479	-1.20380566127375	0.098708318350654	0.5030258698061
AHSG	P02765	-1.21075998745754	0.179813475000273	0.6082300072463
FBLN1	P23142	-1.35383654771774	0.046735962996366	0.4050385217815
Parkin	O60260	-1.86848343903205	0.001477455853893	0.2106742606478
SLC6A8	P48029	-2.02788006501598	0.000108705064546	0.0922191381575

Supplementary table 8.6| 786-O^{EV} and 786-O^{PARK2} protein levels were compared in LC-MS. All proteins, which have |logFC| >1 are displayed in the table, including gene name, protein name, logFC, p-value and adjusted p-value. Table re-used from (Esser et al. in press).

Genes	Protein	LogFC	P-value	Adj. p-value
COX4I1	P13073	2.02299684364024	0.002626618062321	0.2298290804531
CASC4	Q6P4E1	1.66232377434033	0.001028226218881	0.1721161279431
CEP131	Q9UPN4	1.55308522302575	0.000738376379572	0.1496183716502
CAVIN3	Q969G5	1.53427742556365	0.000274286433299	0.1023701382538
IFI35	P80217	1.42911844106106	0.009393500649401	0.2763226602369
LUC7L;LUC7L2	Q9NQ29;Q9Y383	1.39602268198950	0.006132526648753	0.2740423810201
SNRPD1	P62314	1.38795826492697	0.001676293008783	0.2209448908984
UBE2Z	Q9H832	1.36229455746957	$2.56733071426\times10^{-6}$	0.0049421116250
TRAM1	Q15629	1.35945784697475	$8.37101764612\times10^{-5}$	0.0595400876897
OSBPL10	Q9BXB5	1.34696850908152	$2.10071845785\times10^{-6}$	0.0049421116250
GPT2	Q8TD30	1.34366024550536	0.000406661104180	0.1204342500840
HMGB2	P26583	1.33826051880225	0.004570352751060	0.2598362871890
HDAC2	Q92769	1.33682980431010	0.000282952288133	0.1023701382538
P/SMD4/I/SL	P55036;A2A3N6	1.29648957780855	0.000108254704890	0.0595400876897
EXOSC7	Q15024	1.23745440182489	$4.13160862514\times10^{-5}$	0.0530223106893
GSPT1	P15170	1.15323864410210	0.001390308969340	0.2141075812784
IMUP	Q9GZP8	1.12715694395258	0.169038327101307	0.6186288586882
SMARCC1	Q92922	1.10816904200845	0.013898803004954	0.3075309860292
CKS2	P33552	1.09364981784316	0.000548928725298	0.1362545792986
S100A6	P06703	1.07868882146736	0.000537961569681	0.1362545792986
COMMD6	Q7Z4G1	1.07080896550294	0.011289234184196	0.2887936709733
YTHDC1	Q96MU7	1.06113465898051	0.001646529336433	0.2209448908984
SDF2	Q99470	1.05047124837396	0.093578971355801	0.5109353679889
RPL36A/L/	Q969Q0;P83881	1.04839377977204	0.026407724230845	0.3434788455701
STXBP1	P61764	1.04173185206232	0.010159262070567	0.2838184658282
APIP	Q96GX9	1.02699341559930	0.002295531334010	0.2209448908984
PKMYT1	Q99640	1.02502432603127	0.043919472439201	0.3925919948036
RBM22	Q9NW64	1.00951694017168	0.013688266157393	0.3061069636021

GNE	Q9Y223	1.00377464366627	$9.47710403460\times10^{-5}$	0.0595400876897
HMGN4	O00479	-1.00293439862148	0.126707113753121	0.5712113667893
HINT1	P49773	-1.09733278792025	0.009791253345744	0.2830005719640
AFP	P02771	-1.14276615389779	0.376282940974674	0.7790849924300
C3	P01024	-1.15619181849775	0.206817964443813	0.6457208418997
KCNAB2	Q13303	-1.18400824848948	0.063246990153296	0.4459723664656
FBLN1	P23142	-1.58411237545509	0.016682960799257	0.3179372848013
AHSG	P02765	-1.78489300006926	0.044739479646734	0.3932579831962
Parkin	O60260	-1.98312346055540	0.000566252797085	0.1362545792986
SLC6A8	P48029	-2.02968080549596	$5.62204282325\times10^{-5}$	0.0541121621737

Supplementary table 8.7| Clinico-pathological data of the cultured ALI PDOs from different tumor type tissues. Table re-used from (Esser et al. 2020).

ccRCC	**number**
Age	
Range	33-87
Mean	68.53
Median	69
Sex	
m	20
f	6
T Stage	
organ-confined (T1-T2)	18
non-organ-confined (T3-T4)	8
Grading	
G1	5
G2	13
G3	5
G4	3

pRCC	number
Age	
Range	61-84
Mean	69.6
Median	67
Sex	
m	4
f	1
T Stage	
organ-confined (T1-T2)	4
non-organ-confined (T3-T4)	1
Grading	
G1	2
G2	3
G3	-
G4	-
oncocytoma	**number**
Age	
Range	65-68
Mean	66
Median	65
Sex	
m	2
f	1
T Stage	
organ-confined (T1-T2)	-
non-organ-confined (T3-T4)	-
Grading	
G1	-
G2	-
G3	-
G4	-

urothelial carcinoma	number
Age	
Range	46-86
Mean	68.75
Median	70
Sex	
m	5
f	3
T Stage	
organ-confined (T1-T2)	2
non-organ-confined (T3-T4)	6
Grading	
low grade	-
high grade	8

Supplementary table 8.8| Top 20 up-regulated hallmark gene sets for differentially expressed genes in ALI PDOs versus tissue of origin. Table re-used from (Esser et al. 2020).

Hallmark	NES	Raw p-value	FDR q-value	FWER p-value
Allograft rejection	2.365	0.000	0.000	0.000
MTORC1 signaling	1.838	0.000	0.012	0.012
Reactive oxygen species pathway	1.753	0.003	0.012	0.020
MYC targets V1	1.632	0.000	0.030	0.061
Complement	1.600	0.000	0.033	0.082
Epithelial mesenchymal	1.516	0.000	0.065	0.179
Coagulation	1.438	0.025	0.091	0.274
Cholesterol homeostasis	1.395	0.033	0.111	0.353
Inflammatory response	1.389	0.009	0.102	0.367
KRAS signaling up	1.322	0.009	0.146	0.515
Apoptosis	1.309	0.019	0.143	0.542
Unfolded protein response	1.279	0.054	0.161	0.623
Protein secretion	1.278	0.089	0.149	0.627
Interferon alpha response	1.250	0.091	0.170	0.702
Spermatogenesis	1.236	0.131	0.177	0.740
Interferon gamma response	1.227	0.054	0.176	0.763
DNA repair	1.225	0.066	0.168	0.768
IL-2 STAT5 signaling	1.183	0.108	0.213	0.864
IL6 JAK STAT3 signaling	1.132	0.226	0.276	0.933
E2F targets	1.091	0.241	0.339	0.966

Supplementary table 8.9| Top 20 down-regulated hallmark gene sets for differentially expressed genes in ALI PDOs versus tissue of origin. Table re-used from (Esser et al. 2020).

Hallmark	NES	Raw p-value	FDR q-value	FWER p-value
KRAS signaling down	-1.802	0.000	0.009	0.014
WNT beta catenin signaling	-1.782	0.000	0.006	0.020
pancreas beta cells	-1.699	0.012	0.010	0.046
Hedgehog signaling	-1.619	0.014	0.021	0.126
Estrogen response late	-1.510	0.005	0.060	0.370
Estrogen response early	-1.439	0.011	0.098	0.594
TGF beta signaling	-1.403	0.055	0.122	0.738
Angiogensis	-1.395	0.081	0.115	0.769
Notch signaling	-1.332	0.123	0.171	0.919
Hypoxia	-1.278	0.076	0.235	0.975
TNFA signaling via NFKB	-1.212	0.115	0.346	0.998
Mitotic spindle	-1.186	0.155	0.378	0.999
Fatty acid metabolism	-1.166	0.197	0.391	1.000
UV response up	-1.165	0.184	0.365	1.000
Apical junction	-1.151	0.201	0.371	1.000
Xenobiotic metabolism	-1.149	0.205	0.352	1.000
Bile acid metabolism	-1.120	0.276	0.386	1.000
Heme metabolism	-1.116	0.251	0.374	1.000
Peroxisome	-1.095	0.305	0.398	1.000
UV response down	-0.994	0.468	0.598	1.000

9. Publications

Esser, L. K., Branchi, V., Shakeri, F. et al. "Overexpression of Parkin in clear cell renal cell carcinoma decreases tumor aggressiveness by regulating CKS2 levels." (in press). *Int. J. Oncol*.

Branchi, V, **Esser, L. K.**, Boden, C. et al. (2021). "A Combined TLR7/TLR9/GATA3 Score Can Predict Prognosis in Biliary Tract Cancer." *Diagnostics.* 11(9), 1597. doi: 10.3390/diagnostics11091597.

Branchi, V., Jürgensen, B., **Esser, L. K.** et al. (2021). "Tumor Infiltrating Neutrophils are Frequently Found in Adenocarcinomas of the Biliary Tract and Their Precursor Lesions with Possible Impact on Prognosis." *J Pers Med.* 11(3):233. doi: 10.3390/jpm11030233.

Esser, L. K., Branchi, V., Leonardelli, S. et al. (2020). "Cultivation of Clear Cell Renal Cell Carcinoma Patient-Derived Organoids in an Air-Liquid Interface System as a Tool for Studying Individualized Therapy." *Front. Oncol.* 10:1775. doi: 10.3389/fonc.2020.01775.

Simon, A. G., Tolkach, Y., **Esser, L. K.** et al. (2020). "Mitophagy-associated genes PINK1 and PARK2 are independent prognostic markers of survival in papillary renal cell carcinoma and associated with aggressive tumor behavior." *Sci Rep* 10, 18857. doi: 10.1038/s41598-020-75258-4.

Simon, A. G., **Esser, L. K.**, Ellinger, J. et al. (2020). "Targeting glycolysis with 2-deoxy-D-glucose sensitizes primary cell cultures of renal cell carcinoma to tyrosine kinase inhibitors." *J Cancer Res Clin Oncol* 146, 2255-2265. doi: 10.1007/s00432-020-03278-8.

Tolkach, Y., Ellinger, J., Kremer, A., **Esser, L. K.** et al. (2019). "Apelin and apelin receptor expression in renal cell carcinoma." *Br J Cancer*. 120(6):633-639. doi: 10.1038/s41416-019-0396-7.

Esser, L. K., Weiher, H., Schmidt-Wolf, I. (2016). "Increased Efficacy of Brentuximab Vedotin (SGN-35) in Combination with Cytokine-Induced Killer Cells in Lymphoma." *Int. J. Mol. Sci.* 17(7):1056. doi: 10.3390/ijms17071056.

10. Acknowledgements

Zu guter Letzt möchte ich mich bei allen bedanken, die mich während dieser herausfordernden Zeit meiner Promotion begleitet und unterstützt haben.
Allen voran bei meiner Doktormutter Prof. Dr. Marieta Toma, die es mir ermöglicht hat meine Projekte für meine Dissertation in ihren Labor durchzuführen. Sie hat mir jegliche Freiheiten und Unterstützung bei meinen Ideen und Experimenten gewährt.
Des Weiteren danke ich Prof. Dr. Hubert Schorle für die gelungene Kooperation. Er hat meine Projekte von Anfang an begleitet und mir wertvolle Tipps gegeben, die meine wissenschaftlichen Arbeiten sehr bereichert haben. Außerdem hat er sich bereit erklärt als Zweitprüfer für diese Arbeit zu fungieren. Zudem bedanke ich mich bei Prof. Dr. Eva Kiermaier und Prof. Dr. Frank Bigiel für die Bereitschaft als fachnahes und fachfremdes Prüfungsmitglied Teil meiner Prüfungskommission zu sein.
Außerdem gilt mein Dank allen aktuellen und ehemaligen Kollegen der Pathologie. Allen voran Kerstin Fuchs, die mir mit ihrer technischen Unterstützung und Hilfe bei jeglichen Fragen vieles erleichtert hat und auch fernab vom Laboralltag unvergessliche Erinnerungen geschaffen hat. Zudem Carsten Golletz und Vittorio Branchi, die mir mit ihrem wissenschaftlichen und technischen Input das (Labor)leben sehr erleichtert haben und meine Zeit in der Pathologie sehr bereichert haben. Ferner möchte ich mich bei allen ehemaligen Doktoranden und Studenten für die vielen unvergesslichen Momente bedanken.
Mein Dank gilt auch allen Kooperationspartnern für die Hilfe und den wertvollen wissenschaftlichen Austausch: Prof. Dr. Glen Kristiansen (Institut für Pathologie, Universitätsklinikum Bonn), Prof. Dr. Michael Hölzel (Institut für Experimentelle Onkologie, Universitätsklinikum Bonn), Dr. Marc Sylvester (Core Facility Mass Spectrometry, Universität Bonn), Andreas Buness und Dr. Farhad Shakeri (Core Facility Bioinformatics, Universität Bonn), Dr. André Heimbach (Core Facility Next Generation Sequencing, Universität Bonn) und den diagnostischen Labors des Instituts für Pathologie (Universitätsklinikum Bonn).

Außerdem möchte ich mich bei meiner Familie und meinen Freunden bedanken, die mich immer unterstützt haben und ohne die ich diese herausfordernde Zeit nicht so gemeistert hätte.